Encapsulation of particles and cells using stimuli-responsive self-rolling polymer films

DISSERTATION

zur Erlangung des akademischen Grades

Doctor rerum naturalium
(Dr. rer. nat.)

vorgelegt

der Fakultät Mathematik und Naturwissenschaften

der Technischen Universität Dresden

von

Svetlana Zakharchenko

geboren am 2. Oktober 1983 in Moskau, Russland

Die Dissertation wurde in der Zeit von September 2009 bis Oktober 2013
im Leibniz Institut für Polymerforschung Dresden e.V angefertigt.

Gutachter: Prof. Dr. Manfred Stamm
Prof. Dr. Oliver G. Schmidt

Eingereicht am 13. November 2013
Tag der Verteidigung: 09. April 2014

Table of contents

1 Introduction 1

1.1 Motivation 3

1.2 Goals of the work 5

1.3 Outline of the Dissertation 8

2 Theoretical background and literature overview 9

2.1 Self-folding of polymer films 11

2.1.1 Activation of polymer films 12

2.1.1.1 Polymer bilayers 13

2.1.1.2 Cross-linked polymer films with spatial heterogeneities 15

2.1.1.3 Polymer triggers for inorganic films 15

2.1.2 Design and fabrication of self-folding polymer films 16

2.1.3 Stimuli-responsive folding 17

2.1.3.1 Thermoresponsive 17

2.1.3.2 pH- and salt-responsive 19

2.1.3.3 Solvent responsive 19

2.1.3.4 Electro-responsive 20

2.1.3.5 Chemical-responsive 21

2.1.3.6 Light-responsive 21

2.1.4 Conclusions 23

2.2 Methods of cell encapsulation 25

2.2.1 Microgels for cell encapsulation 25

2.2.1.1 Emulsification 25

2.2.1.2 Microfluidics 26

2.2.1.3 Micromolding 26

2.2.1.4 Photolithography 27

2.2.2 Encapsulation using foldable thin films 28

2.3 Bottom-up tissue engineering 30

2.3.1 Assembly of cell-laden microgels 30

2.3.1.1 Random assembly 31
2.3.1.2 Assembly in microfluidic 31
2.3.1.3 Directed assembly on the interfaces 31
2.3.1.4 Molecular interactions 33
2.3.2 Conclusions 33
3 Experimental part 35
3.1 Characterization techniques 37
3.1.1 Null ellipsometry 37
3.1.2 Optical microscopy 40
3.1.3 Confocal microscopy 42
3.1.4 Atomic force microscopy 44
3.1.5 Other methods 46
3.2 Materials 47
3.2.1 Solvents and solutions 47
3.2.2 Polymers 47
3.2.3 Other materials 47
3.2.4 Synthesis 48
3.2.5 Substrates 50
3.2.6 Cells 52
3.3 Fabrication of polymer bilayer films and self-rolled tubes 53
3.3.1 Polymer films deposition 53
3.3.2 Photolithography 58
3.3.3 Modification of the surface of the hydrophobic polymer. 62
3.3.4 Formation of the polymer tubes and their characterization. 62
4 Results and discussion 63
4.1 Thermoresponsive bilayer systems based on poly(N-isopropylacrylamide) 67
4.1.1 Objectives 67
4.1.2 Experimental 67
4.1.3 Results and discussions 69

4.1.3.1 Swelling of PNIPAM-co-polymer thin films 69
4.1.3.2 Formation of thermo-responsive self-rolled tubes 71
4.1.3.3 Diameter of self-rolled tubes 73
4.1.3.4 Rolling direction and tubes morphology 75
4.1.3.5 Reversibility of tube formation 77
4.1.3.6 Encapsulation and release of microparticles inside the tubes 79
4.1.3.7 Design strategy to produce PNIPAM-based self-rolled tubes with desired properties 80
4.1.3.8 Encapsulation of HeLa cells 81
4.1.3.9 Self-rolled tubes with porous walls 84
4.1.3.10 Magneto-sensitive microtubes (manipulation in magnetic field) ... 85
4.1.4 Conclusions 86
4.2 Solvent-responsive bilayer systems based on polysuccinimide 88
4.2.1 Objectives 88
4.2.2 Experimental part 88
4.2.3 Results and discussions 89
4.2.3.1 Swelling of PSI thin films in an aqueous environment 89
4.2.3.2 Formation of the tubes 90
4.2.3.3 Diameter of self-rolled tubes 92
4.2.3.4 Rolling direction and tubes morphology 92
4.2.3.5 Yeast cell encapsulation 94
4.2.4 Conclusions 95
4.3 Thermo-responsive bilayer systems based on gelatin 97
4.3.1 Objectives 97
4.3.2 Experimental part 97
4.3.3 Results and discussions 98
4.3.3.1 Folding of non-crosslinked bilayer 98
4.3.3.2 Folding of crosslinked gelatin/polycaprolactone bilayer 99
4.3.4 Conclusions 101

4.4 Self-assembly of self-rolled polymer tubes into a 3D constructs with aligned pores 105
  4.4.1 Objectives 105
  4.4.2 Experimental part 106
  4.4.3 Results and discussions 108
    4.4.3.1 Assembling and alignment of microtubes in aqueous solution 108
    4.4.3.2 Complex structures consisting of two types of microtubes 120
    4.4.3.3 Fabrication of porous self-assembled tubular constructs filled with yeast cells 122
  4.4.4 Conclusions 124
5 Summary and outlook 125
List of abbreviations 131
Table of figures 133
References 135
Acknowledgments 143
List of publication 145
Contributions to academic conferences 146
Versicherung 149

1 Introduction

1.1 Motivation

The great challenge of regenerative medicine is recapitulation of natural tissue in all complexity, including microarchitecture, and multicellular composition. Realistic tissue models could help to investigate mechanisms of tissue morphogenesis, differentiation and maintenance and are of particular interest for tissue engineering. Besides that, three-dimensional (3D) tissue constructs can be a good alternative to traditional two-dimensional (2D) cell culture.

The design of scaffolds that provide a suitable environment for the growth and division of cells is a keynote procedure for development of efficient approaches for tissues engineering. To facilitate natural behavior of cells the scaffolds must fulfill many requirements such as biocompatibility, biodegradability, porosity, as well as provide a proper chemical and mechanical environment that mimics properties of the extracellular matrix and specific tissue[1]. Most of the developed approaches of scaffold fabrication can be classified either as bottom-up or top-down ones.

In traditional top-down approaches biodegradable polymer scaffolds are first fabricated. It is expected that cells, which are then seeded on it, populate the scaffold and create the appropriate microarchitecture and extracellular matrix. This strategy often suffers from inhomogeneous cells distribution, since most cells are typically seeded on the periphery of the scaffold[2]. Moreover, top-down approaches have difficulties to recreate the complex microstructural features of tissues.

Many natural tissues are made up of assemblies of small and repeating functional units, such as bundles of myofibers in muscles, lobules in liver, islets in pancreas, and nephrons in kidney. In this respect, the bottom-up or modular strategy is particularly perspective for scaffold fabrication. This approach proposes to build tissues by assembling of micro- or nanoscale blocks, which mimic tissue units. These microblocks can be produced using microfabrication techniques, which allow control over microenvironment of individual cells, structure of clusters of cells as well as the interactions between multiple cell clusters. Recently, assembly of cell-laden poly(ethylene glycol) microgel units into hierarchical tissue constructs was reported[3, 4]. The advantages of such mesoscale self-assembling systems are: (i) homogeneous seeding of the cells, as cell encapsulation occurs during gelation process, and (ii) the possibility to reproduce microstructure of tissues. On the other hand, the applicability of the microgel encapsulation approach is limited due to the small size of the pores, which is intrinsic to many hydrogel-based scaffolds. Moreover, post-assembly fixation of the obtained structures using UV light can be harmful for cells.

Wrapping by thin films, which form self-rolled tubes[5] or self-folding particles[6] is an alternative approach for the encapsulation of cells. Self-rolled tubes are thin bilayers which are able to roll due to internal stress produced as a result of thermal expansion[7], lattice mismatch[8, 9], or swelling[10]. Many kinds of tissues such as vessels[11, 12], bones[13] and muscles[14-16] have either tubular or uniaxially aligned porous structure, and therefore tubular tissue units are more suitable to recreate these structural features than amorphous hydrogels. Moreover, microtubes form pores with sizes up to hundreds of micrometers, providing free migration of encapsulated cells.

Recently, encapsulation of cells in self-rolled tubes composed of inorganic materials was reported[17]. However, use of inorganic self-folding films in biotechnological constructs is often limited due to pore biocompatibility, non-biodegradability and rigidity of the used materials. Polymer based systems seem to be more suitable for this purpose. Polymers undergo considerable and reversible changes in volume that can be used as a driving force of rolling. There is a variety of biocompatible and biodegradable polymers already approved for the use in medicine[18]. Using polymers sensitive to different stimuli allows design of structures, which are triggered to roll in response to a specific stimulus, such as temperature, pH or light[19]. Some polymers change their properties in physiological ranges of environmental conditions, which can be utilized for parallel encapsulation of cells during rolling of the tube to achieve homogeneous seeding. Cell-loaded tubes can be potentially assembled into microporous 3D structures. Therefore, self-rolled tubes can offer several advantages over the microgels, when used for cell encapsulation. First, the encapsulation step is separated from the fabrication step, which permits to avoid exposure of the cells to toxic chemical precursors and UV illumination. Second, folding can be reversibly controlled by external stimuli, enabling the triggered capture and potential release.

Several stimuli-responsive polymer self-rolling systems have been reported by the time. Luchnikov *et al.* fabricated poly(4-vinylpyridine)/polystyrene bilayer films that rolled in acidic environment (pH = 2)[5]. Kalaitzidou *et al.* demonstrated thermo-responsive rolling-unrolling of polydimethylsiloxane/gold tubes at 60 - 70 °C[20, 21]. Gracias *et al.* developed an approach for design of self-folding particles made of patterned SU-8 photoresist-polycaprolactone films, which irreversibly fold at 60 °C[6]. The non-biodegradability and non-biocompatibility of these polymers as well as the difficulty to locally control such low pH values and the high temperature hamper the application of these systems in medicine. Therefore, design of biocompatible and biodegradable self-rolling polymer systems triggered by external signal within physiological conditions is strongly desirable.

1.2 Goals of the work

This thesis is focused on the design and development of an approach, allowing the fabrication of biocompatible/biodegradable self-rolled tubes, which are sensitive to stimuli at physiological conditions, can be homogenously filled with cells and are able to self-assemble into a complex 3D construct with uniaxially aligned pores. These constructs are aimed to recreate the microstructure of tissues with structural anisotropy, such as of muscles and bones. The approach is based on the use of microtubes formed by stimuli-induced rolling of polymer bilayers consisting of hydrophobic and stimuli-responsive hydrophilic polymers. As a first step, cells are adsorbed on the top of an unfolded bilayer; triggered rolling results in the parallel encapsulation of the cells inside the tubes. As a second step, the formed self-rolled tubes with encapsulated cells can be assembled in a uniaxial tubular scaffold. The suggested concept is schematically represented in Figure 1.1.

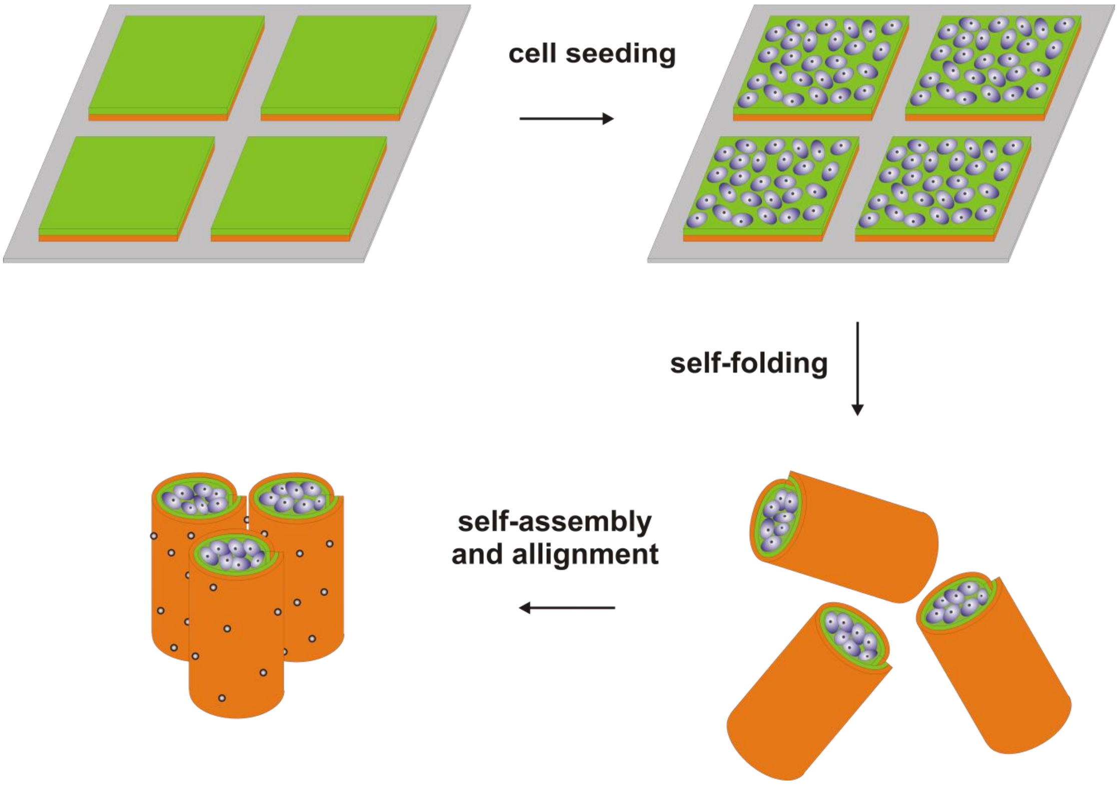

Figure 1.1 | Scheme of the microtubes-based scaffold formation.

In respect to this scheme, three general goals of the present work can be distinguished:

1. Design of biocompatible polymeric bilayers foldable in the range of physiological conditions;
2. Encapsulation of cells;
3. Assembly of individual tubes into a 3D scaffold with aligned pores.

Choice of materials

- *The driving force of folding behavior.* Generally, the rolling of bilayer films can be driven by different forces such as lattice mismatch, unequal thermal expansion or unequal swelling of components in surrounding media. For biotechnological applications, the most promising and straightforward type of polymer activation is a differential swelling of hydrogels. In our approach inhomogeneous swelling is achieved by using lateral bilayer structure of the polymer films. The first layer deposited on a substrate is composed of hydrophilic stimuli-responsive polymer, which is able to swell in aqueous media at specific conditions. The second layer is made of hydrophobic polymer and has to restrict the swelling of an active polymer from the top, in order to provide bending force (see Chapter 2.1).
- *Stimuli-responsiveness.* The approach must provide an opportunity to adsorb cells on the top of unfolded patterned bilayer at physiological conditions. The application of appropriate stimuli triggers swelling of the active component of the bilayer, resulting in rolling of the tubes and cell encapsulation. Both adsorption of the cells and rolling must take place in conditions close to physiological ones. Among possible stimuli, pH and UV light are less favorable to trigger encapsulation of the cells inside the tubes. UV light may cause the damage of DNA due to dimerization of thymine fragments, while even small pH changes affect cell membrane potential. On the other hand, since cells can tolerate variation in temperature in the range between 4 °C and 37 °C, temperature appears to be suitable stimulus to trigger folding.
- *Biocompatibility and biodegradability.* Since the approach is considered for potential biotechnological applications, biocompatibility of at least the passive polymer, which is in a direct contact with cells, is essential. Biodegradability of both components is highly desired.

Fabrication techniques

- *Polymer film deposition.* Typical techniques used for thin film deposition are dip-coating and spin-coating. For the fabrication of bilayer films active and passive polymers must have selective solvents.
- *Photolithography*. Patterning of polymer bilayer has to be performed using photolithography to allow the production of large quantities of microtubes. For this, both components of the polymer bilayer have to be either photocrosslinkable, or can be crosslinked using admixed photocrosslinker.

Cell encapsulation

Parameters of the tubes (inner diameter, morphology) must be optimized in such a way to provide successful encapsulation of the cells as well as their good viability in the tubes. The seeding procedure must result in a homogeneous distribution of the cells within the tubes.

Tube agglomeration and alignment

The procedure of self-assembly of the microtubes into a 3D agglomerates must be tolerable for encapsulated cells. Self-assembled agglomerates of the microtubes must be mechanically stable and possess a good degree of tubes alignment.

1.3 Outline of the Dissertation

The thesis is organized in 5 major Chapters.

In **Chapter 1** the general introduction to the present work is given and the goals of the work are discussed.

Chapter 2 presents the theoretical background and literature overview of the current state of knowledge related to the thesis areas. This chapter is divided into three parts. First, approaches for design of self-folding polymer films, responsive to external stimuli, are summarized. Second, the possibility of cell encapsulation using hydrogels and self-folding films is discussed. Third, an overview of bottom-up tissue engineering strategies, which involve assembly of cell-laden microgels in order to reconstruct larger tissue structures, is given.

Chapter 3 describes characterization techniques and materials used in the present work. Experimental details of fabrication of bilayer films and self-rolled tubes for each designed polymer system are summarized.

Results and discussions are presented in **Chapter 4**, which is divided in two parts. **The first part** is dealing with the design of polymer bilayer systems, which can fold in response to stimuli in conditions tolerable for cells. Three polymer systems are described in this part: two of them thermo-responsive and one solvent-responsive. The details of formation and behavior of individual self-rolled tubes, as well as the possibility to encapsulate microobjects, such as glass beads, yeast cells and mammalian cells, are discussed. **The second part** is focused on the self-assembly of cell-loaded self-rolled tubes into a three-dimensional constructs with parallel orientation of pores.

Finally, the summary of this thesis and possible further investigations are presented in **Chapter 5**.

2 Theoretical background and literature overview

2.1 Self-folding of polymer films

Fabrication of three-dimensional microobjects using controlled bending of two-dimensional thin films, often called microorigami due to similarity to an old Japanese art of paper folding, is a novel and very attractive research field[22, 23]. Spontaneous or stimuli-responsive folding of such 2D structures is typically achieved by manipulation of strain in patterned thin films and can be reversible or irreversible. One of the advantages of this approach is the possibility of quick and reproducible fabrication of 3D hollow objects with controlled chemical properties and morphology of both the exterior and interior.

The microorigami concept arose from the pioneering works of Smela[24] and Jager[25], where reversible folding of patterned gold films with polypyrrole hinges triggered by electric signal was demonstrated. Nowadays, several groups around the world work in this field, using different materials for creation of self-folding structures and proposing latter for the numerous practical applications. So for example, metallic and semiconductor components have been used to fabricate self-folding tubes, containers, and microgrippers using either surface tension or intrinsic thin film stresses as a driving force of folding. Group of O.G. Schmidt focuses on design of semiconductor and metal oxide self-rolled tubes in order to create energy storage elements[26-28], controllable microjets for transport and delivery of microobjects[8, 29, 30], lab-on-a-tube and nanooptic tools [9, 17, 31, 32] and a platform for investigation of behaviour of cells in confinement[33]. Gracias *et al.* developed approaches for fabrication of metal based self-folding microdevices with complex geometry which can be used for a various biotechnological applications, such as microsurgery[34], controlled encapsulation of drugs[35] and cells[36-38] and fabrication of scaffolds for 3D cell growth[39].

However, application of inorganic self-folding films in biotechnological constructs is often limited due to poor biocompatibility, non-biodegradability and rigidity of the used materials. Polymer based systems are more suitable for this purpose. First, polymers undergo considerable and reversible changes in volume that can be used as a driving force of folding and unfolding. Second, using polymers sensitive to different stimuli allows design of structures, which fold or unfold only in response to a specific stimulus, such as temperature, pH, light, etc. rather than spontaneous[19]. Some polymers change their properties in physiological ranges of environmental conditions, which can be utilized for parallel encapsulation of cells during folding. Third, a variety of biocompatible and biodegradable polymers have been already approved for the use in medicine[18]. Forth, since polymer films can be precisely patterned by a number of techniques such as one-step- or multistep-photolithography and molding, a great variety of 2D structures can be fabricated to obtain simple and complex shapes as tubes, spheres and polyhedra.

2.1.1 Activation of polymer films

Design of self-folding materials is generally based on the use of strain-generated bending that facilitates transformation of 2D objects into 3D ones. For inorganic materials such bending can occur as a result of internal stress produced by the lattice mismatch[8, 9, 28, 40] or unequal thermal expansion[7]

Polymer based films, however, often require another type of actuation. That can be for example relaxation of residual thermal stress developed during fabrication of thin films[20, 21]. Another possibility to activate folding of polymer sheets relates to the use of surface tension. For instance, in so called capillary origami folding occurs when water droplet, deposited on a thin film, slowly evaporates[41]. As the volume of droplet decreases, the surface tension of the liquid pulls the sheet around smaller volumes, increasingly curving it. Gracias *et al.* fabricated microcontainers employing minimization of surface tension of the melting polycaprolactone hinges[6].

Possibility to design self-folding objects using shape memory polymers is based on the fact that such polymers can be deformed by application of external stress and fixed in a second, temporary shape, which is stable until an appropriate stimulus is applied to induce the recovery of the original state[42]. However, shape memory polymers response to a limited number of stimuli. Moreover, they can be challenging to pattern using lithographic methods and their shapes often require pre-programming that often restricts miniaturization.

For biotechnological application, most promising and straightforward type of polymer films activation is differential swelling of hydrogels[5, 10, 43]. Hydrogels, which are three-dimensional networks of cross-linked polymer chains imbibed with water, are highly biocompatible soft materials with mechanical characteristics being relatively close to that of living tissues. Hydrogels can exhibit reversible swelling/deswelling under various environmental conditions due to change of interactions of polymer chains with water[44, 45].

In most cases, swelling/shrinking of the hydrogel objects results in an uniform expansion or contraction in all directions, while the shape remains intact (Figure 2.1a). In order to create a self-folding structure using thin hydrogel films, it is necessary to introduce differential stress either along its thickness or lateral dimensions so that a bending moment is generated. Non-uniform swelling or deswelling, which occurs with different magnitudes in different directions, can be achieved either by applying inhomogeneous field to homogeneous materials (Figure 2.1b) or by applying homogeneous stimuli to inhomogeneous materials (Figure 2.1c).

In the first case, applied stimuli are not equal across the object. Lee *et al*. observed bending of polyelectrolyte hydrogel in solution with lateral gradient of pH, formed during electrolysis[46]. Several research groups reported bending deformation by local solvent deposition[47] or due to differential heating of thermo-responsive hydrogel using embedded electronics[48].

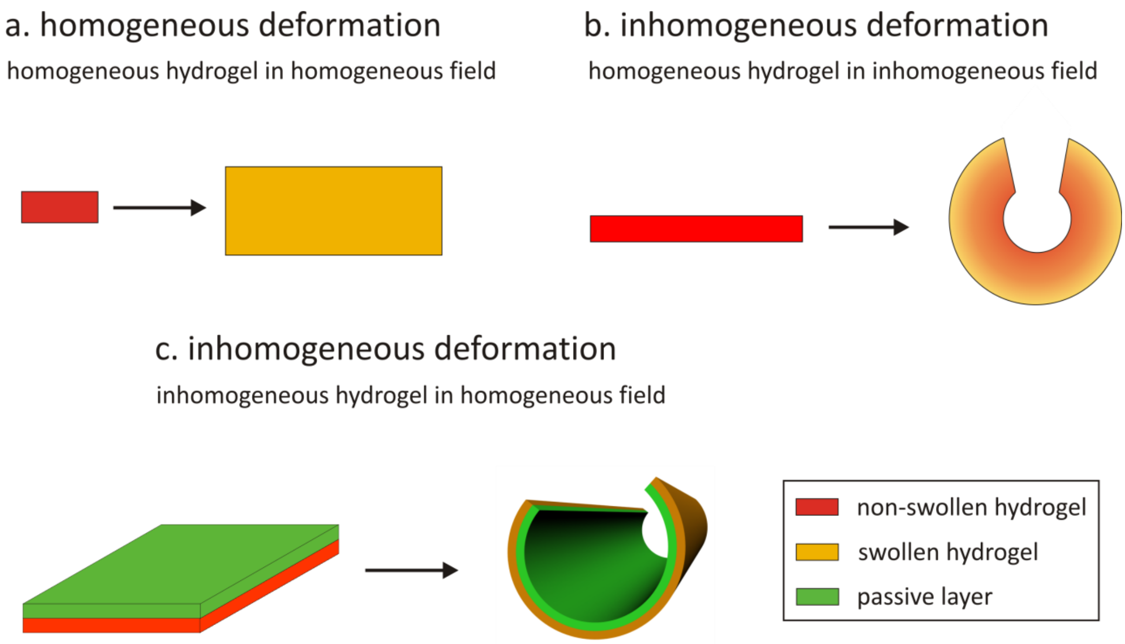
a. homogeneous deformation
homogeneous hydrogel in homogeneous field
b. inhomogeneous deformation
homogeneous hydrogel in inhomogeneous field
c. inhomogeneous deformation
inhomogeneous hydrogel in homogeneous field
non-swollen hydrogel
swollen hydrogel
passive layer

Figure 2.1 | Different scenario of swelling of the hydrogel: (a) homogeneous deformation of homogeneous hydrogel; (b) inhomogeneous deformation of homogeneous hydrogel; (c) inhomogeneous deformation of inhomogeneous hydrogel.

Great majority of polymer-based self-folding systems utilizes difference in swelling characteristics within material itself when homogenous stimulus is applied. To date, three general approaches for design of such polymer activators are reported: (i) polymer bilayers, (ii) cross-linked polymer films with spatial heterogeneities, (iii) inorganic films with polymer trigger.

2.1.1.1 Polymer bilayers

Bilayer actuators have a long history and can be tracked back to the 18th century, when the British clockmaker John Harrison created bimetal strips, which curved upon the temperature changes due to differences in thermal expansion coefficients of two metals. First fundamental investigation of bending of a bilayer was performed by Timoshenko[7] in 1925 for a strip consisting of two metals welded together. When the coefficients of linear expansion of the metals are different, strip uniformly heated from a temperature t_0 °C to t °C bends giving a uniform curvature:

$$\frac{1}{\rho}=\frac{6(\alpha_2-\alpha_1)(t-t_0)(1+m)^2}{h\left(3(1+m)^2+(1+mn)\left(m^2+\frac{1}{mn}\right)\right)}, \qquad (2.1)$$

$$\frac{E_1}{E_2}=n, \qquad (2.2)$$

$$\frac{a_1}{a_2}=m, \qquad (2.3)$$

where α_1 and α_2 denote the coefficients of expansion of the two metals, E_1 and E_2 correspond to their moduli of elasticity, a_1 and a_2 – to the thickness of the layers, h is the total thickness of bilayer film, ρ – radius of curvature. As it comes from the equations (2.1), radius of curvature is inversely proportional to difference in expansion coefficients. Moreover, radius of curvature first decrease and then increase with the increase of m. The resultant curvature is not very sensitive to the difference in stiffness between the two layers, and is mainly controlled by the actuation strain and the layer thickness. The Timoshenko equation applies to a beam bending in only one direction, does not predict the folding direction and is applicable only for reversible elastic deformations.

More recent models have considered complex bending of bilayer in two dimensions. Mansfield found analytical solutions for large deflections of circular[49] and elliptical[50] plates having lenticular cross sections with a temperature gradient through the thickness. Several groups investigated, both theoretically and practically, the preferential rolling direction depending on the aspect ratio of rectangular pattern, consisted of inorganic materials[51-53].

Bending principal for polymer bilayers is similar to that for inorganic systems: one layer demonstrates greater expansion than the second one. However, compared to inorganic bilayers, polymers and especially hydrogels can undergo significantly larger volume changes (up to 10 times) and respond to a variety of stimuli. Generally, self-folding polymer bilayers consist of hydrophobic (passive) and stimuli-responsive hydrophilic (active) polymers. Active layer swells or contracts in response to the change of environmental condition, while passive polymer maintains its volume, restricting uniform swelling of the active one. That results in tensile stress and bending of the film.

Self-folding polymer/polymer and composite polymer/metal bilayers triggered by change in pH, temperature and other conditions have been reported by a number of research groups and are described in more details in Chapter 2.1.3.

2.1.1.2 Cross-linked polymer films with spatial heterogeneities

The concept of differential strain, which is used in bilayer actuators to drive a stimuli-responsive folding, can be adopted for polymer gels having a uniform chemical composition. For that gradients or spatial heterogeneities must be created within a single layer. Such heterogeneities can appear due to unequal degree of crosslinking, created by exposure to different intensities of ultraviolet light using optical filters or photomasks, or due to gradient distribution of co-monomers inside the gel sample. In both cases, differential swelling behaviour is provided.

Crosslinking gradient

Using greyscale photolithography Santangelo *et al.* produced thermoresponsive rectangular strips laterally bisected into discrete regions with greater and lesser degree of crosslinking, which resembles thick but narrow bilayer[54]. When swelled in an aqueous medium, it did not bent to the side of the less swelling component that is the case of “classical” bilayer, but rolled into a three-dimensional shape consisting of two nearly cylindrical regions connected by a transitional neck. The same authors employed this approach for fabrication of even more complicated structures, where highly cross-linked dots were embedded in a less cross-linked matrix[55]. Such swelling patterning resulted in formation of surfaces with constant Gaussian curvature (spherical caps, saddles, and cones) or zero mean curvature (Enneper’s surfaces), as well as more complex and nearly closed shapes.

Jamal *et al*. reported self-folding microstructures with cross-linking gradient along the film thickness, which was generated due to strong molecular absorbance of the used photoresist SU-8 at low ultraviolet wavelengths[56].

Concentration gradient

Flat discs having internal lateral gradients in monomer concentration were produced by programmable mixing of solutions with different monomer concentrations and injection into a Hele-Shaw cell[57]. Fast polymerisation fixed the formed gradients. Due to differential shrinking such discs were able to adopt 3D configuration.

Nasimova *et al.* fabricated gradient gels strip with gradient monomer distribution along its thickness by copolymerization between two surfaces with different hydrophobicity/hydrophilicity properties[58].

2.1.1.3 Polymer triggers for inorganic films

Polymers can be also used to trigger folding of inorganic films. For instance, polymer can be photopatterned atop pre-stressed inorganic bilayer in order to prevent its spontaneous folding. Application of appropriate stimuli, which leads to delamination, softening, dissolution, or degradation of the polymer trigger, results in stress release in underlying strained bilayer and causes the actuation[34, 59, 60].

Inverse approach employs active polymer bilayer template with patterned atop passive inorganic material[61]. Stimuli-responsive folding of the polymer bilayer causes simultaneous deformation of the inorganic film. The polymer template can be then removed by pyrolysis. In both cases folding is irreversible.

2.1.2 Design and fabrication of self-folding polymer films

Two general strategies for design of self-folding films can be distinguished: (i) hinge-free and (ii) hinge-assisted.

In first case, activation occurs in entire film (usually bilayer) and uniform one-step bending results in a formation of rounded hinge-free shapes, such as helixes, tubes and capsules (Figure 2.2a). The type of desired 3D structure is preprogrammed by the bending curvature and the form of film pattern. So for example, tubes can be obtained from rectangular sheets, envelop-like and spherical capsules – form star-like or snowman shapes[62-64].

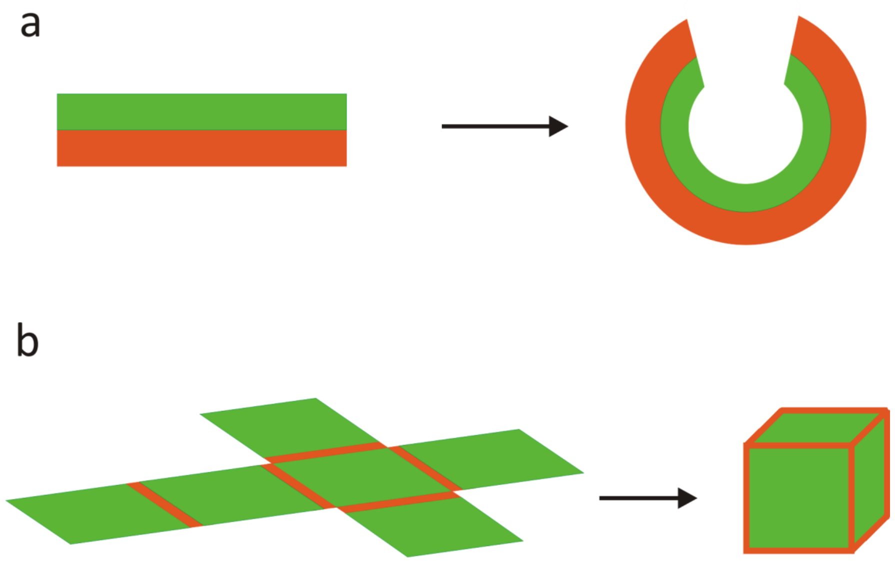

Figure 2.2 | Design of self-folding films: (a) hinge free and (b) hinge-assisted. Passive areas depicted in green, active – in orange.

In second approach, films are complexly patterned and consist of rigid areas connected with flexible joints (hinges). Activation and bending occur only in hinges, which form edges of the folded structure, whereas rigid areas form its faces (Figure 2.2b). This method allows fabrication of a large number of shapes, such as microgrippers[34, 65] and hollow polyhedra[6, 36]. Type of polyhedron is determined by the initial layout. For instance, six square patches produce a cube and twelve regular pentagon patches produce a dodecahedron, etc. The advantage of this approach is not only a great verity of produced microstructures, but also a possibility of step-like activation, when series of stimuli triggers sequential folding/unfolding[34].

Generally, fabrication of self-folding polymer films requires crosslinkability of the used polymers. Experimentally, 2D film layouts can be produced by cutting[5, 20, 21, 66], one-step[10, 62, 67] or multi-step[6, 36, 65] photolithography or using microwell-like substrates[63, 68, 69]. Among them, cutting is the simplest technique and allows the fabrication of millimetre size objects, typically of rectangular shape. No complex patterning is possible in this method. Both microwells technique and one-step photolithography permit a great variety of shapes and are employed for production of hinge-free self-folding structures. Fabrication of patterned polymer films for hinge-assisted folding is the most technically complicated procedure and requires mask alignment during several steps of photolithography, which is time-consuming and difficult to control, but provides the broadest range of shapes of self-folding objects.

2.1.3 Stimuli-responsive folding

As it was already mentioned above, the incorporation of stimuli responsive polymer in self-folding films offers control over the folding behaviour. Folding or unfolding of microstructures is triggered by external signal, such as pH, temperature, electric field or immersion into a solvent. An overview of reported stimuli-responsive polymer self-folding systems is presented below and summarised in Table 2.1.

2.1.3.1 Thermoresponsive

Thermoresponsive self-folding films have been produced using relaxation of residual thermal stress, continuous thermal expansion, shape-memory transition as well as melting.

Lendlein *et al*. reported thermoresponsive macroscopic self-folding cube based on shape memory poly(ε-caprolactone)[70]. At low temperature (below transition temperature of the polymer) the materials are in their temporary shape. Films recover their permanent shape and irreversibly fold by heating. The transition temperature and size of the folded objects was not given in the article.

Kalaitzidou *et al*. demonstrated rolling of polydimethylsiloxane/gold bilayer prepared on a glass substrate covered with polyacrylic acid (PAA)[20, 21]. Upon the dissolution of the PAA in water, microscale tubes and coils were formed as a result of the relaxation of residual thermal stress developed at the polydimethylsiloxane/gold interface during fabrication. Upon heating at 110 °C, unfolding back to a flat shape was achieved, which is due to thermal expansion of the PDMS. The ability of the rolls to capture, transport and release poly(ethylene glycol) molecules was demonstrated.

Gracias *et al*. fabricated all-polymeric containers based on lithographically patterned SU-8 photoresist – polycaprolactone films[6]. Irreversible folding upon heating above 58 °C was driven by a minimization of surface area of the melted polycaprolactone hinges within two-dimensional template. Mammalian cells and bacteria were encapsulated using tumbling approach since the parallel loading during folding was not possible due to high actuation temperature. Design of grippers with chromium/copper/polymer trilayer hinges between metal faces permitted an actuation temperature to be reduced to 40 °C[36, 65]. These structures were used to demonstrate irreversible *in situ* capture of glass beads, fibroblast cells and Triops embryos.

Despite variety of thermoresponsive systems mentioned above, they can be barely used for encapsulation and release of cells as the folding-unfolding conditions are typically harsh. The swelling induced folding of polymer films based on thermoresponsive polymers, which possess Low Critical Solution Temperature (LCST) in aqueous solutions, seems to be more perspective for this goal.

Most recently several self-folding systems based on thermoresponsive poly(N-isopropylacrylamide) (PNIPAM) were reported. In aqueous media, PNIPAM-based hydrogels reversibly swell and shrink below and above LCST, which is 33 °C for homopolymer. By varying the composition of the polymer, its transition temperature can be easily tuned, for instance increased or decreased by copolymerization with hydrophilic or hydrophobic monomer respectively. Peeters *et al*. demonstrated bilayer system, where crosslinked mixture of poly(methyl methacrylate) and diacrylated triblock copolymer of poly(ethylene glycol) and poly(lactic acid) (PLA-b-PEG-b-PLA) restricted swelling of PNIPAM layer[71]. Stimuli responsive bilayer vehicles of sizes varying between 0.25 mm^2 and 1 mm^2 were fabricated and proposed for cardiomyocytes encapsulation and transplantation. Santangelo *et al*. investigated swelling induced deformation of a thin rectangular gel sheet formed of random copolymer of N-isopropylacrylamide, acrylamidobenzophenone, acrylic acid and rhodamine B-labeled methacrylate (poly(NIPAm-co-BPAm-co-AA-co-RhBMA))[54]. Via photolithography sheets were bisected into discrete regions with greater and lesser degree of crosslinking, which results in lesser and greeter swelling in these regions respectively. At 22 °C sheet rolled into a 3D shape consisted of two nearly cylindrical regions connected by a transitional neck. Heating to 50 °C led to fully reversible de-swelling back to a flat structure.

2.1.3.2 pH- and salt-responsive

In pH-responsive self-folding films active layer typically consists of weak polyelectrolyte, which allows switching between charged and uncharged form at different pH. Huck *et al*. reported gold–poly(methacryloxyethyl trimethylammonium chloride) brush composite objects which fold in response to the change in salt concentration to form microcages and microcontainers[72]. Luchnikov and co-workers demonstrated rolling of poly(4-vinyl pyridine)/polystyrene/polydimethylsiloxane trilayer[66] and poly(4-vinyl pyridine)/polystyrene bilayer[5, 73] in aqueous solutions at low pH when nitrogen atom in the pyridine ring is protonated, which results in selective swelling of poly(4-vinyl pyridine) layer. Gracias *et al*. fabricated millimetre size poly(N-isopropylacrylamide-co-acrylic acid)/polyethylene glycol bilayers that fold and unfold in response to changing pH and ionic strength of aqueous media[43].

Bilayers reported by Lee *et al*. were patterned from poly(methyacrylic acid)/poly-(2-hydroxyethyl methacrylate) and folded in contact with biological fluids at pH 6.5 as a result of pH-related swelling differential[63]. Produced self-folding devices were suggested as a microadhesive drug delivery system for preventing drug leakage and improving unidirectional delivery in intestine. For that purpose muco-adhesive patches containing drugs on the surface were priory placed on the surface of the passive layer.

Yang *et al*. fabricated a snowman-shaped bilayer microstructures consisting of an active layer of poly(2-hydroxyethyl methacrylate-co-acrylic acid) and a passive layer of poly(2-hydroxyethyl methacrylate)[64]. The snowman structures folded into microcapsules in aqueous solutions at pH 9. Under neutral conditions, at pH 7, the swelling degree of p(HEMA-co-AA) decreased, and the microcontainer compartments were opened. Further decrease of pH down to pH 4 resulted in a planar snowmanshaped configuration, indicating completed unfolding. In situ encapsulation (at pH 9) and triggered release (at pH 4) of target materials, was demonstrated on example of 1 µm polystyrene particles and dextran with molecular weight of 2000 kDa.

Gradient gels obtained by copolymerization of N-isopropylacrylamide with acrylic acid sodium salt between two surfaces with different degrees of hydrophobicity/hydrophilicity were demonstrated by Nasimova *et al.*[58] Such gels demonstrate pH-induced bending/straightening behaviour due to gradient distribution of acid units inside the gel sample. In acidic media at pH 3 gel strips reversibly bend, whereas incubation at pH 7 results in uniform swelling without any changes of the sample shape.

2.1.3.3 Solvent responsive

In most reported solvent-responsive systems spontaneous folding of microstructures takes place in contact with water. The folding is typically immediate and irreversible. For example, Jeong and Jang *et al*. fabricated 3D actuating objects in a shape of helixes, tubes, cubes, pyramids and phlat balls, where transformation of programmed 2D structures was achieved via bending, twisting and folding mechanisms[74]. The driving force of the actuation was selective swelling of water-swellable poly-urethane/2-hydroxyethyl methacrylate restricted by hydrophobic polydimethylsiloxane.

Lee *et al*. fabricated partially biodegradable bilayers, where active and passive layers consisted of poly(polyethylene glycol methacrylate-co-polyethylene glycol dimethacrylate) resin (poly(PEGMA-co-PEGDMA)) and chitosan respectively[69]. Capsule-like microstructures were formed in water. Later related system consisted of polyvinyl alcohol/chitosan and possessed similar behaviour was reported[68]. Huck demonstrated gold/poly(glycidyl methacrylate) brush composite system which folded on immersion in methanol.

An example of reversible solvent-responsive system was reported by Mei and Yu *et al*., who fabricated tubes and springs using bilayers of pre-strained metal and poly(vinyl alcohol)-poly(acrylic acid) (PVA–PAA)[75]. The ability of the micro-scrolls to roll and unroll was due to the swelling and shrinking of the polymer layer in response to different solvents, namely water and ethanol respectively.

2.1.3.4 Electro-responsive

Pioneering work of Smella *et al*. introduced microactuators consisting of conducting polypyrrole/gold bilayers which connected rigid plates to each other and to a silicon substrate[24]. Electrically controlled and reversible bending of the hinges allowed precise three-dimensional positioning of the plates to fabricate such structures as cube. Five years later Jager *et al*. presented micrometer-size manipulator based on the same polypyrrole/gold system[25]. This microrobotic arm was able to pick up, lift, move, and place micrometer-size objects (glass bead) within an area of 250 µm x 100 µm and was proposed by authors as a tool for single-cell manipulation.

Whitesides *et al*. created a variety of proof-of-concept 3D actuators and soft-robotic devices, which consisted of polydimethylsiloxane with aligned cardiomyocytes[76]. The polymer-cell film adopted three-dimensional conformations when an electric signal was applied and cardiomyocytes were shortened during reversible synchronous contraction. The centimetre-scale constructs capable of gripping, pumping, walking, and swimming were fabricated. The same system was further used for calculating the contractile stresses of a 2D anisotropic muscle tissue cultured on a flexible polymer film[77].

2.1.3.5 Chemical-responsive

Folding and unfolding can be triggered by a presence of particular chemicals, which cause softening, degradation, dissolution or delamination of the trigger layer. Such self-folding is typically irreversible.

To achieve folding and unfolding of microgrippers, Randhawa *et al*. used the sequential chemical etching of hinges prepared from a chrome/copper/polymer trilayer[59]. Folding was triggered by the dissolution of the polymer in an aqueous acetic acid solution, whereas unfolding started upon the dissolution of copper layer when H_2O_2 was added.

Enzyme-sensitive self-folding films were developed for the first time by Gracias *et al*.[34] In this approach self-folding metallic grippers were constructed using multilayer hinges that employed intrinsic strain energy and biopolymer triggers. Two kinds of biodegradable polymers were used to form a polymer layer that prevented bending of hinges. The gripper, unfolded in the initial state, folds when the first polymer is degraded after addition of the first enzyme. Unfolding took place when another enzyme was added to degrade the second polymer. As a result one circle of folding and unfolding was achieved. The possibility to use such microdevices was demonstrated by gripping and releasing an alginate bead as well as by the biopsy of liver tissue from a model organ system. Enzymatic approach seems to be very promising for it allows fabrication of smart materials and devices that autonomously reconfigure in response to specific biological environments.

2.1.3.6 Light-responsive

Several examples of self-folding systems triggered by light were reported. One of the possible approaches to convert light energy into mechanical energy is based on the use of light-sensitive molecules which undergo conformational or chemical changes upon irradiation. For example, Ikeda and co-workers observed light-induced bending behaviour of a film, which consisted of a liquid-crystal network containing an azobenzene chromophore[78]. The film bent in different directions in response to irradiation by linearly polarized light with wavelength of 366 nm and different angles of polarization. Bending was reversible and film flattened again by visible light with wavelength longer than 540 nm. The photomechanical effect resulted from a photoselective volume contraction due to trans-cis isomerization of the azobenzene moieties. Aoyagi *et al*. proposed a fabrication of self-bending actuators utilizing a photo-triggered pH jump reaction[79]. For this a photo-initiated proton-releasing agent of o-nitrobenzaldehyde (NBA) was integrated in polyacid/polybase bilayer. Upon UV irradiation phototransformation of NBA induced local pH decrease inside the pH-responsive bilayer gels resulting in quick and reversible bending of the actuators.

Another approach to design light-responsive systems involves localized conversion of light energy into heat. So for example, self-folding of thin pre-strained polystyrene sheets where hinges were created by printing black ink on a transparent polymer was achieved using unfocused light[80]. Black ink provided a localized light absorption, which heated the underlying polymer to temperatures above its glass transition. At these temperatures hinges relaxed and shrank, and thereby caused the planar sheet to fold irreversibly into a 3D object. The system was activated in air. A system foldable in water was reported by Javey *et al*.[81] and consisted of low density polyethylene (LDPE) sheets with second layer of poly(N-isopropylacrylamide)/single-walled carbon nanotubes composite hydrogel (PNIPAM/SWNT) in hinges. Irradiation with near-IR laser led to the folding of such structures as cube and flower due to the shrinking of the hydrogel induced by the local heat generated from near-IR absorption of SWNTs. Folding was completely reversed by switching of the irradiation. Gracias with co-workers demonstrated sequential folding of microstructures by directed heating of pre-stressed Cr/Au bilayer hinges with polymer trigger atop using low power lasers[82]. On heating above its T_g the polymer in hinges softened and no longer restrained the stressed bilayer, which resulted in spontaneous bending. Folding can be also induced with patterned light rather than patterned hinges[83].

Table 2.1 | Reported examples of stimuli/responsive self-folding polymer films (modified from Ref [84])

System	Stimulus	Folding conditions	Biodegradability	Reversibility	Ref.
Thermoresponsive					
Poly(ε-caprolactone)	T	Not given	Full	-	[70]
Polydimethylsiloxane/gold	T	60 - 70 °C	No	+	[20, 21]
SU-8 photoresist/polycaprolactone	T	60 °C	Partial	-	[6]
Photoresist/metals	T	40 °C	No	-	[36, 65]
Poly(N-isopropylacrylamide)/mixture of poly(methyl methacrylate) and diacrylated triblock copolymer of poly(ethylene glycol) and poly(lactic acid) (PLA-b-PEG-b-PLA)	T	Below 32 °C	Partial	+	[71]
Poly(NIPAm-co-BPAm-co-AAc-co-RhBMA)	T	22 °C	No	+	[54]
pH- and salt-responsive					
Poly(methacryloxyethyl trimethylammonium chloride)/gold	pH, salt	Not given	No	-	[72]
Poly(4-vinyl pyridine)/polystyrene	pH	pH = 2	No	+	[5, 66, 73]
Poly(N-isopropylacrylamide-co-acrylic acid)/polyethylene glycole	pH	pH = 2.5-7.5	No	+	[43]

Poly(2-hydroxyethyl methacrylate)/poly(methacrylic acid)	pH	pH=6.5	No	+	[63]
Poly(2-hydroxyethyl methacrylate-co-acrylic acid)/poly(2-hydroxyethyl methacrylate)	pH	pH=9	No	+	[64]
Poly(methacrylic acid)/poly-(ethyleneglycol dimethacrylate)	pH	No information	No	+	[69]
Gradient Poly(N-isopropylacrylamide-co-acrylic acid)	pH	pH = 3	No	+	[58]
Solvent responsive					
Poly-urethane/2-hydroxyethyl methacrylate/polydimethylsiloxane	Water	Immediate folding	No	-	[74]
Poly(PEGMA-co-PEGDMA/Chitosan	Water	Immediate folding	Partial	-	[69]
Polyvinyl alcohol/chitosan	Water	Immediate folding	Partial	-	[68]
Poly(glycol methacrylate)/gold	Methanol	Immediate folding	No	-	[72]
Poly(vinyl alcohol)-poly(acrylic acid)/metal	Water	Immediate folding	No	+	[75]
Electro responsive					
Polypyrrole/gold	Electric	1 V	No	+	[24, 25]
Polydimethylsiloxane/cardiomyocytes	Electric	10 V	Partial	+	[76, 77]
Chemical triggering					
Metals/photoresist	Acetic acid	> 60 %	No	One cycle	[59]
Metals-gelatine-carboxymethylcellulose	Enzyme		Partial	One cycle	[34]
Light responsive					
Liquid-crystal network containing azobenzene chromophore	Light	366 nm, air	No	+	[78]
Poly(N-isopropylacrylamide-co-2-carboxyisopropylacrylamide)/poly(N-isopropylacrylamide-co-N,N'-dimethylaminopropylacylamide), integrated o-nitrobenzaldehyde	Light	365 nm, water	No	+	[79]
Polystyrene/black ink	Light	air	No	-	[80]
Low density polyethylene/poly(N-isopropylacrylamide) loaded with single-walled carbon nanotubes	Light	Near-IR (785 nm), water	No	+	[81]
Metals/photoresist	Light	532 nm, air	No	-	[82]
Poly(pentaerythritol tetra(3-mercaptopropionate)-co-2-methylene-propane-1,3-di(thioethylvinylether)-co-ethylene glycol di(3-mercaptopropionate))	Light	365 nm, air	No	-	[83]

2.1.4 Conclusions

Stimuli-responsive self-folding polymer films are very promising for controlled encapsulation and release of drugs and cells, as well as for investigation of cell growth in confinement. In comparison to cells locked in crosslinked hydrogel matrix, cells entrapped inside self-folded objects are free to move, which is very attractive for tissue engineering.

Importantly, cells can tolerate relatively narrow range of environmental conditions, making it impossible to use most of reported self-folding systems for parallel loading. From this point of view such signals as immersion to aqueous media, change in pH or temperature are preferable for cell encapsulation. However, solvent-responsive folding is often immediate that lets less time for cells to adhere on the top of unfolded film and makes encapsulation inefficient. On the other hand, only few types of cells can tolerate large changes of pH, and as it is difficult to design self-folding system that undergoes transformation upon insignificant pH changes, this kind of triggering cannot be seen as a common solution. The use of temperature as a stimulus is more suitable, since cells readily withstand temperature variation.

Another limitation, especially relevant for tissue engineering applications, is the lack of biodegradability. To the best of our knowledge, no fully biodegradable system which is triggered to fold in physiological conditions has been reported by now. In future, these two limitations must become the main focus of the research in this field.

2.2 Methods of cell encapsulation

Cell encapsulation technology, which involves immobilization of cells within a semi-permeable polymer membrane or hydrogel matrix, is of great importance for a large number of biomedical applications. So for instance, encapsulation and subsequent cell culture can be used for exploratory purposes, such as cell visualization, single-cell bioassays, drug screening[85], cell viability studies within different microenvironments[86], and for investigation of intercellular interactions[87]. Cell encapsulation therapy, employed to treat diseases or to repair damaged tissue, provides possibility for cell transplantation without the need for immunosuppression. In this case, encapsulation prevents contact of transplanted cells with the host immune system, while permitting the transport of oxygen, nutrients, growth factors, waste, and therapeutic products[88, 89]. Besides that, cell-laden microgels can be used as modules for bottom-up tissue engineering, which will be discussed further (Chapter 2.3).

Generally, three strategies for cell encapsulation can be distinguished: using (i) capsules, (ii) microgels and (iii) foldable films. Here, two last approaches will be discussed, while information about the first one can be found elsewhere[89-92].

2.2.1 Microgels for cell encapsulation

Hydrogels are particularly attractive materials for fabrication of building blocks for bottom-up tissue engineering, because of their highly hydrated tissue-like environment for cell and tissue growth, biomimetic mechanical properties, cytocompatibility, porosity, as well as potential biodegradability[93, 94]. Microfabrication techniques allow control over the size and shape of produced microgels.

Encapsulation of cells within polymer matrix occurs during gelation process, which puts limitations on chemicals, formulations and conditions used for microgel synthesis. Release of cells can occur due to degradation of polymer. Cell-laden microgels can be produced through four distinct methods: conventional emulsion-templating, microfluidics, micromolding, or photolithography.

2.2.1.1 Emulsification

One of the most ease and widely used methods to fabricate microgels is based on emulsification. In this process, small aqueous droplets of the hydrogel precursors are generated in a continuous oil phase by stirring. Droplets are stabilizes with surfactants or particles and can be gelled using a variety of crosslinking mechanisms to obtain spherical microgels. This process can be used for a variety of materials including alginate, collagen and agarose. When added to the aqueous phase, cells can be trapped and encapsulated in hydrogel network of resultant microgels.

Although the size of the droplets can be controlled by such process parameters as degree of mechanical agitation, viscosity of each phase and the presence of surfactant, the method results in a high size distribution. Furthermore, emulsification provides little control over the shape of microgels as the droplets are typically spherical.

2.2.1.2 Microfluidics

Monodisperse emulsion droplets with controlled features can be produced using microfluidic devices[95]. Similarly to the first fabrication method microfluidic systems generate cell-laden microparticles by using multiphase systems with cells dispersed in aqueous phase. The transformation of the cell-laden droplets into microgels can be achieved by the photopolymerization or ionic gelation[96]. Sizes and shapes of resulting microgels can be controlled by proper design of microfluidic channels. For instance, by varying the flow rates and dimensions of the microchannels it is possible to fabricate spherical and rod-shaped hydrogels[97]. Moreover, microfluidic fabrication allows control over the morphology of resulting microgels: uniform, gradient[98], core-shell[99], Janus[100] structure can be fabricated.

2.2.1.3 Micromolding

Although microfluidic emulsification approaches are very efficient (approximately 1000 drops can be produced per second), drop-based techniques present several limitations. First, an immiscible oil phase must be used to generate water drops, which can reduce the viability of cells. Second, the microgel particle shape is limited to spherical or another shape with high isotropy.

Micromolding technique provides better possibility to generate microgels with controllable features. In this method, prefabricated poly(dimethyl siloxane) (PDMS) molds are covered with aqueous precursor solution to fill the hole-patterns of the template. Residual solution is then removed from the top of the mold and precursors, which remain in the holes, are gelled to generate structures of a variety of shapes and sizes[101, 102]. Resulting microgels can be than released. A variety of materials has been used to create micromold fabricated hydrogels, among them hyaluronic acid[101], chitosan[103], PEG[104], alginate and fibrine[105].

In addition to PDMS, other materials could also be used for micromolding. For instance, Tekin *et al*. developed thermo-responsive size-controllable PNIPAM mold to create microgels composed of multiple components[106]. Primarily an agarose solution containing first cell type was molded and crosslinked at the temperature below the LCST of PNIPAM template. The temperature was then elevated above LCST in order to shrink thermo-responsive mold and to form a gap between the microgel and template walls. As a second step, this gap was filled with an agarose solution containing another cell type. Resulting microgels had a 2D core-shell structure, where one cell type was spatially arranged around the second cell type in a defined microenvironment. Therefore this technique can be successfully used to prepare a cell co-culture within a microgel.

2.2.1.4 Photolithography

Much larger variety of microgel shapes can be achieved by using photolithography techniques. To encapsulate cells using this method thin films of pre-polymers in aqueous solution are polymerized by exposure to UV light through a photomask. Selective crosslinking occurs in the transparent regions of a mask, resulting in the microgels of corresponding shapes.

Compared to conventional photolithography where polymer films are typically deposited from organic solvents and dried prior to UV irradiation, aqueous solutions of pre-polymers have low polymer content and therefore low viscosity. To prevent flow of solutions during photopolymerisation, they can be confined within microchamber. Du *et al*. used this technique to prepare cell-laden microgels with various shapes[4]. The same authors reported fabrication of donut shape microgels consisting of two concentric regions[107]. These microgels were fabricated by sequential photocrosslinking through two overlaying masks and contained encapsulated endothelial cells in inner ring and smooth muscle cells in outer ring, mimicking the native vasculature.

Although photolithography enables fabrication of microgels with complex shapes, the production throughput is very low. Merging microfluidic techniques with photolithography provides possibility to produce microgels continuously, which significantly improves efficiency of the process. In this method that is called flow lithography, the hydrogel precursor solution containing cells flow in microfluidic channel past a light source. The exposure time is controlled by shutter, and the microgel shape – by the used mask. However, when exposure time is relatively long compared to the flow rate resulted microgels are elongated along the direction of flow. To prevent this stop-flow lithography was developed. In this process the flow is temporally stopped during UV exposure. Panda *et al*. used stop-flow lithography to fabricate uniform cell-laden polyethylene glycol microgels with square shapes were prepared by stop-flow lithography to produce cell-laden microgels[108].

Disadvantages of photolithography are necessity of photocrosslinkable materials and potential effects of UV irradiation on cell function.

2.2.2 Encapsulation using foldable thin films

Another approach for cell encapsulation employs self-folding thin films. General principles of design and fabrication of such structures were already discussed in Chapter 2.1. In this case, cells entrapment occurs when prefabricated foldable 2D film is immersed into a media with suspended cells and then triggered to transform into 3D hollow structure.

Self-folding microstructures can offer several advantages over the microgels when used for cell encapsulation. First, the encapsulation step is separated from the fabrication step, which permits to avoid exposure of the cells to toxic chemical precursors and UV illumination. Second, folding and unfolding can be reversibly controlled by external stimuli, enabling the triggered capture and release. Third, release occurs upon unfolding of the 3D structure, which does not involve degradation and allows the repeated use of self-folding film.

Obviously, parallel entrapment of the cells during film folding is only possible when folding conditions are close to physiological and can be tolerated by cells. As it was already discussed in a previous section, only few self-folding systems fulfil this requirement. Among them chromium/copper/polymer hinge-assisted sheets which were used to encapsulate fibroblasts during irreversible folding at the temperature of 40 °C[36, 65]. Enzyme-sensitive microgrippers consisted of metals, gelatine and carboxymethylcellulose were successfully used to perform biopsy of liver tissue from a model organ system in the presence of corresponding enzymes[34]. Poly(methyacrylic acid)/poly-(2-hydroxyethyl methacrylate) bilayers bent at pH 6.5, attaching to a tissue, and were proposed as a smart plaster to direct diffusion of the drugs and prevent their leakage[63]. Using PNIPAM-based bilayer system reported by Peeters *et al.*, it was possible to encapsulate cardiomyocytes at the temperature below 32 °C[71].

Zhang and Jiang *et al.* offered a strategy for fabrication of tubular structures mimicking blood vessels by utilizing spontaneous folding of stress induced rolling membrane[109]. Here, an elastic polydimethylsiloxane film was stretched to produce stress, permitting spontaneous rolling process to take place upon release of the ends of the film. Rolling could be performed at mild conditions: in the cell-culture medium at room temperature and without heating or etching. Different types of cells, deposited on the top of prestressed membrane, were entrapped during tube rolling and formed walls, composed of multilayers of endothelial cells, smooth muscle cells and fibroblasts. The folding process is, however, irreversible and spontaneous.

Most recently an elegant method of parallel cell encapsulation was reported by Takeuchi *et al.*[110] To drive the folding process, this technique, called cell origami, utilizes cell traction force that is generated by actomyosin interactions and actin polymerization, and pulls toward the centre of the cell body. First, cells were stretched and adhered across multiple parylene microplates. Upon detaching the microplates from a glass substrate cell traction force caused the plates to lift and fold according to a prescribed pattern. By changing the geometry of the patterned 2D plates various 3D cell-laden microstructures such as dodecahedron and cylindrical helical tube, could be fabricated. Cell origami seems to be highly biocompatible and simple approach as it does not require any special materials for the microplates and hinges to induce folding.

Not for all systems folding conditions allow parallel cell encapsulation. When conditions of 2D-3D transformation are harsh, several post-filling approaches could be used. For instance, Gracias *et al*. used tumbling method to load already folded 3D containers with cells[6]. Cells diffused inside non-porous containers through 5-10 µm hinge gaps from media with a high cell concentration. Similarly Huang and Mei *et al*. filled self-rolled SiO/SiO_2 microtubes with yeast cells[33]. Other strategies employed such type of devices as µ-syringe[9] or optical tweezers[17], which were used to bring cells, suspended in medium, inside the self-rolled inorganic tubes. Since such microstructures have optical transparent walls, they enable microscopic visualisation and in situ monitoring of encapsulated cells in 3D environments and can be used as 3D micro-Petri dishes. However, post-filling approaches do not use the advantages of self-folding films for cell encapsulation.

2.3 Bottom-up tissue engineering

The great challenge of regenerative medicine is recapitulation of natural tissue in all complexity, including microarchitecture, and multicellular composition. Realistic tissue models could help to investigate mechanisms of tissue morphogenesis, differentiation and maintenance and are of particular interest for tissue engineering. Three-dimensional polymer scaffolds aim to support cells in their growth and differentiation. Most of the developed approaches of scaffold fabrication can be classified either as bottom-up or top-down ones.

In traditional top-down approach biodegradable polymer scaffold is first fabricated. It is expected that cells, which are then seeded on it, populate the scaffold and create the appropriate microarchitecture and extracellular matrix. This strategy often results in inhomogeneous cells distribution inside the scaffold, caused by their slow migration. Moreover, top-down approaches often have difficulty to recreate the complex microstructural features of tissues.

Many natural tissues are made up of the assemblies of small and repeating functional units, such as bundles of myofibers in muscles, lobules in liver, islets in pancreas, and nephrons in kidney. In this respect bottom-up or modular strategy is very perspective for scaffold fabrication. This approach proposes to build tissues by assembling of microscale building blocks mimicking those units. Microfabrication techniques, used for production of such building blocks allow control over microenvironment of individual cells, structure of clusters of cells as well as the interactions between multiple cell clusters.

2.3.1 Assembly of cell-laden microgels

One of the major challenges of the modular approach is to assemble fabricated units into macroscale engineered tissues. The main difficulty of such process is to retain the microarchitecture as well as cellular behaviour of engineered tissue, while creating a construct with robust mechanical properties. In this chapter, general techniques used to assemble cell-laden microgels will be discussed, leaving aside such methods of bottom-up scaffold fabrication as tissue printing and cell sheet technology. A key aspect that must be considered for microgel assembly is the type of forces that are used to drive the assembly process. The bottom-up assembly of microgel building blocks was achieved using manual manipulation[101], random assembly[111], microfluidic-directed assembly[112, 113], hydrophobic-hydrophilic interactions[3, 4, 107, 114-117] and molecular recognition[118, 119]. Obtained constructs often require stabilization by secondary cross-linking step.

2.3.1.1 Random assembly

Sefton and colleagues introduced an approach to modular scaffold formation in 2006[111]. Sub-millimetre sized collagen rods seeded with HepG2 hepatocytes were produced by cutting a tubular gel and then coated with endothelial cells. The modules then were randomly assembled in larger tube to form construct with interconnected channels through which blood or medium could be perfused. Random assembly of microgel modules is rapid and simple, but lacks the control over the final structure of the hydrogel aggregate. To assemble these microgels, manual manipulations may be used[101], which is however relatively slow and non-scalable for fabrication of large tissues.

2.3.1.2 Assembly in microfluidic

Microfluidic devises can be used to fabricate highly sophisticated microgel assembly architectures. Chung and Park *et al*. assembled hydrogel building blocks in a railed microfluidic device to achieve constructs with precise organization of cells[112]. Two sorts of hydrogel blocks containing HeLa and HEK293 cells moved along the grooved microchannels to create 2D self-assembled matrix micropatterned of two different cell types.

Three-dimensional assembly of hydrogels using microfluidic platform was reported by Whitesides *et al*.[113] Cylindrical-shaped collagen modules containing fibroblast cells and HepG2 cells were assembled in a microchannel. The ratio of the dimensions of the channels to the dimensions of the modules determined the extent of ordering in the packing arrangement. When the channels were much wider than the modules, random packing occurred. In channels approximately twice the width of the modules, the soft modules became noticeably more organized. Channels with widths comparable to the dimensions of the modules resulted in the greatest degree of organization.

Disadvantages of the microfluidic method are long operational times and complex equipment.

2.3.1.3 Directed assembly on the interfaces

Khademhosseini and co-workers have intensively investigated the assembly of cell-laden microgels by manipulating the hydrophilicity of surfaces and interfaces. Their approach exploits the tendency of hydrophilic and hydrophobic substances to minimize the interaction with each other.

In one case, cell-laden microgels of different shapes (i.e., square, lock-and-key shape) were assembled at oil-water interface[4]. Upon manual mechanical agitation microscale hydrogels in a bulk oil phase are driven together to minimize unfavorable surface interactions, which is similar to formation of water droplets in oil. Control over assembly process could be achieved by variation of microgel shapes. It was possible to create ‘‘lock-and-key’’ assemblies, where the shape of different microgels was matched to create mesoscale hydrogels with controlled microarchitectures. Furthermore, a mathematical model of microgel assembly in oil-like media was developed[114].

Assembly of microfabricated poly(ethylene glycol) microgel rings into tubular structures was performed in mineral oil by swiping a needle underneath them[107]. By stacking concentric microgel arrays containing endothelial cell-laden inner ring and smooth muscle cell-laden outer ring blood vessel-like structures were obtained.

In another case, cell-laden microgels of various shapes were assembled at an air-liquid interface while floating on the solvent perfluorodecalin[3]. Individual building blocks of hydrophilic hydrogels were induced to aggregate due to forces present at the air-liquid interface. This technique permitted to create tightly packed tissue-like sheets in a centimeter scale with either single cell types or homogeneously distributed co-culture.

The abovementioned strategies require the use of mineral oil or other hydrophobic organic solvents, which limit its application for sensitive cells. To overcome this problem Khademhosseini *et al*. developed an approach of directed assembly of cell-laden microgels in PBS buffer[115]. For that, glass slide substrate was patterned with hydrophobic and hydrophilic regions and PBS dispersion of microgels was deposited on it. After excess solution was poured off, the buffer remained in the hydrophilic regions of the slide, trapping microgels in the remaining liquid. Driven by surface tension, the microgels tended to assemble into sheets within the aqueous droplets.

However, the approaches described above are inherently 2D and therefore it is difficult to use them to create 3D mesoscale tissue-like constructs.

To address this limitation, a micro-masonry assembly process has been developed[116]. By using two interfaces, oil-water and a wetting substrate, assembled microgels could be wrapped around a substrate to generate 3D structures. Individual building blocks of HepG2 cell-laden hydrogels suspended in a solution of PEG-methacrylate with photoinitiator were placed on PDMS surface with cylindrical-shapes. When excess of pre-polymer solution was removed, capillary forces brought the microgels together around the template. After secondary photopolymerization, which was used to bind the building blocks together, PDMS template was removed to generate hollow tube-like structures.

Alternatively 3D constructs can be obtained by stacking pre-fabricated microgel self-assembled sheets[117]. For example, hexagonal microgels, produced by photopolymerization of PEG or the calcium-induced gelation of alginate, were assembled in two-dimensional arrays on a glass substrate by removing the excess pre-polymer solution around the microgels. The resulting clusters were crosslinked and stacked on one another to fabricate thick 3D constructs that were greater than 1 cm in width and 3 mm in thickness. Additionally, pores were generated by chelating calcium to dissolve the integrated alginate microgels.

2.3.1.4 Molecular interactions

Recently, Harada *et al*. demonstrated self-assembly of millimeter sized gels due to molecular recognition of the cyclodextrins (host) and hydrocarbon (guest) groups, immobilized on the gels' surfaces[118]. By changing the size and shape of the host and guest units, different gels could be selectively assembled and sorted into distinct macroscopic structures that were on the order of millimeters to centimeters in size.

Elbert *et al*. fabricated macroporous scaffolds by assembly and chemical reaction of hydrogel microspheres[119]. Microspheres with different functions (structural, drug delivery and porogenic) were synthesized from reactive poly(ethylene glycol) derivatives and proteins and possessed reactive groups, which allowed crosslinking upon mixing and centrifugation and resulted in a scaffold formation. The crosslinking was mild enough to be performed in the presence of living cells. Pores were produced by the dissolution of porogenic microspheres.

2.3.2 Conclusions

Discussed examples of bottom-up approach for scaffold fabrication demonstrate the potential utility of this technique to create complex tissue-like structures with possibility to recreate microarchitecture and multicellular composition. However, some potential disadvantages of this process have to be taken into account. One of them is difficulty to create structures that are tens of centimetres in length. Such structures will require strong secondary crosslinking to ensure stable bonding between microgels, and, if free standing, will require building blocks with mechanical properties sufficient to support the weight of the structure.

3 Experimental part

3.1 Characterization techniques

In the present work, a combination of several analytical techniques was used to obtain information about each step of the experiment. Characterisation of the polymer films in unfolded state was performed using ellipsometry and AFM. The process of bilayer folding, basic characteristics of self-rolled tubes as well as the possibility to encapsulate particles and cells were then investigated using different microscopic techniques. The most used methods are described in this chapter.

3.1.1 Null ellipsometry

The thickness of dry and swollen polymer layers was determined using null ellipsometry. **Basics.** Ellipsometry is a non-destructive optical technique that uses the change in the state of light polarization upon reflection from the sample to characterize thin films, interfaces and surfaces[120]. The method allows defining film thickness for single or multilayers in the range from several angstroms to few micrometers.

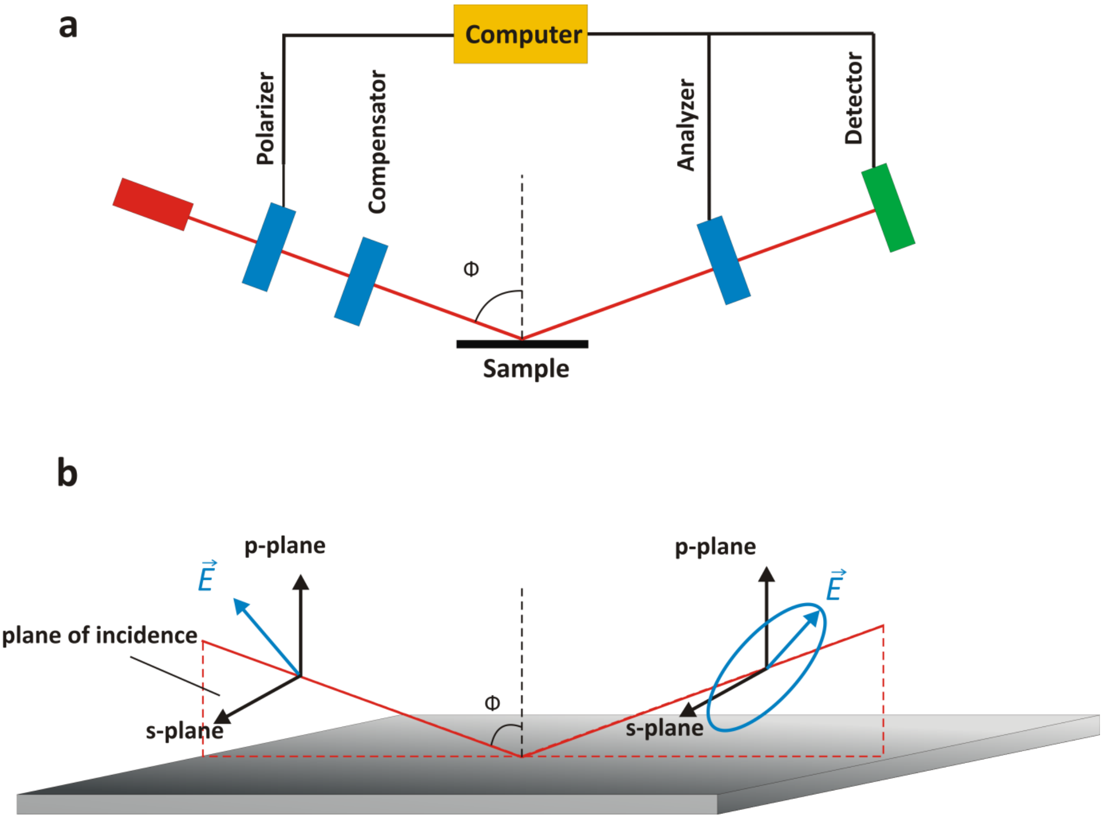

Figure 3.1 | (a) Simplified principle of null ellipsometry; (b) scheme of an ellipsometric experiment.

The primary setup elements for collecting ellipsometry data are: light source (often monochromatic, such as laser), polarization generator, sample, polarization analyzer, and detector (Figure 3.1a). Generally, in ellipsometric measurements, monochromatic light with a known state of polarization is incident on a sample surface. The reflected light differs in its state of polarization and these changes are measured and analyzed. The Figure 3.1b represents the typical scheme where the incident light is linearly polarized and reflected light is elliptically polarized. Mathematically the state of polarization is determined by the superposition of the orthogonal components of the electric field vector of two linearly polarized light waves. The coordinate system used is p-s coordinate system, where p-direction is parallel to the plane of incidence and s-direction is perpendicular to it.

In experiment, the position of polarizer and analyzer at minimum and maximum intensity gives the amplitude parameter – relative amplitude ratio tanψ and the phase parameter – relative phase shift Δ. The relation of these parameters to the Fresnel reflection coefficients R_p and R_s for p- and s- polarized light is described by the fundamental equation of ellipsometry:

$$\rho = \frac{R_p}{R_s} = \frac{E_{rp}/E_{ip}}{E_{rs}/E_{is}} = \tan(\psi)e^{i\Delta} = F(\Phi_0, \lambda, N_S, n_0, n_t, k_t, d_t) \quad , \qquad (3.1)$$

where E_{ip}, E_{is} and E_{rp}, E_{rs} are electric-field components (p- and s- polarized) for incident and reflected light respectively. The amplitude and the phase parameters are complex functions of the angle of incidence Φ_0, the wavelength λ, the optical constants of the substrate (N_s), the ambient medium (n_0), the layers (n_t, k_t), and the layer thicknesses (d_t).

Ellipsometry is an indirect method, meaning that measured Δ and ψ cannot directly provide information about the thickness and the optical constants of the sample. The unknown parameters in the optical model are varied to find the best fit to the experimental data. The layer model considers the optical constants (refractive index or dielectric function tensor) and thickness parameters of all individual layers of the sample including the correct layer sequence. For proper analysis the sample must consist of a small number of discrete and well-defined layers, which are optically homogeneous and isotropic.

Experiment. Ellipsometric measurements were carried out with a null-ellipsometer (Multiscope, Optrel GbR, Berlin, Germany) equipped with He/Ne laser as a monochromatic light source (λ = 632.8 nm). The ellipsometric parameters were fitted using the *Elli* program developed by Optrel GbR.

Thickness calculations were performed using layer modeling with following optical constants: silicon substrate, n(Si) = 3.858 - i0.018[121]; silicon oxide, n(SiO_2) = 1.4598[121]; (3-aminopropyl)triethoxysilane, n(APS) = 1.422[122]; poly(N-isopropylacrylamide), n(PNIPAM) = 1.496; polymethylmethacrylate, n(PMMA) = 1.489[123]; polysuccinimide n(PSI) = 1.50; polycaprolactone, n(PCL) = 1.476; gelatin, n (Gelatin) = 1.54[124]; water, n(H_2O) = 1.3329; phosphate buffered saline, n(PBS) = 1.3347; air, n(air) = 1.

The thickness of layers in a dry state was measured at RT and 40 - 50 % relative humidity with angle of incidence fixed at 70°. Measurements were performed after each step of wafer modification and polymer deposition. Obtained results were used for the further ellipsometric simulation (modeling).

Thickness of SiO_2 layer was typically in the range of 1.5 ± 0.2 nm, thickness of APS layer was 0.9 ± 0.2 nm. Thickness of the polymer bilayer films was calculated using a four-layer model (silicon/silicon oxide/polymer-1/polymer-2/air as an ambient). Thickness of thick or inhomogeneous (rough) films was confirmed by AFM scratch test (Chapter 3.1.4).

In situ ellipsometric measurements were carried out to investigate the swelling behaviour of polymer hydrogels in aqueous solutions at different temperatures. Typically, the films with a dry layer thickness around 20 - 40 nm were used to define swelling degree of the polymer. Polymer under investigation was deposited on APS modified Si-wafer and crosslinked using UV illumination. Uncrosslinked polymer was removed by submerging in a corresponding solvent for several minutes. After drying the sample was measured first in a dry and next in a swollen state.

Temperature-dependent measurements were performed using home-made heating table based on Peltier element with possibility to regulate temperature using control device.

After measurement in a dry state, sample was put into a cuvette and fixed with a home-made holder. The incident angle was changed to 68° to achieve perpendicular irradiation of the side windows of the cuvette. After the dry film thickness was again measured, the cell was filled with 4 ml of water or phosphate buffered saline.

The swelling of PNIPAM and PNIPAM-co-polymer thin films at RT was usually so fast (maximum swelling degree was achieved within less than one minute after exposure to solvent), that kinetics was not detectable, and only maximal thickness of polymer film in a swollen state was measured. After changing the temperature or solvent the sample equilibrated for approximately 10 min before the next measurement.

For gelatin and polysuccinimide thin films swelling kinetics was measured at different temperatures for several hours. The plateau value was taken to calculate swelling degree.

The thickness of the polymer in a swollen state was calculated using a four-layer model (silicon/silicon oxide/APS/polymer hydrogel/water or PBS buffer as an ambient. Refractive index for swollen polymer film was calculated by the program within the range: n(ambient) as a lower limit and n(dry polymer) as an upper limit, and was typically around 1.37.

A polymer layer bound to a substrate swells in 5 directions but for layers with relation of height/width/length larger than 1/10/10 the swelling ratio can be determined approximately by the change of the height only [125]. Therefore, swelling degree (SD) of hydrogels was calculated as a ratio of the maximal thickness of the swollen polymer film (d_{max})to the thickness of dry polymer (d_{dry}):

$$SD = \frac{d_{\max}}{d_{dry}} \qquad (3.2)$$

3.1.2 Optical microscopy

Basics. Optical microscopes are instruments which produce magnified visual or photographic images of objects invisible to the naked eye, using the principles of transmission, absorption, diffraction, and reflection of light waves. Production of informative image depends on the magnification of the object, its contrast with respect to its internal or external surroundings, and the ability of the microscope to resolve structural details[126-128].

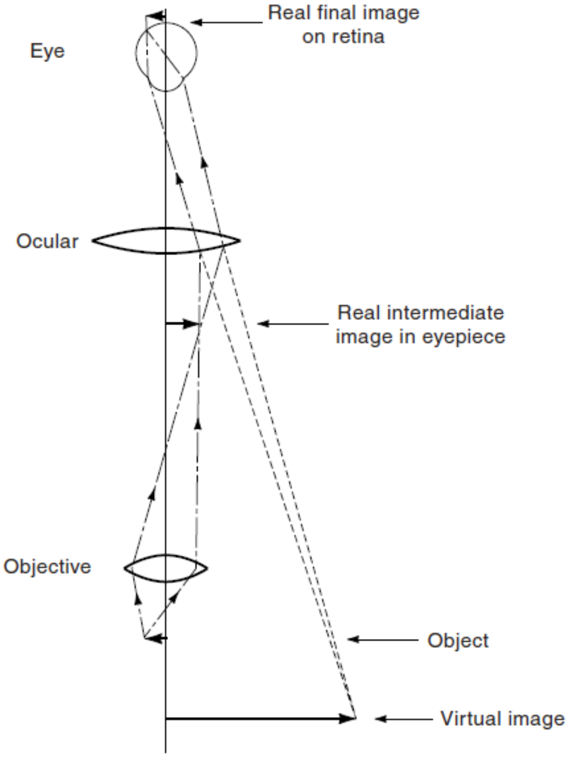
Eye
Real final image on retina
Ocular
Real intermediate image in eyepiece
Objective
Object
Virtual image

Figure 3.2 | Perception of a magnified virtual image in the microscope (from Ref.[127]).

The microscope optical pathway typically consists of illuminator (light source and collector lens), condenser, specimen, objective, eyepiece, and detector, which is either observer’s eye or camera. The visible diapason of wavelength is used in optical microscope to illuminate the sample. A most common light source is the tungsten halogen lamp which emits a continuous spectrum of light centered at 3200 K. The condenser lens focuses light from the illuminator onto a small area of the specimen.

Modern compound microscope combines two lens systems to obtain magnified image: the objective and the eyepiece. The objective, which is typically composed of several lens elements, collects light transmitted through or reflected from the specimen and forms a magnified real image at the real intermediate image plane near the eyepieces. The intermediate image is further magnified by the eyepiece to produce a secondary enlarged virtual image of the specimen, which is observed by microscopist (Figure 3.2). The total magnification of a microscope is determined by multiplying the individual magnifications of the objective and eyepiece.

Experiment. In the present work, most of the samples under investigation were prepared on a silicon substrate, which made usage of trans-illumination impossible, therefore reflected microscopy was used to observe self-rolled tubes formation and for definition of tubes diameter. The minority of the samples, prepared on a glass substrate was characterized using trans-illumination microscopy.

Two different microscopic techniques have been used depending on the sample characteristics and goal of observation: bright-field microscopy and dark-field microscopy.

In ***bright-field microscopy***, contrast results from absorbance of illuminating light in dense areas of the specimen. The background is bright, and absorbing structures within the specimen appears darker. Thus, bright field microscopy is ideal for objects with high natural absorption.

To introduce contrast into transparent colorless samples, ***dark-field illumination*** can be used. Dark-field microscopy is a specialized technique that uses oblique illumination to enhance contrast in specimens that are not imaged well under normal bright-field illumination conditions. After direct light has been blocked by an opaque stop in the condenser, light reaches the specimen from oblique angles that cannot be accepted by the objective’s aperture. As a result, only highly diffracting or scattering structures can be observed forming a bright image on a dark background. Dark field illumination technique is especially good to reveal outlines, edge, and boundaries of objects.

For light microscopy imaging a Zeiss Axio microscope equipped with Zeiss air objectives: Epiplan 5x/0.13 HD, Epiplan 10x/0.20 HD, LD EC Epiplan-NEOFLUAR 20x/0.22 HD DIC, LD EC Epiplan-NEOFLUAR 50x/0.55 HD DIC and LD EC Epiplan-NEOFLUAR 100x/0.75 HD DIC and digital color camera with CCD chip was used. The obtained image stacks were processed and analyzed using free *Fiji* software. To perform microscopic observation at different temperatres, sampes were placed on the home-made thermo-stage based on Peltier element, which allows very fast change of the temperature within several seconds.

3.1.3 Confocal microscopy

Basics. Modern confocal microscopes can be considered as completely integrated electronic systems where the optical microscope plays a central role in a configuration that consists of one or more electronic detectors, a computer, and several laser systems combined with wavelength selection devices and a beam scanning assembly[129-131].

Confocal fluorescence microscopy offers several advantages over conventional optical microscopy, including controllable depth of field and the elimination of image degrading out-of-focus information.

In conventional wide field light microscopy, the entire field of view of a specimen is simultaneously illuminated and fluorescence emission is excited throughout the whole depth of the specimen, rather than just in a focal plane. Therefore, image-forming light comes not only from the selected focal plane, but also from bellow and from above it. This out-of-focus blur degrades final image by reducing contrast and sharpness and is especially problematic for specimens having a thickness greater than 2 µm.

In contrast, in the confocal approach one or more focused beams of light, usually from a laser, are scanned across the specimen. A confocal imaging aperture in the optical system prevents the light, emanating from regions above and below the focal plane, from contributing to the final image, which thus contains only in-focus information. The images produced by scanning the sample in this way are called optical sections. The 3D reconstructions of transparent objects can be generated by collecting serial optical sections from thick specimens.

The confocal principle in epi-fluorescence laser scanning microscopy is schematically presented in Figure 3.3. Coherent light emitted by the laser system passes through a pinhole aperture that is situated in a conjugate plane (confocal) with a scanning point on the specimen and a second pinhole aperture positioned in front of the detector (a photomultiplier tube). As the laser is reflected by a dichromatic mirror and scanned across the specimen in a defined focal plane, secondary fluorescence emitted from points on the specimen (in the same focal plane) pass back through the dichromatic mirror and are focused as a confocal point at the detector pinhole aperture.

The significant amount of fluorescence emission that occurs at points above and below the objective focal plane is not confocal with the pinhole and forms extended Airy disks in the aperture plane. Because only a small fraction of the out-of-focus fluorescence emission is delivered through the pinhole aperture, most of this extraneous light is not detected by the photomultiplier and does not contribute to the resulting image. Refocusing the objective in a confocal microscope shifts the excitation and emission points on a specimen to a new plane that becomes confocal with the pinhole apertures of the light source and detector.

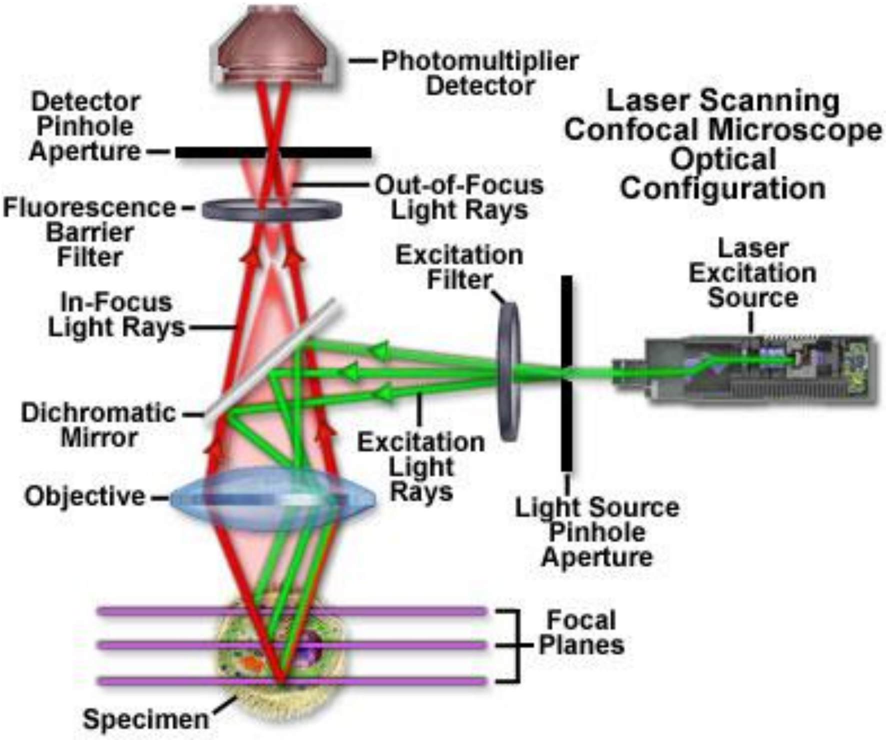
Photomultiplier Detector
Laser Scanning Confocal Microscope Optical Configuration
Detector Pinhole Aperture
Out-of-Focus Light Rays
Fluorescence Barrier Filter
Excitation Filter
Laser Excitation Source
In-Focus Light Rays
Dichromatic Mirror
Excitation Light Rays
Objective
Light Source Pinhole Aperture
Focal Planes
Specimen

Figure 3.3 | Principle of confocal microscopy (from Ref.[132]).

Experiment. In the present work, a Zeiss LSM 780 NLO microscope equipped with Zeiss Plane-Apochromat 20x/0.8 air objective was used for confocal imaging. As a fluorophores quantum dots (QDs, Chapter 3.2.3) were used, which allowed us to minimize bleed-through of fluorescence emission, exhibited by many of the common fluorophores.

Samples for imaging were prepared in a following way: assembled self-rolled tubes were pulled out of the aqueous solution and fixed on a microscope slide using small pieces of a double-sided tape. A cover slip was fixed above the sample in a distance of several mm, forming a kind of cell, which was filled with DI water just before imaging.

Samples were exited at 405 nm and imaged using GaAsP spectral detector with 32 channels (detector range was set to 400 - 700 nm) in a Lambda-mode. Spectral unmixing has been done using Zen 2010 B Software. The obtained image stacks were processed and analyzed using free *Fiji* and *Zeiss* software. Pseudocolors were chosen in respect to the maximum of fluorescence for correspondent QDs, i.e. tubes contained green fluorescent QDs were colored in green.

3.1.4 Atomic force microscopy

Basics. The atomic force microscopy (AFM) is a high resolution imaging technique, in which sharp tip scans the sample surface[133]. The tip is typically less than 5 µm tall and often less than 10 nm in diameter at the apex and located at the free end of the cantilever. Interaction between the atoms of the tip and the sample, which appear due to different forces, such as Van der Waals, capillary, electrostatic forces etc., results in the cantilever bending, or deflection. A detector measures the changes in the cantilever position as the tip is scanned over the sample. Most atomic force microscopes use optical techniques for detection, in which laser beam is reflected from the back of the cantilever onto a position-sensitive photo-detector (PSPD). The laser beam changes its position on the detector, as the canteliver deflects. Hook's law of elasticity ($F = -kz$) describes the dependency of force F, stiffness of the cantilever k and the bending of the cantilever z. The output of the detector is processed by a computer giving a topography of the sample surface or other sample features. This basic scheme of AFM experiment is depicted in Figure 3.4a.

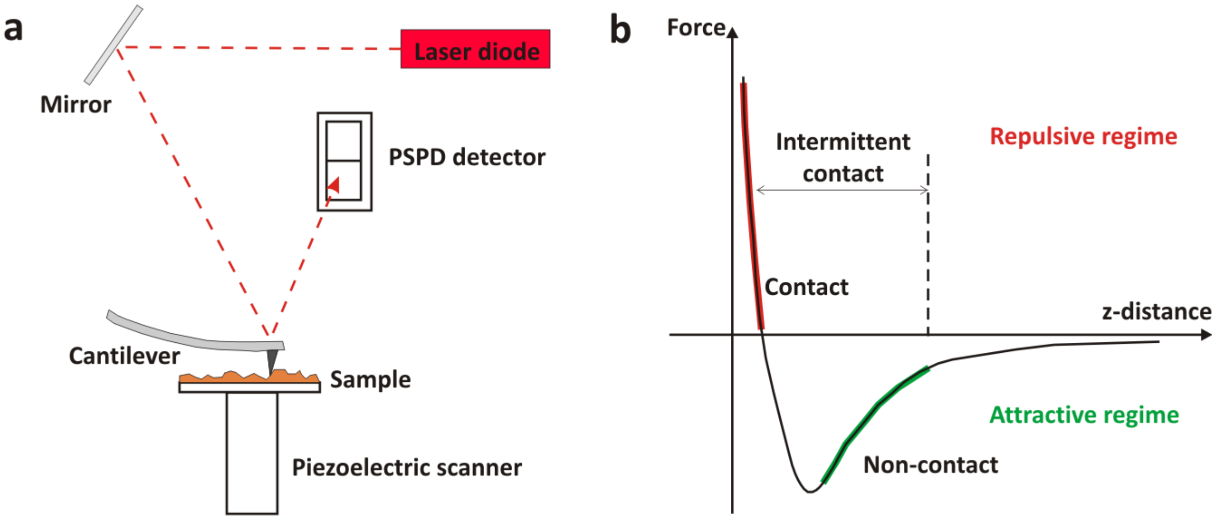

Figure 3.4 | (a) The basic scheme of optical detection in AFM; (b) typical force-distance curve with indicated repulsive (red) and attractive (green) forces, z-distance corresponds to tip-to-sample separation.

To a large extent, the distance regime (Figure 3.4b) determines the type of force that will be sensed. AFM can be operated using different modes, which are primarily defined in terms of the type of force being detected and how it is measured. All experiments in the present work have been done in a **tapping-mode**, in which tip intermittently touches the surface during vertical oscillation of the cantilever. The cantilever's oscillation amplitude changes with sample surface topography, as cantilever comes closer (farther) to the surface. The z-position of the cantilever is controlled by an electronic servo to keep oscillation amplitude constant. The measurements are displayed as a topografic image of the sample surface.

Experiment. In the present work atomic force microscopy in a tapping mode operated in air was used to control surface morphology of the polymer films as well as to determine the thickness of the layers thicker than 300 nm by using scratch test (Figure 3.5). For all AFM measurements DI Scanning Probe Microscope Nanoscope III, Dimension 3100 (Veeco, USA) equipped with silicon cantilevers with radius of 10 - 20 nm, spring constant of 30 N/m and resonance frequency of 250 - 300 kHz was used.

The root mean square (RMS) roughness σ_{RMS} was evaluated with the help of the free WSxM software[134] according to the equation:

$$\sigma_{RMS} = \sqrt{\frac{\sum_{i=1}^{N}(Z_i - Z_{ave})^2}{N}}, \qquad (3.3)$$

where Z_i is the current height value, Z_{ave} is the average height value, and N is the number of points within a given sample area. The roughness characteristics were typically obtained from 100 x 100 µm^2 sized images.

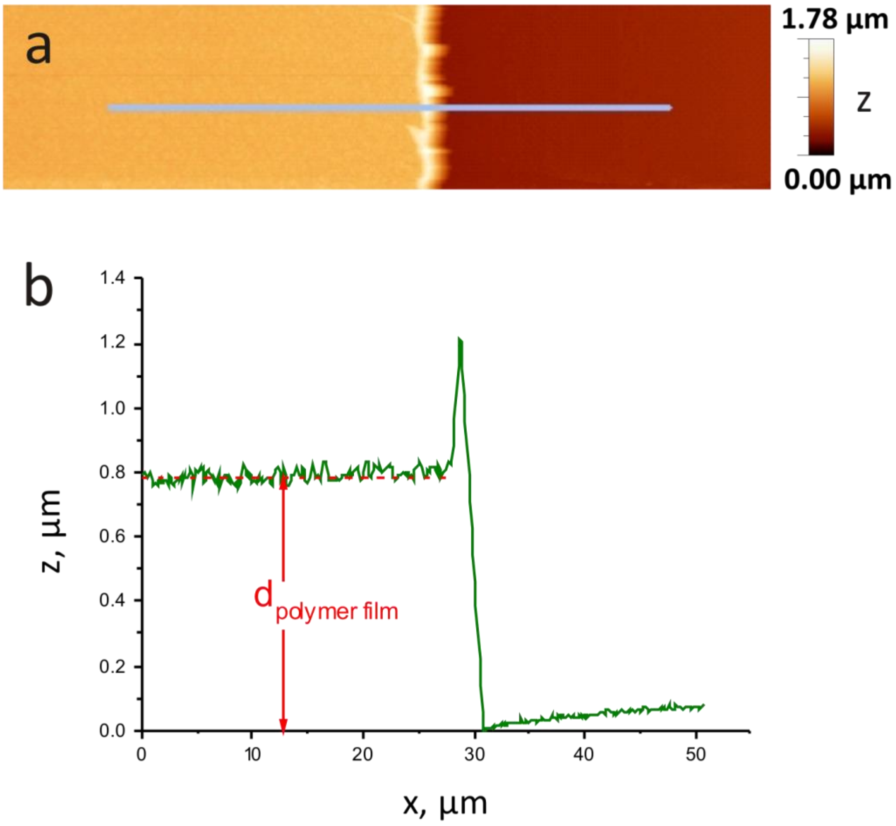

Figure 3.5 | Illustration of scratch test experiment: (a) AFM image of polymer film scratched with a blade, (b) cross-section profile corresponding to the blue line on the AFM scan shows the difference in height between polymer film surface and the substrate, allowing determination of the polymer layer thickness, $d_{polymer\ film}$.

3.1.5 Other methods

Scanning electron microscopy.

The scanning electron microscopy was performed with a Zeiss NEON 40 microscope by an acceleration voltage of 3 kV using secondary electron (SE) and InLens detection modes. Before SEM imaging all samples were coated with 3 nm platinum layer using low vacuum sputter coater.

^{1}H-NMR spectra were recorded on a Bruker DRX-500 spectrometer operating at 500.13 MHz for ^{1}H using $CDCl_3$ as a solvent. The spectra were referenced on the solvent peak ($\delta(^1H) = 7.26$ ppm).

Gel Permission Chromatography (GPC) measurements were carried out on Agilent 1100 Series (Agilent) normal-temperature size exclusion chromatograph, equipped with refractive index detector and one column PL Gel MIXED-B (Polymer Laboratories, U.K.) using chloroform or dimethylacetamide as an eluent and flow rate of 1 ml/min. Calibration was based on polystyrene standards obtained from Polymer Standards Service (PSS, Germany).

Drop shape analysis technique (DSA)

Contact angle (CA) measurements were performed by the sessile drop method using a Krüss DSA 10 drop shape analyzer (Germany). The advancing contact angle was measured by supplying deionized water into the drop at constant velocity. When the pump is reversed, the drop volume started to decrease linearly and the receding contact angle was measured. All investigations were carried out at 24 ± 0.5 °C and relative humidity of 40 ± 3 %.

3.2 Materials

3.2.1 Solvents and solutions

Deionized (DI) water was obtained using TKA ultra-purification system (Germany), conductivity 0.055 µS/cm. *Phosphate-buffered saline (PBS)* biotechnology grade with ionic strength 0.15 M (0.138 M NaCl, 0.0027 M KCl), pH 7.4 was prepared by dissolving crystal PBS buffer (Sigma) in 1000 ml of deionized water. Dulbecco's Modified Eagle's Medium with 15 mM HEPES and sodium bicarbonate, without L-glutamine, liquid, sterile-filtered, suitable for cell culture (Sigma) and Alpha Medium with 2 g/l $NaHCO_3$, without L-Glutamate, without nucleosides (Biochrom) were used with addition of Penicillin-Streptomycin solution to the concentration 100 U/ml of penicillin and 100 µg/ml of streptomycin. Following chemicals were used as received: *ethanol* absolute (VWR); *toluene* ACS grade (Acros organics); *chloroform* ACS grade, stabilized with amylene (Acros organics); *dichloromethane* ACS grade, stabilized with amylene (Acros organics) – was used for photolithography development; *dichloromethane* p.a., stabilized with amylene (Sigma) – was used for synthesis; *diethyl ether* ACS grade (Merck); *n-Hexane* ACS grade (Merck); *N,N-Dimethylformamide* p.a. (DMF, Sigma) – was used for synthesis; *N,N-Dimethylformamide* ACS grade (Sigma) – was used for preparation of polymer solutions; a*mmonia solution* 28 - 30 wt.% (Acros organics); *hydrogen peroxide* 30 % (Merck); *phosphoric acid* 85 % ACS grade (Sigma-Aldrich); *hydrochloric acid* 37 % ACS grade (Merck).

3.2.2 Polymers

Polycaprolactone (PCL, Aldrich) M_n = 70 000 - 90 000 g/mol, g*elatin* from porcine skin, gel strength 300 g Bloom, Type A (Sigma) were used as received.

3.2.3 Other materials

2,2'-Azobis(2-methylpropionitrile) 98 % (AIBN, Fluka) was recrystallized from ethanol; *N-Isopropylacrylamide* 97 % (NIPAM, Aldrich) was recrystallized from hexane; *acrylic acid* (AA, Aldrich), *methyl methacrylate* 99 % (MMA, Alrich), *2-(dimethylamino)ethyl methacrylate* (DMAEMA, Aldrich) were purified by filtration through basic or neutral Al_2O_3 column before polymerization.

Aluminum oxide activated, basic, Brockmann I (Al_2O_3, Sigma-Aldrich), *aluminum oxide* activated, neutral, Brockmann I (Al_2O_3, Sigma-Aldrich), sand (Sigma-Aldrich), *sodium sulfate* ACS grade, ≥ 99.0 %, anhydrous (Sigma-Aldrich), *(3-aminopropyl)triethoxysilane* 98 % (APS, Aldrich), *4-hydroxybenzophenone* (BPhOH, Fluka), benzophenone (BPh, Aldrich), *4,4'-Diazido-2,2'-stilbenedisulfonic acid disodium salt tetrahydrate* (DAz, Fluka), *acryloyl chloride* (Fluka), *N,N-diisopropylethylamine* (Aldrich), *N,N,N′,N′′,N′′-pentamethyldiethylenetriamine* (PMDTA, Aldrich), *2-bromoisobutyrate* (EBiB, Aldrich), *copper (II) bromide* ($CuBr_2$, Aldrich), *L-Aspartic acid* (Aldrich); *Penicillin-Streptomycin* (Pen/Strep) solution, containing 10 000 units penicillin and 10 mg streptomycin/mL, sterile-filtered, BioReagent, suitable for cell culture (Sigma-Aldrich)were used as received.

Glass Particles (Duke Standards 9000 Series) 10 µm ± 1 µm were purchased from Thermo Scientific.

The toluene soluble *quantum dots* (QDs) were kindly provided by Christian Waurisch, Stephen G. Hickey and Alexander Eychmüller, TU Dresden (Figure 3.6). Green emitting $CdSe/Cd_{1-x}Zn_xSe_{1-y}S_y/ZnS$ QDs (QD-266) with a maximum of fluorescence at 540 nm were synthesized following a procedure of Bae *et al.*[135] Red emitting CdSe QDs (QD-275) with a maximum of fluorescence at 605 nm were synthesized following a modified procedure of Qu *et al.*[136]

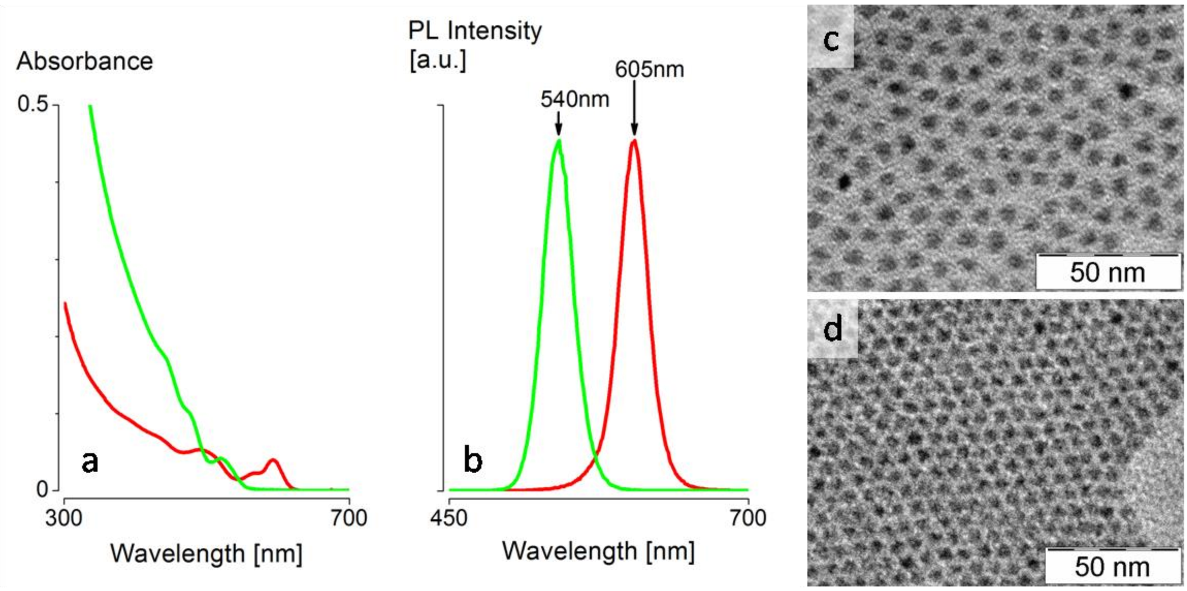

Figure 3.6 | Quantum dots: (a) absorbance and (b) fluorescence spectra of QD-275 (in red) and QD-266 (in green); TEM images of (c) red emitting quantum dots QD-275 and (d) green emitting quantum dots QD-266. Images are kindly provided by Christian Waurisch and Stephen G. Hickey and Alexander Eychmüller, TU Dresden.

3.2.4 Synthesis

Synthesis of 4-acryloylbenzophenone (BA). 4-Hydroxybenzophenone (20 g, 0.1009 mol), N,N-diisopropylethylamine (19.3 ml, 0.1110 mol) and 80 ml of methylene chloride were added into 200 ml three-necked round-bottom flask fitted with an overhead stirrer, a thermometer, and an addition funnel with acryloyl chloride (9.02 ml, 0.1110 mol) solution in 20 ml of methylene chloride. The acryloyl chloride solution was added dropwise into the flask under cooling (0 - 5 °C) for ca. 3 hours. The methylene chloride was removed by rotary evaporation. The residue was washed with 80 ml of

20 % HCl, 80 ml of saturated solution of sodium hydrocarbonate and dried over sodium sulfate. The solution was passed through a silica gel column with chloroform as the eluent. Chloroform was removed by a rotary evaporator. Finally, 24.44 g (95 %) of ABP was obtained. 1H NMR ($CDCl_3$, 500 MHz): 6.05 (dd, J1 ¼ 10.40, J2 ¼ 1.26, 1H), 6.34 (dd, J1 ¼ 10.40, J3 ¼ 17.34, 1H), 6.64 (dd, J3 ¼ 17.34, J2 ¼ 1.26, 1H), 7.27 (m, 2H), 7.49 (m, 2H), 7.59 (m, 1H), 7.80 (m, 2H), 7.86 (m, 2H).

Synthesis of poly(N-isopropylacrylamide-co-benzophenoneacylate), p(NIPAM-BA(1 mol. %)). BA (0.02253 g, 0.089 mmol), NIPAM (1 g, 0.0885 mol), AIBN (0.01453 g, 0.089 mmol) were added in 10 ml test tubes. Components were dissolved in 6 ml 1,4-dioxane and oxygen was removed from reaction mixture by bubbling nitrogen through it for 30 min. Test tubes were tightly sealed and placed into a shaker (70 °C, 90 rpm) for 24 hours. Then the mixtures were cooled to room temperature and copolymers slowly poured into 500 ml of diethyl ether. Products were filtered and dried under vacuum. LCST (DI water) ≈ 28 °C, LCST (PBS buffer 0.1 M, pH 7.4) ≈ 28°C.

Synthesis of poly(N-isopropylacrylamide-co-acylic acid-co-benzophenoneacylate), p(NIPAM-AA(4.8 mol.%)-BA(1.6 mol. %)). NIPAM (6.4798 g, 55.62 mmol), BA (0.224 g, 0.89 mmol); AA (0.1912 g, 2.66 mmol), AIBN (0.0507 g, 0.31 mmol) were dissolved in 30 ml of ethanol and oxygen was removed from reaction mixture by bubbling nitrogen through it for 30 min. The polymerization was carried at 70 °C with mechanical stirring for 24 hours. Then the P(NIPAN-AA-BA)polymerization mixture was cooled to room temperature and poured slowly into 750 ml of diethyl ether. Precipitated polymer was filtered and dried under vacuum. Molecular weight of polymer characterized by GPC was M_n = 24 kg/mol, M_w = 80 kg/mol, M_w/M_n = 3.33. LCST (DI water) ≈ 33 °C, LCST (PBS buffer 0.1 M, pH 7.4) ≈ 40 °C.

Synthesis of poly(methylmethacrylate-co-benzophenoneacylate), p(MMA-BA(1.6 mol. %)). MMA (4.5 g, 44.95 mmol), BA (0.182 g, 0.73 mmol) and AIBN (0.075 g, 0.46 mmol) were dissolved in 25 ml of N,N-dimethylformamide (DMF). The mixture was purged with nitrogen for 30 min. The polymerization was carried at 70 °C under nitrogen atmosphere with mechanical stirring overnight. After cooling down to the room temperature, the mixture was poured in 800 ml diethyl ether; the precipitate was filtered and dried under vacuum at 40 °C. Molecular weight of polymer characterized by GPC was M_n = 13 kg/mol, M_w = 37 kg/mol, M_w/M_n = 2.84.

Synthesis of polysuccinimide, PSI. PSI was synthesized by acid-catalyzed thermal polycondensation of L-aspartic acid. A typical synthesis procedure was as follows. Powdery L-aspartic acid (20 g, 150 mmol) and 85% o-phosphoric acid (10 g, 87 mmol) were kept at 200 °C for 6.5 h under nitrogen flow. The mixture was cooled to room temperature and dissolved in N,N-dimethylformamide (DMF). The solution was poured into a large amount of deionized water (Millipore), and the precipitate was washed several times with water until the filtered water became neutral. The obtained PSI was characterized by GPC: M_n = 15.7 kg/mol, M_w = 44.9 kg/mol, M_w/M_n = 2.86.

Synthesis of magnetic particles. The oleic acid stabilized iron oxide nanoparticles were prepared as described by Agrawal et.al.[137]. The average particle sizes obtained from the TEM micrographs was 15 nm for the toluene dispersion.

Preparation and modification of silica particles.

Silica particles (SP-1000) were prepared by Stöber synthesis with further modification (3-aminopropyl)triethoxysilane (SP-NH_2) and 2-Bromo-2-methylpropionyl bromide (SP-Br) as described by Puretskiy et.al.[138].

Polymerisation of 2-(dimethylamino)ethyl methacrylate (DMAEMA). 1 g of SP-Br particles was placed in 50 ml round-bottom flask and 15 ml DMF were added. The mixture was sonicated for 10 min. Further 15 ml DMAEMA, 190 µl 0.5 M solution N,N,N′,N′′,N′′-pentamethyldiethylenetriamine (PMDTA) in DMF, 190 µl 0.1 M solution copper(II) bromide ($CuBr_2$) in DMF, 0.75 µl ethyl 2- bromoisobutyrate (EBiB) were added. To remove the excess of oxygen from the reaction mixture, nitrogen was bubbled through it for 10 min. Then, 400 µl tin(II) 2-ethylhexanoate were added to reaction mixture and the flask was placed on an oil bath at 101 °C and stirred at 700 rpm. After 1 hour the flask was removed from the oil bath and the particles were centrifuged and washed several times with DMF and ethanol and then dried in a vacuum oven at 50 °C overnight. Approximately 1 g of SP-PDMAEMA particles was obtained. Thickness of the polymer brushes, grafted from the particles, was estimated by the parallel reaction on a modified silica wafer and the value of approximately 60 nm was determined. Molecular weight of PDMAMEA obtained as a side product is M_w = 21 kg/mol. Average size of the particles determined by SEM was 1 µm ± 0.1 µm.

Quaternization of SP-PDMAEMA. 0.2 g SP-PDMAEMA was places in 10 ml vial and sonicated in 5 ml ethanol for 2.5 hours. To the dispersion of the particles in ethanol 4 ml iodomethane were added, dispersion was sonicated for 20 minutes and then stirred for 2 hours at 700 rpm. Particles were centrifuged, washed several times with ethanol and dried at 60 °C in vacuum oven overnight; 0.21 g of SP-PTMAEMA was obtained.

3.2.5 Substrates

Silicon substrate

Polished silicon wafers (100) with a native oxide layer of about 2 nm, purchased from the Si-Mat Silicon Materials (Germany), were used as a substrate for thin polymer films preparation. Wafers were first cut into rectangular pieces (typically 12 mm x 30 mm) using a diamond cutter. They were then placed in a custom-designed Teflon holder and cleaned by sonication in dichloromethane at RT for 15 min, followed by submerging in a mixture of ammonia solution (NH_4OH, 28 - 30 %), hydrogen peroxide (H_2O_2, 30 %) and deionized water (1:1:2) at 72 °C for 1 hour[139]. Subsequently, the wafers were rinsed thoroughly with DI water. The cleaning procedure leads to hydrophilization of the substrate due to enrichment of the Si wafer surface with silanol groups (Si-OH). The water contact angle after washing was approximately 0°. Cleaned wafers were stored under DI water no longer than 1 month and blown dry with nitrogen before usage. The ellipsometric thickness of SiO_2 layer was 1.5 ± 0.2 nm.

Glass substrate

Alternatively, glass substrate was used instead of silicon wafers, which was necessary for imaging using transmitted light microscope. For this either 1 mm thick microscope slides (Menzel-Gläser) or 0.5 mm thick cover slips (Menzel-Gläser) were cut into appropriate size and modified using procedure for Si wafers, described above.

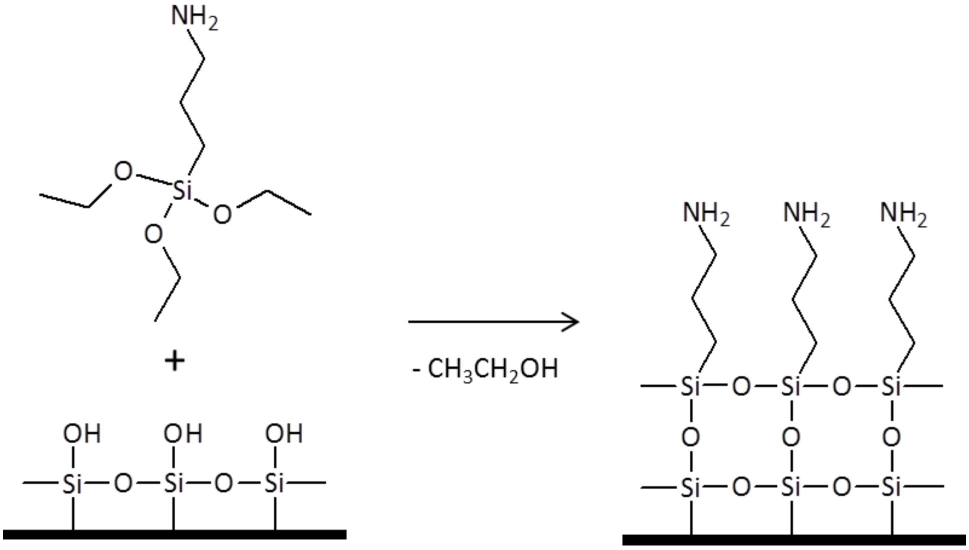

Figure 3.7 | Scheme of chemisorption of 3-aminopropyltriethoxysilane on a silica surface.

Silanization of substrate

For investigation of the swelling behavior of the polymer hydrogels, photocrosslinked polymer film deposited on the substrate have to be covalently grafted to it to avoid detachment during the experiment. For this purpose aminosilanized silicon wafers or glasses have been used as a substrate. Cleaned substrate (after $NH_4OH/H_2O_2/H_2O$ treatment) was immersed into 2 Vol. % solution of (3-aminopropyl)triethoxysilane (APS) in ethanol absolute at RT and stirred at 260 rpm for 2 h. The substrate was then removed from the solution, rinsed several times with ethanol and blown dry with nitrogen. The ellipsometric thickness of the APS layers was 0.9 ± 0.2 nm, which corresponds to the monolayer thickness. During the modification APS attaches to a surface via siloxane bonds (Si-O-Si) to form an amine-terminated surface (Figure 3.7) which can be then used to graft polymer layer to a substrate upon UV-irradiation.

3.2.6 Cells

Baker's yeast was used as a model cells for encapsulation inside self-rolling tubes.All experiments with **HeLa Kyoto GFP-tub H2B-mcherry cells** were performed together with Britta Koch in Leibniz Institute for Solid State and Materials Research Dresden (IFW) in collaboration with group of Prof. O. G. Schmidt and Dr. S. Sanchez.

3.3 Fabrication of polymer bilayer films and self-rolled tubes

The general scheme of the fabrication of polymer bilayer films for self-rolled tubes production is depicted in Figure 3.8. First, active (responsive) polymer was deposited on a Si-wafer or glass substrate, next, passive polymer was deposited from a selective solvent on the top of the first polymer film. The patterning of the polymer bilayer was achieved using photolithography.

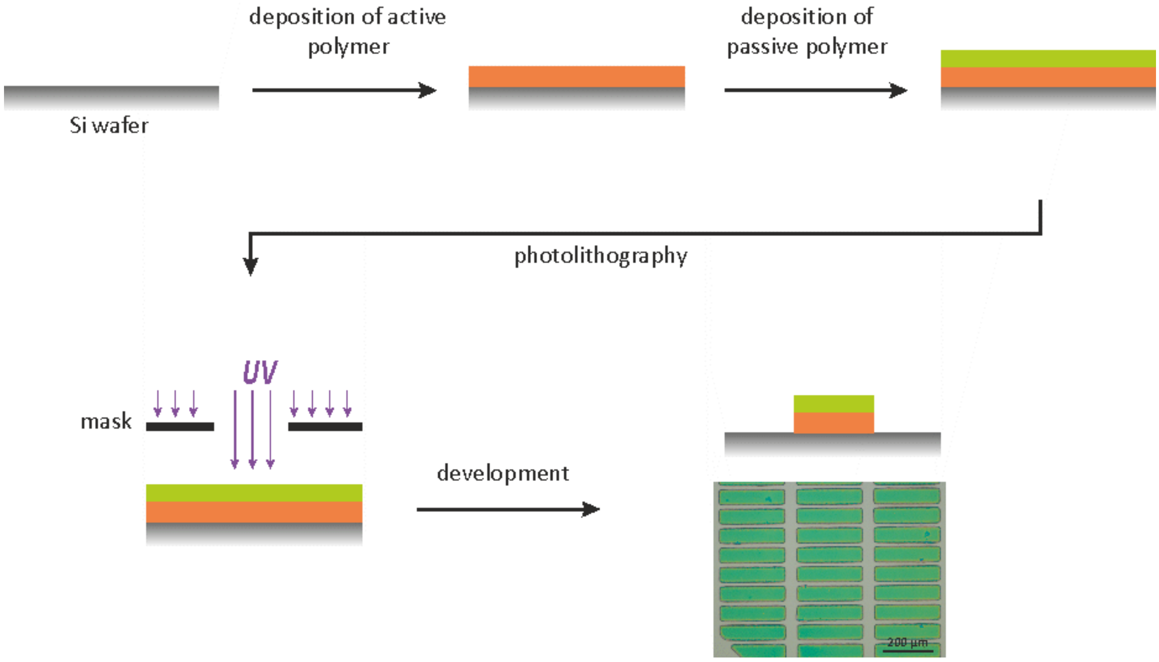

Figure 3.8 | Scheme of patterned polymer bilayer film fabrication.

3.3.1 Polymer films deposition

The deposition of thin polymer films was done using spin-coating or dip-coating. For each polymer the most optimal technique and conditions of deposition, which allowed the production of homogeneous layer with less defects and crystallinity, have been defined experimentally by the method of trial and error.

Basically, spin-coating was used for the deposition of polymers from non-volatile solvents, such as DMF or water. About 200 - 500 µl of a polymer solution was dispensed on the substrate at zero rotation, followed by spinning in one period. When using DMF as a solvent, it was necessary to heat the sample immediately after spin-coating up to the temperature above the boiling point of the DMF to avoid dewetting of the polymer film and to remove the rests of the toxic solvent.

Manual dip-coating was used to obtain polymer films with a thickness of more than 500 - 700 nm. In most other cases, an automatic dip-coater, which allows controlling the withdrawal speed in a range from 0.6 mm/s up to 2 mm/s, was used. The first polymer layer was dried prior to the deposition of the second polymer.

Table 3.1 | Parameters of polymer films deposition

Function of the polymer	Polymer	Solvent for deposition (selective solvent)	Deposition method and parameters
Active polymer	p(NIPAM-BA)	Ethanol absolute	***Automatic dip-coating****:* polymer solution temperature 25 °C, substrate stays 10 s in solution, withdrawal speed 1 mm/s. ***Manual dip-coating:*** solution temperature 20 - 25 °C; substrate stays 20 s in solution, withdrawal speed is not controlled.
	p(NIPAM-AA-BA)	Ethanol absolute	***Automatic dip-coating****:* solution temperature 25 °C, 10 s in solution, withdrawal speed 1 mm/s. ***Manual dip-coating:*** solution temperature 20 - 25 °C, 20 s in solution, withdrawal speed is not controlled.
	PSI	DMF	***Spin-coating:*** solution temperature 20 - 25 °C; 3000 rpm, 2000 rpm/s, 10 - 15 s, in one period (rotation speed, acceleration and spin time). Immediate heating on a heating plate at 170 °C for 1 min. All manipulations were performed under the fume hood.
	Gelatin	DI water with addition of Pen/Strep solution up to concentration 100 U/ml penicillin, 100 µg/ml streptomycin	***Spin-coating:*** solution temperature 37°C, 2000 rpm, 1500 rpm/s, 25 s. Drying on air before second polymer layer deposition (5 - 30 min depending on gelatin layer thickness).
Passive polyme	p(MMA-BA)	Toluene	***Automatic dip-coating****:* solution temperature 20 - 25 °C, 10 s in solution, withdrawal speed 1 mm/s. ***Manual dip-coating:*** solution temperature 20 - 25 °C, 20 s in solution, withdrawal speed is not controlled (for deposition of films with thicknesses from 700 nm up to 2 µm).
	PCL	Toluene	***Spin-coating:*** solution temperature 20 - 25 °C; 3000 rpm, 2000 rpm/s, 40 s. ***Automatic dip-coating****:* solution temperature 20 - 25 °C; withdrawal speed 1.1 mm/s.

It is essentially important for second layer, which is a passive polymer, to be deposited from a selective solvent, since only in this case first layer stays intact (do not dissolve or swells) resulting in well-defined bilayer structure. The used solvents and techniques of the polymer deposition process are summarized in the Table 3.1.

The concentration of polymer solutions, used for deposition, varied from 1 % to 12 %, calculated as the mass of dissolved polymer [gram] to the volume of the solvent [ml]. All solutions with concentration less than 8 % were filtered through 0.2 µm PTFE filter prior to use. Otherwise, pre-filtered solvent was used for the solution preparation. Increase of the solution concentration led to the increase of the film thickness, which varied between 50 nm and 2 µm and was determined using either ellipsometry (Chapter 3.1.1) or scratch test (Chapter 3.1.4).

The polymer film homogeneity and roughness were controlled using AFM on the each step of the polymer deposition. The typical σ_{RMS} values calculated for 100 x 100 μm^2 sized images for responsive and passive polymer layers are listed in the Table 3.2.

Table 3.2 | Typical surface roughness for selected dry polymer layers

Layer	Polymer	Concentration of the polymer solution for film deposition, %	Film thickness, nm	σ_{RMS}, nm
Responsive layer	p(NIPAM-BA)	7	740	0.4
	p(NIPAM-AA-BA)	7	740	0.4
	PSI	7	200	0.3
	Gelatin	7	400	0.6
Passive layer	p(MMA-BA)	4	100	1.6
	PCL	3	230	12.3
		4	310	16.8
		7	950	28.0
		9	1200	76.3
	PCL*	7	950	49.6
	PCL**	7	950	22.9

* PCL treated by heating at 130 °C and cooling down to −78.5 °C

** PCL treated by heating at 130 °C and cooling down to −196 °C

All responsive polymers formed homogeneous films with the roughness less than 1 nm independently on the concentration of the solution for film deposition. The situation was different with the polymers, used for the passive layer preparation. While p(MMA-BA) formed smooth films with roughness of approximately 1 - 2 nm in all range of used layer thicknesses, the PCL films were highly crystalline. The roughness and the size of crystallites for PCL were dependent on the concentration of deposition solution. So, for films deposited from 3 %, 7 % and 9 % solutions, σ_{RMS} increased dramatically from 12.3 nm to 28.0 nm and 76.3 nm respectively. At the same time the average size of crystallites decreased from approximately 100 µm to 25 µm and 8 µm respectively (Figure 3.9a-c). Even though the films of PCL were always continuous, the crystallites formed deep cracks with the depth often reaching 50 % of the layer thickness.

The following procedure has been tested to decrease the crystallinity of PCL layers. After deposition of the polymer film and before the photocrosslinking, the sample was heated up to 130 °C for 1 minute to melt PCL ($T_{m,PCL} = 60$ °C) and then quickly cooled down on a metal plate placed either on a dry ice (T = −78.5 °C) or in liquid nitrogen (T = −196 °C). The photolithography was done immediately after that. In Figure 3.9 the AFM images for the films deposited from 7 % solution of PCL and treated this way are shown: 100 x 100 µm^2 scan after cooling using dry ice (e), 100 x 100 µm^2 scan and 10 x 10 µm^2 close-up (f, g respectively) – after cooling using liquid nitrogen. For each image the cross-section profile is displayed as inset to demonstrate the depth of the cracks formed by crystallites.

When compared to untreated film of the same thickness (Figure 3.9b), it is clear that for both cooling temperatures the procedure led to a significant decrease of crystallite size. Nevertheless, cooling at −78.5 °C seems to even worsen the film quality. Although by treatment, crystallite size decreased from 25 µm to 3 - 5 µm, the depth of cracks increased from 15 % to 23 % of polymer film thickness and at the same time roughness (σ_{RMS}) increased up to 49.6 nm. Contrary, cooling at −196°C improved roughness a bit (22.9 nm), decreased both the size of the crystallites (to less than 1 µm) and the depth of cracks (to 8 % of polymer film thickness), resulting in a better quality of polymer film.

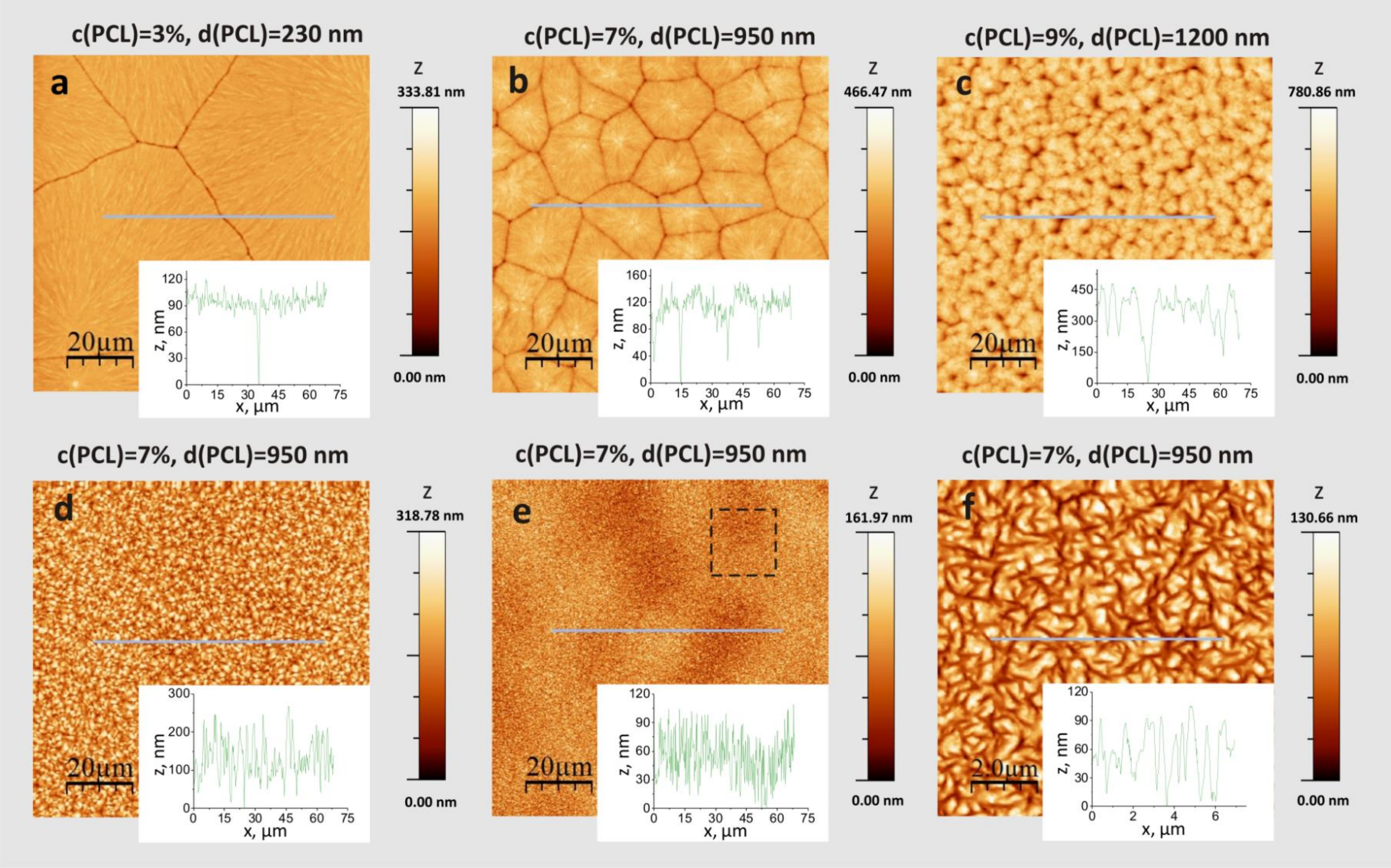
c(PCL)=3%, d(PCL)=230 nm
a
Z
333.81 nm
0.00 nm
20µm
120
90
60
30
0
z, nm
0
15
30
45
60
75
x, µm
c(PCL)=7%, d(PCL)=950 nm
b
Z
466.47 nm
0.00 nm
20µm
160
120
80
40
0
z, nm
0
15
30
45
60
75
x, µm
c(PCL)=9%, d(PCL)=1200 nm
c
Z
780.86 nm
0.00 nm
20µm
450
300
150
0
z, nm
0
15
30
45
60
75
x, µm
c(PCL)=7%, d(PCL)=950 nm
d
Z
318.78 nm
0.00 nm
20µm
300
200
100
0
z, nm
0
15
30
45
60
75
x, µm
c(PCL)=7%, d(PCL)=950 nm
e
Z
161.97 nm
0.00 nm
20µm
120
90
60
30
0
z, nm
0
15
30
45
60
75
x, µm
c(PCL)=7%, d(PCL)=950 nm
f
Z
130.66 nm
0.00 nm
2.0µm
120
90
60
30
0
z, nm
0
2
4
6
x, µm

Figure 3.9 | AFM images of PCL thin films, demonstrating different size of PCL crystallites in dependence on the concentration of deposition solution: (a) 3 %, (b) 7 % and (c) 9 %. Change of PCL film morphology after heating and cooling (d) at −78.5 °C and (e, f) at −196 °C. Additionally the cross-section profile is displayed as an inset in each image for a path of (a-e) 70 µm and (f) 7 µm, marked as a blue line.

3.3.2 Photolithography

The patterning was performed using contact photolithography. Typically, both polymers, used for bilayer preparation, were either photosensitive due to copolymerization with photosensitive monomer (BA) or contained small amount of admixed photocrosslinker (BPhOH or DAz). Admixing, but not copolymerization, was preferred in case when commercially available polymers were used (PCL, gelatin) or when copolymerization led to undesirable changes of polymer properties, such as exceeding decrease of LCST of PNIPAM-copolymers when contained more than 2 mol.% of 4-acryloylbenzophenone. In the last case the admixing of the photocrosslinker allowed us to vary the swelling degree of the polymer hydrogels without varying their chemical properties. Mechanism of the polymer UV light crosslinking using benzophenone derivatives is depicted in Figure 3.10: UV irradiation activates benzophenone fragments, which produce free radicals and lead to polymer crosslinking in the irradiated areas. Notably, other similar compounds including benzophenone, 4-carboxybenzophenone, and 2,4-dihydroxybenzophenone were found to be almost inefficient for the cross-linking of the used polymers. This may be related to a difference in mixability of crosslinker with polymer.

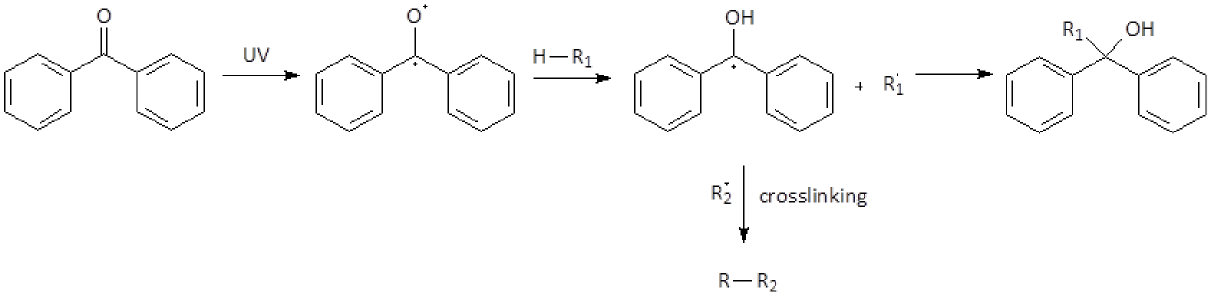

Figure 3.10 Scheme of polymer UV light crosslinking using benzophenone derivatives

For the crosslinking of gelatin the usage of benzophenone derivatives was impossible due to insolubility of the latter in water, which is the only solvent for gelatin film deposition. Therefore water soluble DAz was used as photocrosslinker. Type and amount of crosslinker used for a given polymer are listed in the Table 3.3.

For photolithography UV hand lamp (NH-15, Herolab, Germany) with two possible wavelengths of 254 nm or 364 nm was used. Irradiance at the distance of 3 cm from the lamp was ~ 330 µW/cm^2 for 254 nm and ~ 1100 µW/cm^2 for the 354 nm UV light source. The irradiation was performed through a photomask (Toppan Photomasks Inc., Germany) with rectangular patterns of appropriate size. The photomask was placed on a sample and fixed using a special home-made box so that the distance from the sample to the lamp was 3 cm.

Table 3.3 | Choice of crosslinker for used polymers

Polymer	PNIPAM-co-polymers	PSI	Gelatin	p(MMA-BA)	PCL
Crosslinker	Copolymerization with 1-1.5 mol.% of BA. By additional admixing of BPhOH degree of hydrogel crosslinking can be increased.	Admixing of 1-2 wt.% of BPhOH.	Admixing of 12 wt.% of DAz.	Copolymerization with 1.5-2 mol.% of BA.	Admixing of 4-5 wt.% of BPhOH.

One of the most critical steps for bilayer pattern production is a development after photolithography was performed. During this step uncrosslinked polymers in non-illuminated areas have to be removed. At the same time, crosslinked areas of polymer bilayer should stay possibly intact, do not detach from the substrate and form well-defined patterns. The optimal results were demonstrated when a common solvent exists for both, active and passive polymers and development occurs in one step. It is important to notice that to achieve a good quality of photolithography, both crosslinked polymers should swell in a non-selective solvent more or less equally, which is especially important for the thick polymer films (with thickness close to 1 µm). Unequal swelling of the polymers can result in the deformation of patterns, detachment of the polymer bilayers from the substrate or even folding. In Figure 3.11a an example of an unsuccessful development of p(NIPAM-BA)/PCL bilayer in THF is presented.

Moderate difference in swelling of two layers results in a rather acceptable quality of pattern formation, especially if it is the second layer that swells more intense. However the modulus mismatch between the bilayers creates a compressive stress resulting in wrinkling similar to spontaneous surface patterning described in the work of Bowden *et al.*[140] and in other reports[141-143]. This kind of surface changes has been observed for PNIPAM-co-polymer/p(MMA-BA) bilayers when using chloroform or dichloromethane as a non-selective solvent (Figure 3.11 b). Wrinkling led to the increase of RMS roughness up to 31.5 nm, but did not disturb further tube formation and therefore the solvents were considered as acceptable for the development of such bilayers.

In the absence of common solvent, the development has to be done in two steps: first, unkrosslinked passive polymer should be removed, than the development of the active polymer layer can be done. The second step should be performed very carefully, since the swelling of only the first layer can lead to immediate tubes formation (Figure 3.11c). In this case, it is also possible to leave active polymer intact and combine development step with the step of tube formation when sample is placed in aqueous media. It can be done when the presence of small amount of dissolved responsive polymer in solution is not disturbing for further experiment.

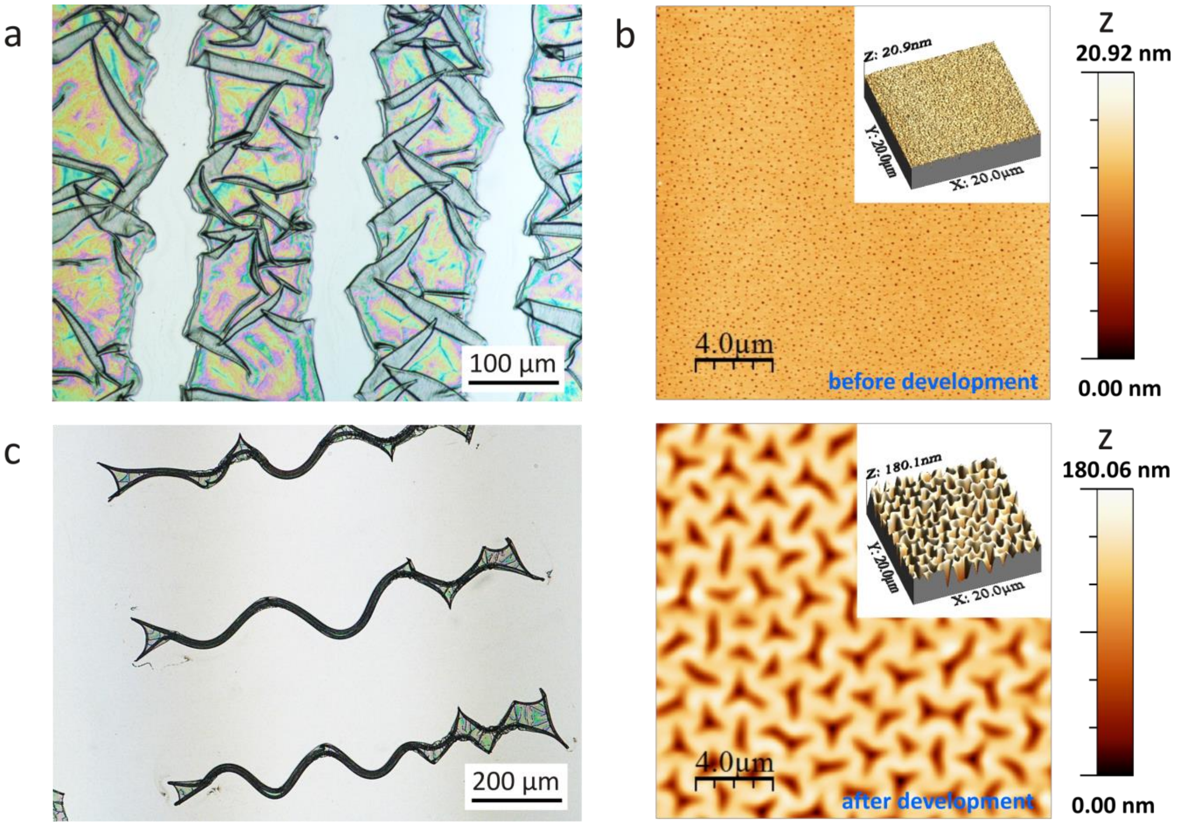
a
100 µm
b
Z: 20.9nm
Y: 20.0µm
X: 20.0µm
4.0µm
before development
Z
20.92 nm
0.00 nm
c
200 µm
Z: 180.1nm
Y: 20.0µm
X: 20.0µm
4.0µm
after development
Z
180.06 nm
0.00 nm

Figure 3.11 | The defects of patterns due to development step: (a) detachment of p(NIPAM-BA)/PCL bilayer from the substrate during development in THF; (b) wrinkling of p(NIPAM-BA)/p(MMA-BA) surface; (c) rolling of the p(NIPAM-BA)/p(MMA-BA) bilayer during two step development in toluene and ethanol.

Occasionally, additional steps were required. For instance, non-volatile solvents were removed by washing the sample in an appropriate solvent, often in ethanol. Prior to cell experiments samples were kept in vacuum oven at T = 50 °C at least for 2 h to eliminate the rests of the solvents. The conditions of photolithography and development for polymer bilayers used in the present work are summarized in the Table 3.4.

Table 3.4 | Parameters of photolithography(I) and polymer bilayer development (II)

Passive polymer **Active polymer**	**PCL,** **Layer thickness ≤ 0.5 µm**	**PCL,** **Layer thickness ≥ 0.5 µm**	**p(MMA-BA),** **Layer thickness ≤ 0.5 µm**	**p(MMA-BA)** **Layer thickness ≥ 0.5 µm**
p(NIPAM-BA), Layer thickness ≤ 0.5 µm	I. UV-254 nm lamp: 1 h II. $CHCl_3$, 2 min – development of both layers	I. UV-254 nm lamp, 1.5 h II. CH_2Cl_2, 5 min – development of both layers	I. UV-254 nm lamp: 1 h II. $CHCl_3$, 2 min – development of both layers*	—
p(NIPAM-BA), Layer thickness ≥ 0.5 µm	I. UV-254 nm lamp, 1 h II. $CHCl_3$, 2 min – development of both layers	I. UV-254 nm lamp, 1.5 h II. CH_2Cl_2, 5 min – development of both layers	I. UV-254 nm lamp, 1 h II. CH_2Cl_2, 5 min – development of both layers*	I. UV-254 nm lamp: 1.5 h II. CH_2Cl_2, 5 min – development of both layers*
p(NIPAM-AA-BA), Layer thickness ≤ 0.5 µm	I. UV-254 nm lamp, 1 h II. $CHCl_3$, 2 min – development of both layers	I. UV-254 nm lamp, 1.5 h II. CH_2Cl_2, 5 min – development of both layers	I. UV-254 nm lamp: 1 h II. $CHCl_3$, 2 min – development of both layers*	—
p(NIPAM-AA-BA), Layer thickness ≥ 0.5 µm	I. UV-254 nm lamp: 1.5 h II. $CHCl_3$, 5 min – development of both layers	I. UV-254 nm lamp, 1.5 h II. CH_2Cl_2, 5 min – development of both layers	I. UV-254 nm lamp: 1 h II. $CHCl_3$, 5 min – development of both layers*	I. UV-254 nm lamp: 1.5 h II. CH_2Cl_2, 5 min – development of both layers*
PSI	I. UV-254 nm lamp: 1.5 h II. 1) $CHCl_3$, 10 min – development of PCL layer 2) DMF, 10 min – development of PSI layer 3) EtOH, 6 min, two times – elimination of DMF*		—	
Gelatine	I. Simultaneously UV-254 nm lamp (for BPhOH activation) and UV-354 nm lamp (for DAz activation), 30 min II. 1) $CHCl_3$, 5 min – development of PCL layer 2) Water, 37 °C, 2 min – development of gelatin layer 3) EtOH, 30 s – to accelerate drying of the bilayer		—	

* Prior to cell experiments samples were kept in vacuum oven at T = 50 °C at least for 2 h to eliminate the rests of the solvents

3.3.3 Modification of the surface of the hydrophobic polymer.

The promising possibility to functionalize the inner wall prior to tube formation have been already discussed by Luchnikov *et al.*[5] Indeed, when bilayer patterns are unfolded, it is easy to modify surface of the passive polymer that can be important for controlling cell adhesion inside the tube. In the present work, by a simple O_2-plasma treatment hydrophilization of the passive polymer surface was achieved. When carefully applied, plasma treatment did not decrease the thickness of the second polymer layer and did not influence the rolling behavior of the bilayer film. The decrease of water contact angle for PCL surface after plasma treatment is demonstrated in the Table 3.5. The roughness characteristics of the surface stayed unchanged.

Table 3.5 | Plasma modification of PCL polymer layer

Conditions of film preparation	Treatment of PCL surface	Water contact angle (Adv), °	Film thickness, µm	σ_{RMS}, nm
Deposition from 9 % solution of PCL in Toluene with admixed 5 wt.% of BPhOH (related to the mass of dry polymer), spin-coating, UV crosslinking	w/o treatment	72.2	1.2	75.2
	O_2 plasma 10 s, power 35	63.2	1.2	75.2
	O_2 plasma 10 s, power 65	60.1	1.2	75.2
	O_2 plasma 30 s, power 65	58.5	1.1	75.1

3.3.4 Formation of the polymer tubes and their characterization.

The tubes were fabricated by exposure of patterned bilayers in DI water, buffer solution or cell culture medium at the temperature conditions correspondent to the system used. The rolling was observed using optical microscope.

4 Results and discussion

INDIVIDUAL SELF-ROLLED POLYMER TUBES: ROLLING BEHAVIOR AND ENCAPSULSATION OF MICROOBJECTS

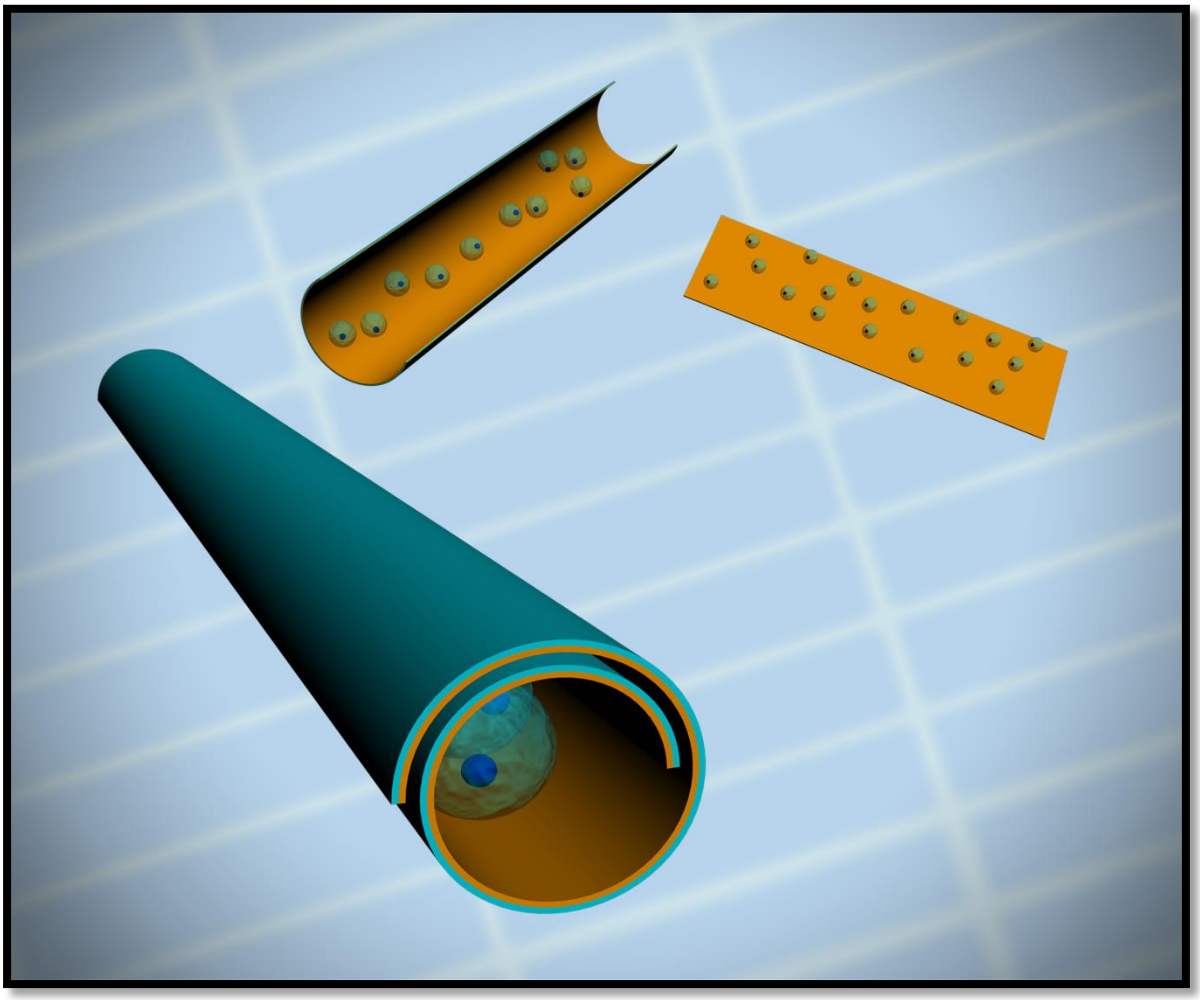

4.1 Thermoresponsive bilayer systems based on poly(N-isopropylacrylamide)

4.1.1 Objectives

In this chapter, the design of partially biodegradable temperature-sensitive microtubes is described. Thermoresponsive poly(N-isopropylacrylamide)-based copolymer was used as an active component of the bilayer. In aqueous media, poly(N-isopropylacrylamide) homopolymer (PNIPAM) reversibly changes its solubility at the Low Critical Solution Temperature (LCST ~ 33 °C). Due to its thermoresponsive properties, PNIPAM has been already applied for diverse biotechnological applications, such as controlled adhesion of cells[144], directed protein adsorption[145], control of biomolecular motors[146, 147], protein purification[148], photolithography[149] and drug delivery[150]. As a passive – hydrophobic – component of bilayer polycaprolactone or polymethylmethacrylate was used. Polycaprolactone (PCL) is a semicrystalline polyester that undergoes hydrolytic degradation due to the presence of hydrolytically labile aliphatic ester linkages[18]. Biodegradability of PCL has been used for development of various micro- and nano-sized drug delivery vehicles[151]. Moreover, due to its excellent biocompatibility, PCL is a very perspective material for design of scaffolds for tissue engineering[152, 153]. Polymethylmethacrylate (PMMA) is not biodegradable, but has a good degree of biocompatibility and is broadly used in dentistry as a main organic component of dental fillings, in manufacture of rigid intraocular lenses [154] and in orthopedic surgery as a bone cement in order to affix implants and to remodel lost bone[155].

The bilayer film made of these polymers is able to self-roll and unroll due to swelling and collapse of PNIPAM at low and elevated temperatures, respectively. This behavior allowed controlled encapsulation and release of microobjects, triggered by temperature changes in the range of 25 - 37 °C.

4.1.2 Experimental

Materials. As a responsive layer random copolymer of NIPAM and BA poly(N-isopropylacrylamide-co-benzophenoneacylate), p(NIPAM-BA(1 mol.%)), or copolymer of NIPAM, AA and BA poly(N-isopropylacrylamide-co-acylic acid-co-benzophenoneacylate), p(NIPAM-AA(4.8 mol.%)-BA(1.6 mol.%)), were used. Random copolymer of MMA and BA poly(methylmethacrylate-co-benzophenoneacylate), p(MMA-BA(1,6 mol.%)) was used for preparation of the passive layer. Polymers were synthesized using free radical polymerization as described earlier in Chapter 3.2.4.

Fabrication of polymer bilayers and self-rolled tubes. The bilayer films were fabricated by sequential deposition of PNIPAM-co-polymer and PCL or p(MMA-BA) layers on a silicon substrate using dip-coating (Table 3.1). The solution concentration for polymer deposition was typically 2 - 8 % for PNIPAM-co-polymer, 0.5 - 5 % for PCL and 2 - 7 % for p(MMA-BA). To provide UV-photocrosslincability, polycaprolactone solutions contained 5 wt. % of 4-hydroxybenzophenone with respect to the weight of dry polymer. The thickness of polymer layers varied in the range of 170 - 1200 nm for PNIPAM-co-polymer, 40 - 400 nm for PCL and 60 - 360 nm for PMMA.

The polymer bilayers were patterned using photolithography (3.3.2) through masks with following pattern sizes of 65 µm x 825 µm, 90 µm x 948 µm, 126 µm x 1327 µm, 200 µm x 1600 µm or 300 µm x 1800 µm. The irradiated film was rinsed with chloroform in order to remove non-crosslinked polymers leaving rectangular bilayers.

Patterned bilayers were then exposed in DI water or PBS (0.15 M, pH 7.4) at elevated temperature, which was above LCST of PNIPAM-co-polymer. Decreasing the temperature below LCST resulted in formation of the tubes within 1 - 10 minutes.

Preparation of magneto-sensitive tubes. For the preparation of magneto-sensitive self-rolled tubes, 0.7 wt.% of oleic acid-coated Fe_3O_4 nanoparticles[137] were admixed into PNIPAM-co-polymer chloroform solution used for polymer film deposition. Parameters of polymer film deposition were taken as for the ethanol solution. Further procedure has been performed as described above.

Mammalian cells. All experiments with HeLa Kyoto GFP-tub H2B-mcherry cells were performed in Leibniz Institute for Solid State and Materials Research Dresden (IFW), Institute for Integrative Nanosciences (Prof. Dr. Oliver G. Schmidt) in collaboration with Dr. Samuel Sanchez Ordonez and Britta Koch.

Cell line details:

- Human epithelial cell line taken from a cervix carcinoma (cancer cell line).
- Labelling: GFP protein (green fluorescence) fused to alpha-tubulin (Protein of the cytoskeleton); mcherry (red fluorescence) fused to H2B (histone protein where the DNA in its condensed state is coiled around, therefore shows the location of the cell nucleus).

Live-cell imaging. Live-cell imaging was performed in IFW Dresden using a Zeiss Axio Observer Z1 inverse microscope equipped with a 37 °C heated stage and a CO_2 chamber. The software *Axio Vision Rel. 4.8* (Carl Zeiss, Inc.) was used for the image acquisition.

4.1.3 Results and discussions

4.1.3.1 Swelling of PNIPAM-co-polymer thin films

In an aqueous environment, PNIPAM homopolymer undergoes reversible coil-globule transition at the Low Critical Solution Temperature (LCST) of 32 - 33 °C, changing from a hydrophilic state below this temperature to a hydrophobic state above it[156]. Copolymerization of NIPAM with hydrophilic or hydrophobic monomers increases or decreases the LCST of a given co-polymer respectively[149].

In order to provide photocrosslinkability of the polymer, benzophenoneacylate photosensitive groups were incorporated into the PNIPAM chains giving a random poly(N-isopropylacrylamide-co-benzophenoneacylate) copolymer (p(NIPAM-BA)). The hydrophobic nature of BA resulted in a lowered LCST, which was 28 °C both in DI water (pH = 5.5) and in PBS buffer (0.15 M, pH = 7.4) for polymer containing 1 mol. % of BA co-monomer. Additional incorporation of ionisable acrylic acid units into polymer backbones increased LCST and enabled phase transitions and solubility changes dependent on pH. So, random poly(N-isopropylacrylamide-co-acylic acid-co-benzophenoneacylate) copolymer (p(NIPAM-AA-BA)), which contained 4.8 mol.% of AA and 1.6 mol. % of BA units, possessed LCST of 33 °C in DI water and of 40 °C in PBS buffer. Thus, both synthesized PNIPAM-copolymers demonstrate thermoresponsive behavior in the temperature range close to physiological conditions.

The swelling behavior of photocrosslinked hydrogel thin films (20 - 30 nm) produced of PNIPAM-co-polymers was investigated at 20 °C and 37 °C using null ellipsometry as described in Chapter 3.1.1. Thermoresponsive hydrogels swell and shrink at reduced and elevated temperature, respectively. Swelling of PNIPAM-co-polymers films was very fast and maximal swelling degree was usually achieved within less than one minute after exposure to a solvent at the temperature below LCST. Above LCST for a given polymer and solvent no swelling was observed. For p(NIPAM-BA) swelling degree, calculated using equation (3.2), was equal in DI water and PBS buffer and at 20 °C was 3.5. At 37 °C in both solvents polymer films stayed shrunk (Figure 4.1a). Swelling of thermo- and pH-responsive p(NIPAM-AA-BA) co-polymer was dependent on the solvent used: at 20 °C swelling degree was 3.2 and 4 for DI water and PBS buffer respectively. At 37 °C polymer films swelled only in buffer (Figure 4.1b) that correlates with LCST values. The increase of swelling degree with the increase of ionic strength and pH of the aqueous solution is due to boosted dissociation of acrylic acid (pK_a = 4.5) and correspondent repulsion of ionized carboxylic groups within PNIPAM hydrogel. By admixing of additional low-molecular photocrosslinker BPhOH, the degree of hydrogel crosslinking could be increased that resulted in the decrease of the swelling degree, while transition temperature was unchanged (Figure 4.1c).

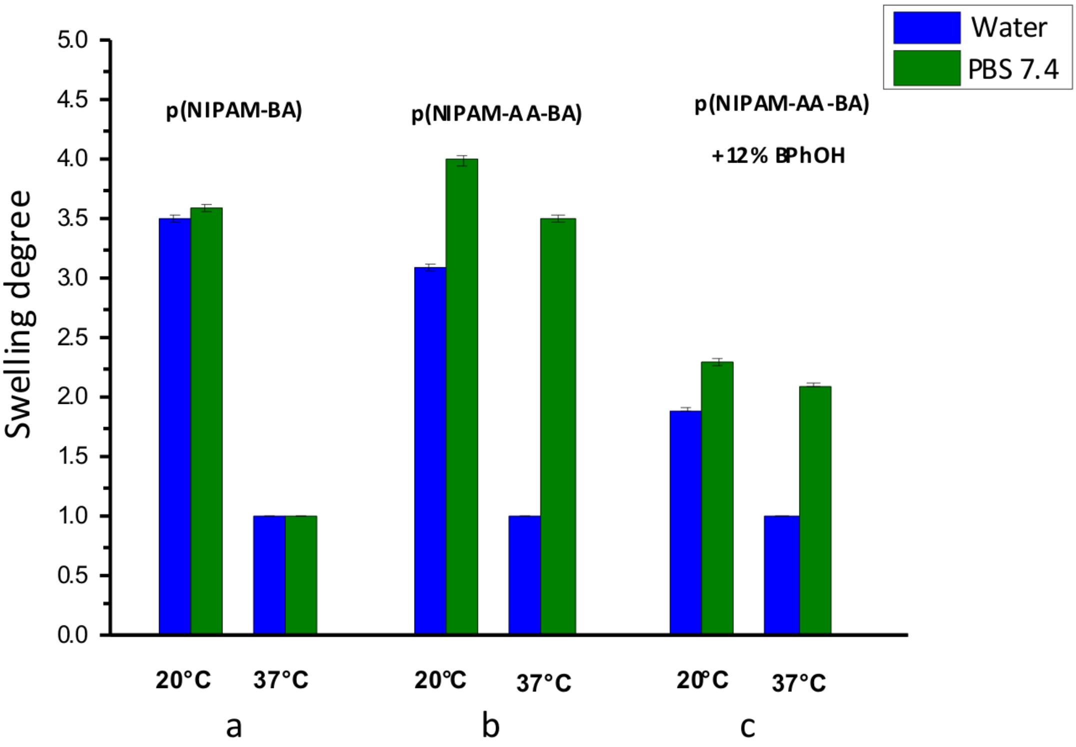

Figure 4.1 | Swelling degree of PNIPAM-co-polymers in DI water and PBS buffer (0.15 M, pH = 7.4) at the temperature of 20°C and 37°C: (a) p(NIPAM-BA(1 mol.%)); (b) p(NIPAM-AA(4.8 mol.%)-BA(1 mol.%)) and (c) p(NIPAM-AA(4.8 mol.%)-BA(1 mol.%)) with admixed 12 wt.% of BPhOH (in relation to the mass of dry polymer).

The swelling of p(NIPAM-BA) and p(NIPAM-AA-BA) films is reversible and swelling-shrinking cycles can be repeated many times in a reproducible manner (Figure 4.2a). While p(NIPAM-BA) is only thermo-responsive, p(NIPAM-AA-BA) co-polymer is sensitive to both temperature and pH. Therefore, for p(NIPAM-AA-BA) films, swelling-shrinking cycles can be performed not only by changing the temperature, but also by exchanging the solvent. When temperature is fixed in the range $LCST_{DI\ water} < T < LCST_{PBS\ buffer}$, exchange of DI water with PBS buffer results in a reversible swelling of p(NIPAM-AA-BA) film (Figure 4.2b).

Switching between swelling and shrinking by changing the temperature was very fast and was finished within several seconds (3-10 s), switching by solvent exchange was slower and usually took several minutes. For investigations presented further in this chapter, the p(NIPAM-BA) copolymer was chosen. Self-rolled tubes based on p(NIPAM-AA-BA) are described in Chapter 4.4.

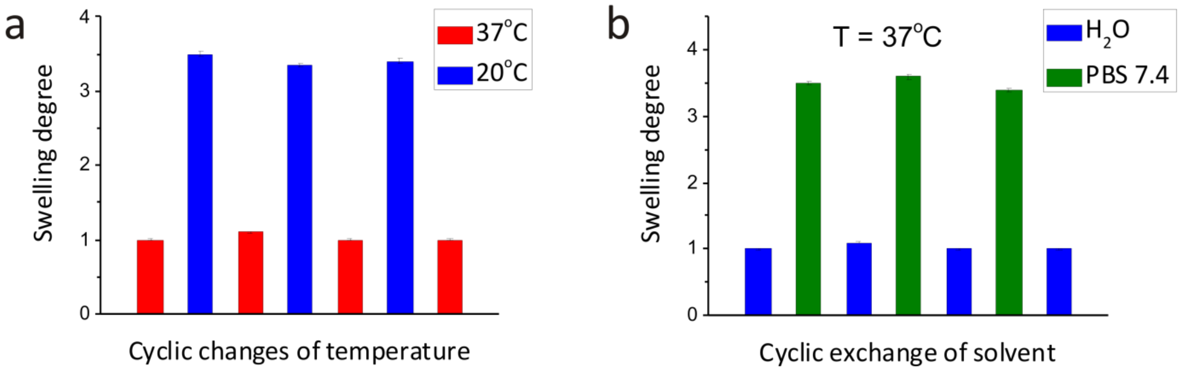

Figure 4.2 | Cyclic changes of swelling degree of PNIPAM-co-polymers (a) thin film of p(NIPAM-BA(1 mol.%)) swells and shrinks in response to the cyclic changes of temperature from 37 °C to 20 °C; (b) thin film of p(NIPAM-AA(4.8 mol.%)-BA(1 mol.%)) swells and shrinks in response to the cyclic exchange of the solvent (DI water and PBS buffer) at the temperature fixed at 37 °C.

4.1.3.2 Formation of thermo-responsive self-rolled tubes

Next, the formation of thermo-responsive self-rolled polymer tubes in aqueous environment was investigated. Polymer bilayers were prepared on a silicon substrate using thermo-responsive p(NIPAM-BA) as an active component, and hydrophobic polycaprolactone (PCL) or random copolymer poly(methylmethacrylate-co-benzophenone acrylate) (p(MMA-BA)) as a passive one. Bilayer films remain undeformed when exposed to aqueous environment at the temperature above LCST of PNIPAM-co-polymer (T > 28 °C) (Figure 4.3a). When the temperature decreases below the LCST of p(NIPAM-BA), the active layer starts to swell, at the same time hydrophobic layer of PCL or p(MMA-BA) restricts swelling from the top of bilayer system. As a result of inhomogeneous swelling, the bilayer pattern folds, forming a self-rolled tube (Figure 4.3b).

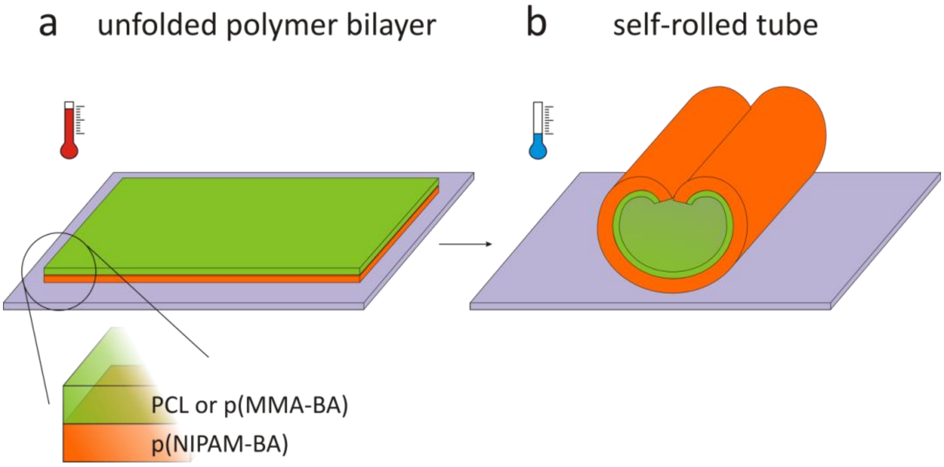

Figure 4.3 | Scheme of temperature triggered formation self-rolled tube: (a) in aqueous environment at the temperature above LCST of PNIPAM-copolymer, the bilayer film is unfolded; (b) a decrease of the temperature below LCST results in a rolling of the bilayer and formation of a tube.

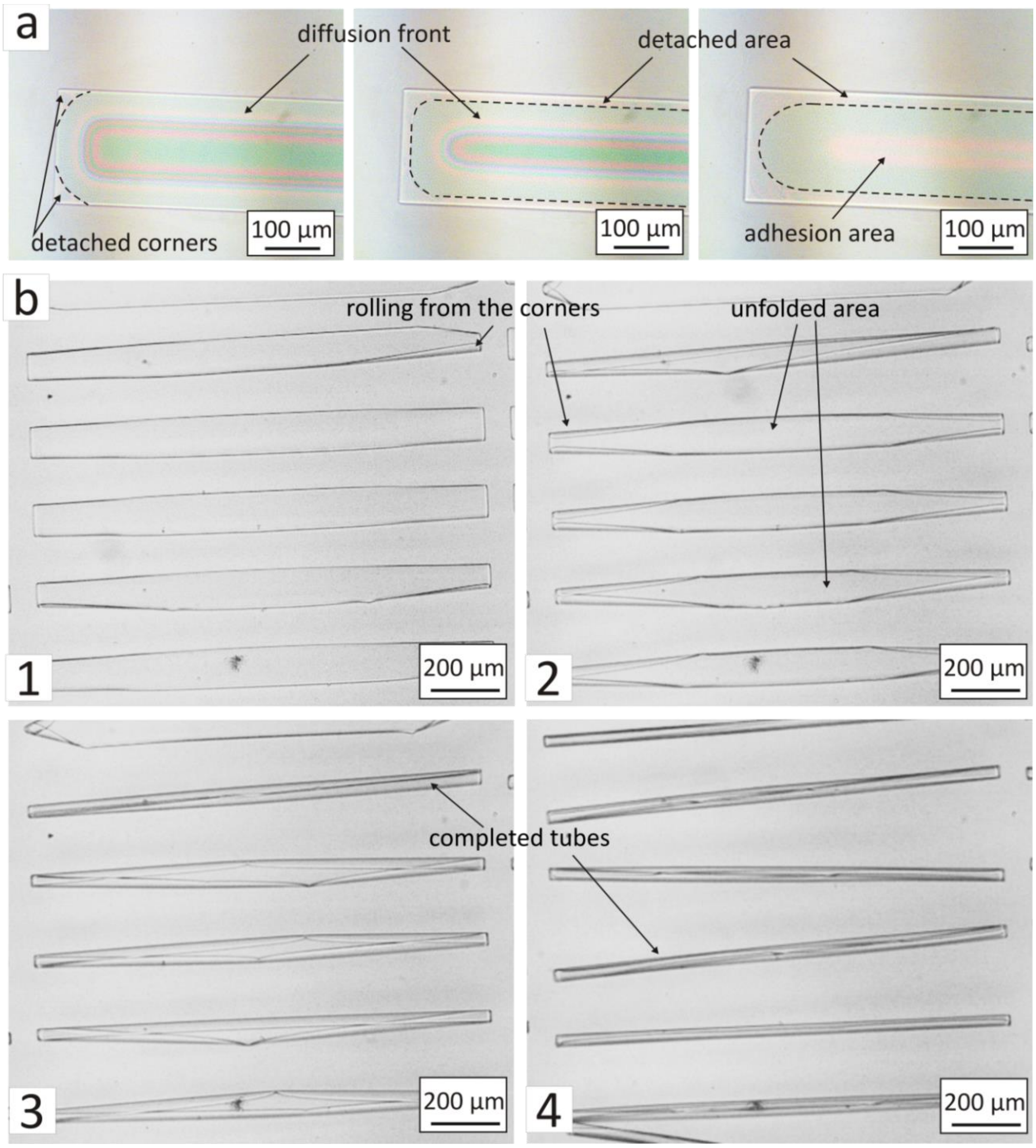
a
diffusion front
detached area
detached corners
adhesion area
100 µm
100 µm
100 µm
b
rolling from the corners
unfolded area
completed tubes
1
2
3
4
200 µm
200 µm
200 µm
200 µm

Figure 4.4 | Microscopic images of (a) time-resolved propagation of the diffusion front into an active layer of p(NIPAM-BA)/p(MMA-BA) bilayer film ($th_{p(NIPAM-BA)}$ = 500 nm, $th_{p(MMA-BA)}$ = 300 nm, pattern size 200 µm x 1600 µm) and (b) formation of the tubes ($th_{p(NIPAM-BA)}$ = 1.2 µm, $th_{p(MMA-BA)}$ = 320 nm, pattern size 126 µm x 1327 µm; diameter of the tube d = 25 µm). Both samples were placed in PBS buffer (0.15 M, pH = 7.4) at the temperature of 37 °C. Swelling of the PNIPAM layer and rolling of the tubes started when the temperature was decreased down to 20 - 25 °C.

In bilayer pattern, diffusion of water into a PNIPAM-co-polymer layer is restricted from the top by the hydrophobic layer of the passive polymer and from the bottom by the substrate, so that swelling of an active layer starts from the edges of the photolithographically produced patterns. The propagation of the solvent diffusion front into a hydrogel can be observed microscopically as a change of interference colors, which reflect changes in the film thickness. First color changes are observed on the corners of the rectangular pattern and the diffusion front has an oval shape (Figure 4.4a). Indeed, since on the corners diffusion occurs from two edges simultaneously the swelling there is faster, than on the sides of the pattern. When PNIPAM hydrogel achieves a swelling degree sufficient to produce a bending moment great enough to overcome the adhesion of the polymer to the substrate, the bilayer detaches from the substrate and starts to bend. The detachment of the rectangular pattern starts from the corners, followed by detachment along the whole perimeter. Detached corners of the bilayer pattern bend (Figure 4.4b1) and after coming into contact with each other, they form tubes on the end sides of the pattern, while the middle part of the pattern still being attached to the substrate and unfolded (Figure 4.4b2). The rolling then propagates towards the middle of the pattern, resulting in a completed tube (Figure 4.4b3-4). Thus, the formation of the tubes is regulated both by inhomogeneous solvent diffusion into an active layer and by adhesion of the pattern to the substrate.

The kinetics of tubes rolling depends on the stiffness of the passive polymer. When soft PCL (Young's modulus is around 0.3 GPa[157]) was used as a hydrophobic layer, the rolling was very fast and, independently of the thickness of deposited PCL, was typically completed within 5 - 10 s. When stiff PMMA (Young's modulus is around 1.8 GPa[158]) was used, formation of the tubes was considerably slower and for passive layers thicker than 100 nm could take tens of minutes.

4.1.3.3 Diameter of self-rolled tubes

While for the bending of bimetal strips the Timoshenko formula[7] provides a theoretical basis for the prediction of bending curvature, it is not directly applicable for quantitative description of the polymer bilayer films, because mechanical properties of the hydrogels are changing during swelling. Since by now there is no theory that adequately models folding of polymer bilayers, the experimental investigation of the tube's formation process and resulting diameters is required.

The rolling curvature and therefore the diameter of the tube depends on a number of factors, such as stiffness of the polymers, degree of crosslinking and swelling degree of an active layer, the thickness of each layer and the thickness ratio[10]. The swelling degree of an active polymer varies depending on the crosslinking degree that is determined by the amount of crosslinker and intensity of UV exposure dose. This influence was investigated by Kumar *et al*. for poly(4-vinylpyridine)/polystyrene bilayers that were able to roll in acidic aqueous solutions due to swelling of poly(4-vinylpyridine) layer. It was found that the diameter of the rolled tubes continuously decreased with the increase of the exposure dose, until some constant diameter value was reached that obviously corresponded to the maximal achievable crosslinking degree[10]. In the present work, the parameters of the photolithographic process were chosen in such a way that the PNIPAM-co-polymer layer was crosslinked to a maximal degree possible for a given amount of crosslinker. Solvent characteristics can also influence swelling of the active polymer layer. Considering the fact that pH and ionic strength of cell culture media is close to these parameters of PBS buffer (0.15 M, pH = 7.4), the swelling behavior of PNIPAM layer and therefore diameters of the tubes are expected to be similar in both cases. However, it has to be taken into account that addition of bovine serum albumin into a culture medium can alter the swelling/deswelling behavior of the PNIPAM layer due to adsorption of proteins with polymeric hydrogel[159]. In this chapter, all diameter measurements have been done for tubes rolled in PBS buffer.

At the same time, one of the critical factors for folding is the nature of substrate and therefore the strength of polymer adhesion to it. Indeed, when adhesion of the polymer to the substrate exceeds the gain of energy due to bending, no rolling takes place. Remarkably, the diameter of the tubes produced on the silica wafer differed from that of the tubes produced on the glass slides, even though the substrate modification was the same (Chapter 3.2.5). However, the investigation of substrate influence on the tubes' diameter was beyond the present study, since the great majority of polymer bilayers were prepared using only one type of the substrate, namely hydrophilized silicon wafers.

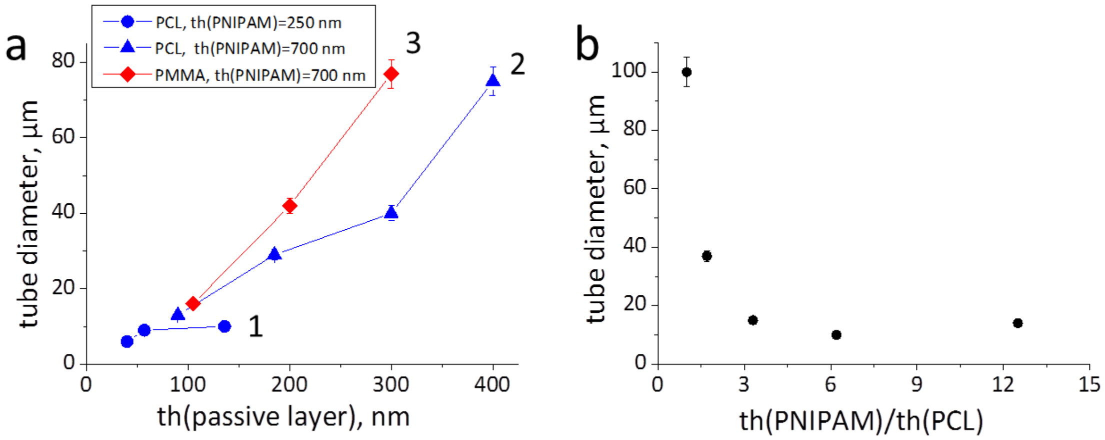

Figure 4.5 | Effect of the thickness of the polymer layers on the tube's diameter. (a) Dependence of the tube diameter on the thickness of the passive layer: (1) thickness of the PNIPAM layer is 250 nm, PCL is used as a passive layer; (2) thickness of PNIPAM is 700 nm, PCL is used as a passive layer; (3) thickness of the PNIPAM is 700 nm, PMMA is used as a passive layer. (b) Dependence of the tube diameter on the thickness ratio th(PNIPAM)/th(PCL) (thickness of both layers was varied). Thickness of the active layer is given for a dry state. When tubes with multiple revolutions were formed, the diameter of the first curl was taken as a characteristic value (inner diameter of the tube, d_{inn}).

The straightforward way to control the diameter of the tubes is to vary the thickness of both – active and passive – polymer layers, which can be easily done by choosing an appropriate deposition technique and concentration of polymer solution. It was found that for PNIPAM/PCL bilayers, the diameter of the tubes increased with the increase of the thickness of each layer (Figure 4.5a curves 1 and 2). In general, smaller thickness ratio of the PNIPAM and PCL layers (r = th(PNIPAM) / th(PCL)) led to a larger diameter of the formed tubes (Figure 4.5b). For the same layer thicknesses, the diameter of the tube almost doubled, when stiffer PMMA was used instead of PCL (Figure 4.5a curves 3). It is important to mention, that when a passive layer is much thicker or much thinner than an active layer, no rolling is observed. In the first case, the bending curvature is too large to be measured in experimental conditions. In the second case, the thin passive layer does not generate enough strain to cause the film to bend. Tubes with inner diameter ranging from 4 µm up to 100 µm were fabricated. Importantly, inner diameter was independent from the size of the bilayer pattern.

4.1.3.4 Rolling direction and tubes morphology

The most important factors that determined morphology of self-rolled PNIPAM/PCL and PNIPAM/PMMA tubes were the proportions of bilayer pattern (aspect ratio of pattern length to pattern width, *L/W*) and the relation of pattern width to the inner diameter (d_{inn}) of the tube (ratio of pattern width to the circumference of the first roll formed by the tube, W/C, $C = \pi d_{inn}$).

In general, for a rectangular bilayer, folding may occur in three different directions: (i) short-side rolling, when the rolling axis is parallel to the short side of the pattern, (ii) long-side rolling, when the rolling axis is parallel to the long side of the pattern and (iii) diagonal rolling, when the bending of the bilayer occurs from the corner towards the middle part of the pattern (Figure 4.6a). Several groups have investigated, both theoretically and practically, the preferential rolling direction depending on the aspect ratio of a rectangular pattern, consisting of inorganic materials[51-53]. So for example, Smela *et al*. found that short-side rolling was preferential and the preference increased with increase of the pattern *L/W* aspect ratio. The system under investigation was polypyrrole/gold bilayers, where stress-free films were first released from the substrate by underetching and then triggered to roll by homogeneous electrical actuation[51]. Contrary, Hsia and Li *et al*. demonstrated the preference of long-side rolling, when $In_xGa_{1-x}As/GaAs$ bilayers were progressively etched from a substrate[52]. Actuation mechanism of hydrogel-based films significantly differs from that of inorganic bilayers. As it was already mentioned above, actuation of polymer bilayers occurs from the edges of the pattern, and propagation of a solvent diffusion front inside the pattern is restricted by swelling kinetics of an active layer. At the same time, adhesion of the film to the substrate plays an important role. Therefore, actuation of a polymer bilayer is generally inhomogeneous.

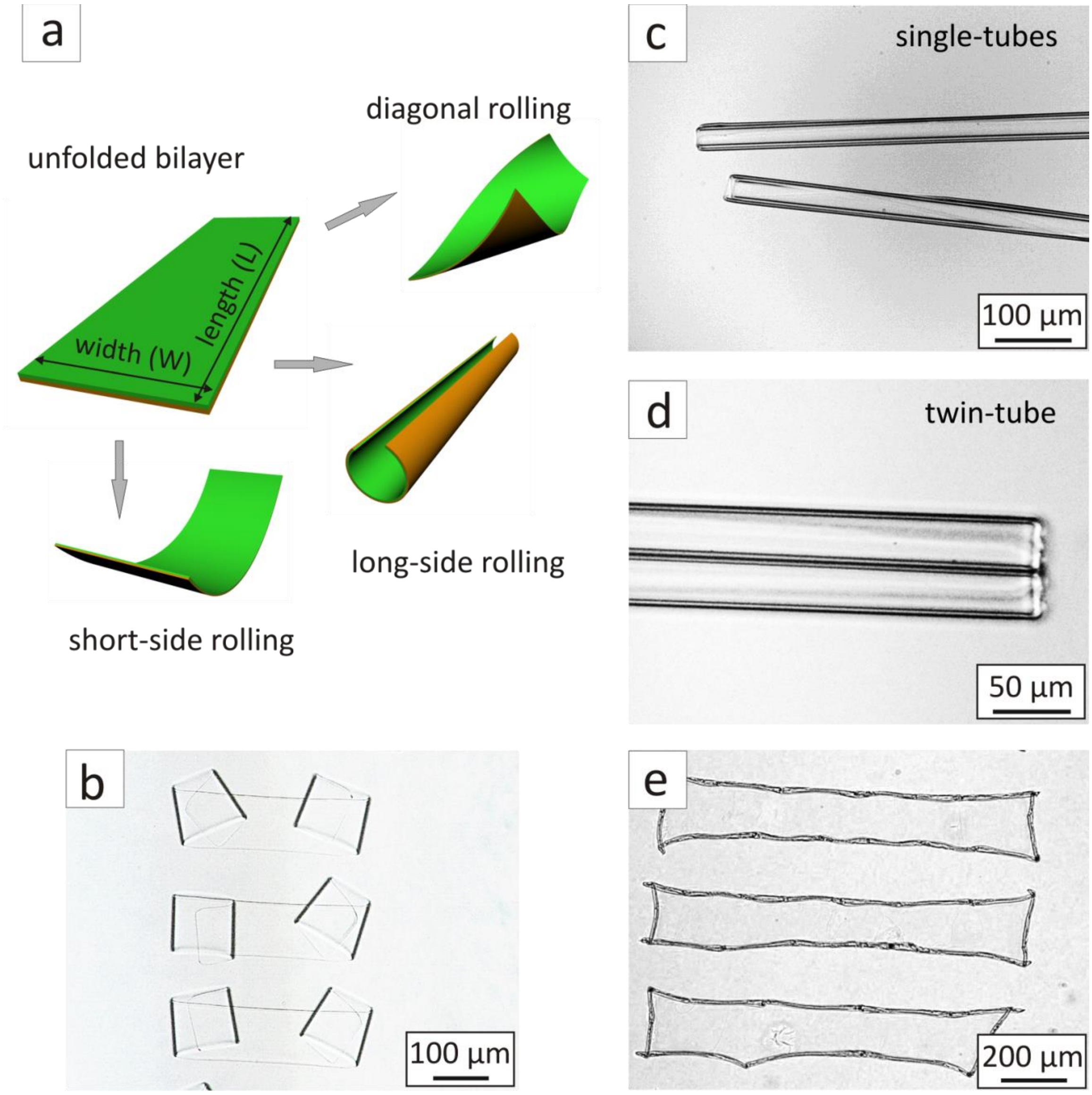
a
unfolded bilayer
width (W)
length (L)
diagonal rolling
long-side rolling
short-side rolling
b
100 µm
c
single-tubes
100 µm
d
twin-tube
50 µm
e
200 µm

Figure 4.6 | (a) Scheme of the possible rolling directions for rectangular bilayers: short-side rolling, long-side rolling and diagonal rolling. Microscopic images of the tubes, formed by rolling of p(NIPAM-BA) /p(MMA-BA) in PBS at 25 °C, demonstrating different morphologies: (b) short-side rolling, W/C = 0.27; (c) long-side rolling resulted in a single-tube formed by multiple revolutions, W/C = 2.5; (d) long-side rolling resulted in a twin-tube formed by multiple revolutions W/C = 3.8; (e) rolling form all sides, W/C = 15.

In the present work, patterns with high aspect ratio (L/W = 6 - 10) have been investigated. Depending on the ratio of the pattern width to the circumference of the first roll of the tube (*W/C*), tubes of different morphologies were obtained (Table 4.1). Bilayer patterns rolled from the short sides when *W/C* ratio was smaller than 0.5 (Figure 4.6b). Increase of *W/C* value led to the change of rolling scenario to the long-side rolling. When the width was comparable with the circumference, long-side rolled single-tubes were formed, wherein the number of revolutions increased upon the increase of the pattern width (Figure 4.6c). The number of revolutions could be estimated in assumption of compact formed rolls as $n \sim W/\pi d_{inn}$, and confirmed from microscopic images. Upon further increase of *W/C* ratio twin-tubes were formed (Figure 4.6d). As it was reported by Kumar *et al.,* asymmetric photo-patterning could be used to prevent formation of twin-tubes[10]. However, since in the present work the patterns were produced symmetrically and rolling from each of the long sides of the pattern was energetically equal, twin-tube morphology predominated when *W/C* exceeded a value of 3. In the case of twin-tubes, number of revolutions could be estimated as $n \sim W/2\pi d_{inn}$. Finally, rolling from all sides (Figure 4.6e) occurred when the pattern width was much larger than circumference ($W/C > 10$). Diagonal rolling was generally untypical for the PNIPAM/PMMA and PNIPAM/PCL systems and was only observed as an initial step of pattern detachment from the substrate, when bending started from the corners (Figure 4.4b2). Diagonal rolling immediately switched to a long-side one as soon as the perimeter of the bilayer film was detached from the substrate. Thus, for used bilayer patterns with high *L/W* aspect ratios long-side rolling generally dominated over the other scenarios.

Table 4.1 | Morphologies of self-rolled tubes in dependence on W/C ratio

W/C	Predominant morphology of the tubes	Figure
W/C < 0.5	Short-side rolling	Figure 4.6b
0.5 < W/C < 1	Long-side rolling, non-completed tubes	–
1 < W/C < 3	Long-side rolling, single-tubes, number of revolutions $n \sim W/\pi d_{inn}$	Figure 4.6c
W/C > 3	Long-side rolling, twin-tubes, number of revolutions of the each tube $n \sim W/2\pi d_{inn}$	Figure 4.6d
W/C > 10	All-side rolling	Figure 4.6e

Interestingly, for the same pattern dimensions, the rolling of film, detached from the substrate prior to actuation, occurs preferentially from the short-side or as a mixture of short-side rolling and diagonal rolling, i.e. in correspondence with the case of homogeneous actuation, described by Smela *et al.*[51] Theoretical considerations for the preferential rolling direction in conditions of inhomogeneous and homogeneous actuation as well as detailed experimental investigation of the rolling behavior of PNIPAM/PMMA and PNIPAM/PCL bilayers with great variety of *L/W* aspect ratios was reported by Stoychev *et al.*[160]

4.1.3.5 Reversibility of tube formation

Since swelling and collapsing of PNIPAM upon temperature changes is a fully reversible process, heating affects morphology of the formed microtubes. In particular, the microtubes produced by single revolution were able to unroll at elevated temperatures, i.e. when p(NIPAM-BA) was collapsed (Figure 4.7a). The kinetic of unrolling strongly depended on the stiffness of the passive polymer. For soft PCL rapid unfolding was completed within several seconds, while for PMMA the process took tens of minutes. The cycles of rolling-unrolling could be repeated many times. Interestingly, when a tube was detached from the substrate during unrolling, following decrease of temperature resulted in rolling according to the original scenario which was typical for inhomogeneous, but not homogeneous swelling of an active layer. That was probably due to residual stress in the bilayer that was not completely released upon unrolling and predetermined following cycles of bilayer folding.

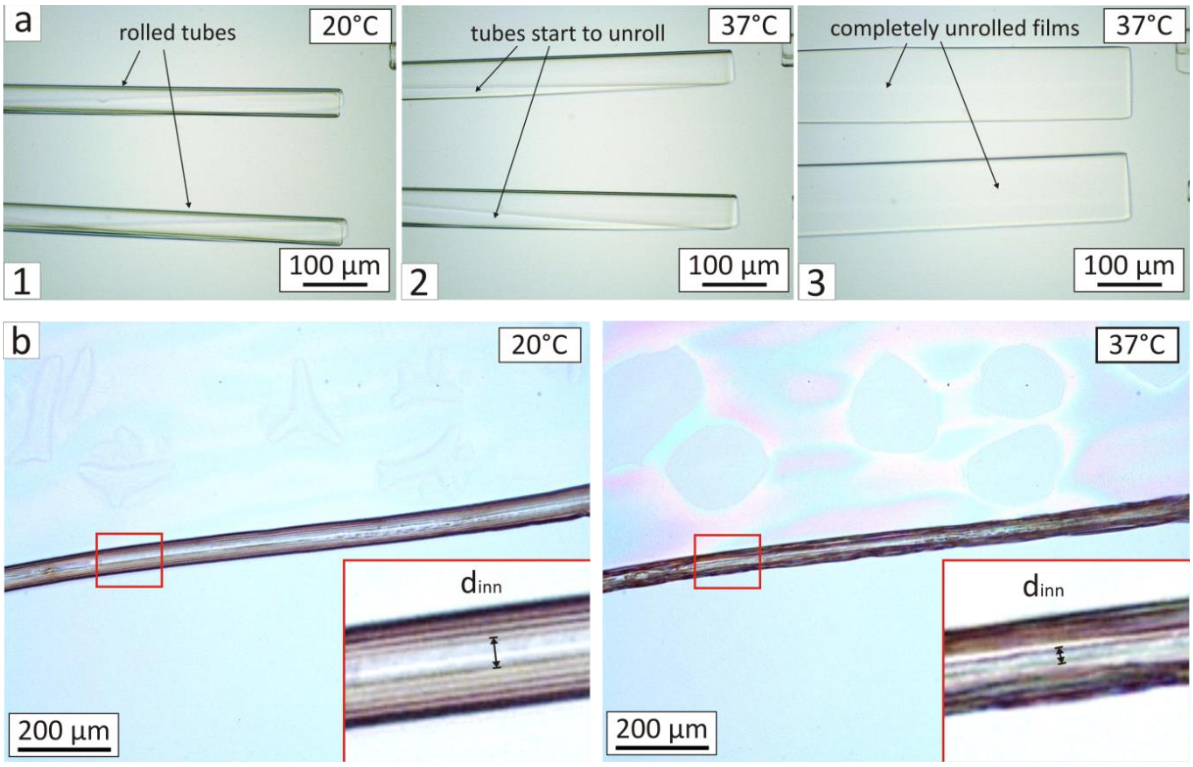

Figure 4.7 | Reversibility of tube formation: (a) microscopic images of the unrolling of the tubes, formed by one revolution (1), upon increase of the temperature above LCST of PNIPAM-co-polymer (2-3); (b) shrinking of the tube, formed by multiple revolutions, at elevated temperature: inner diameter decreased in 3 times.

Contrary, tubes formed by multiple revolutions were unable to unroll at elevated temperature, but either shrunk or kept their diameter constant (Figure 4.7b). Obviously, in this case collapse of PNIPAM layer did not lead to the unfolding of the film due to friction between the walls of the multiple rolls. Tubes, where passive layer was formed by PCL, decreased their inner diameter in 2 - 3 times at elevated temperatures. Stiffer PMMA layers resisted shrinking and for layers with thickness less than 300 nm, inner diameter decreased only in 1.3 - 1.5 times. For thicker PMMA layers, no changes in inner diameter of the tubes were observed. The lack of a theoretical model, describing reversible rolling of the responsive polymer bilayer, does not allow quantitative prediction of the degree of shrinking in each particular case.

4.1.3.6 Encapsulation and release of microparticles inside the tubes

The possibility to encapsulate micro-objects using self-rolled thermo-responsive tubes was investigated using 10 µm sized SiO_2 particles. For this, microparticles were deposited from their aqueous dispersion on the top of a patterned polymer bilayer film at elevated temperature when p(NIPAM-BA) was collapsed and the bilayer was unfolded (Figure 4.8a1). Decrease of the temperature triggered the formation of the tubes accompanied by the entrapment of the microparticles (Figure 4.8a2).

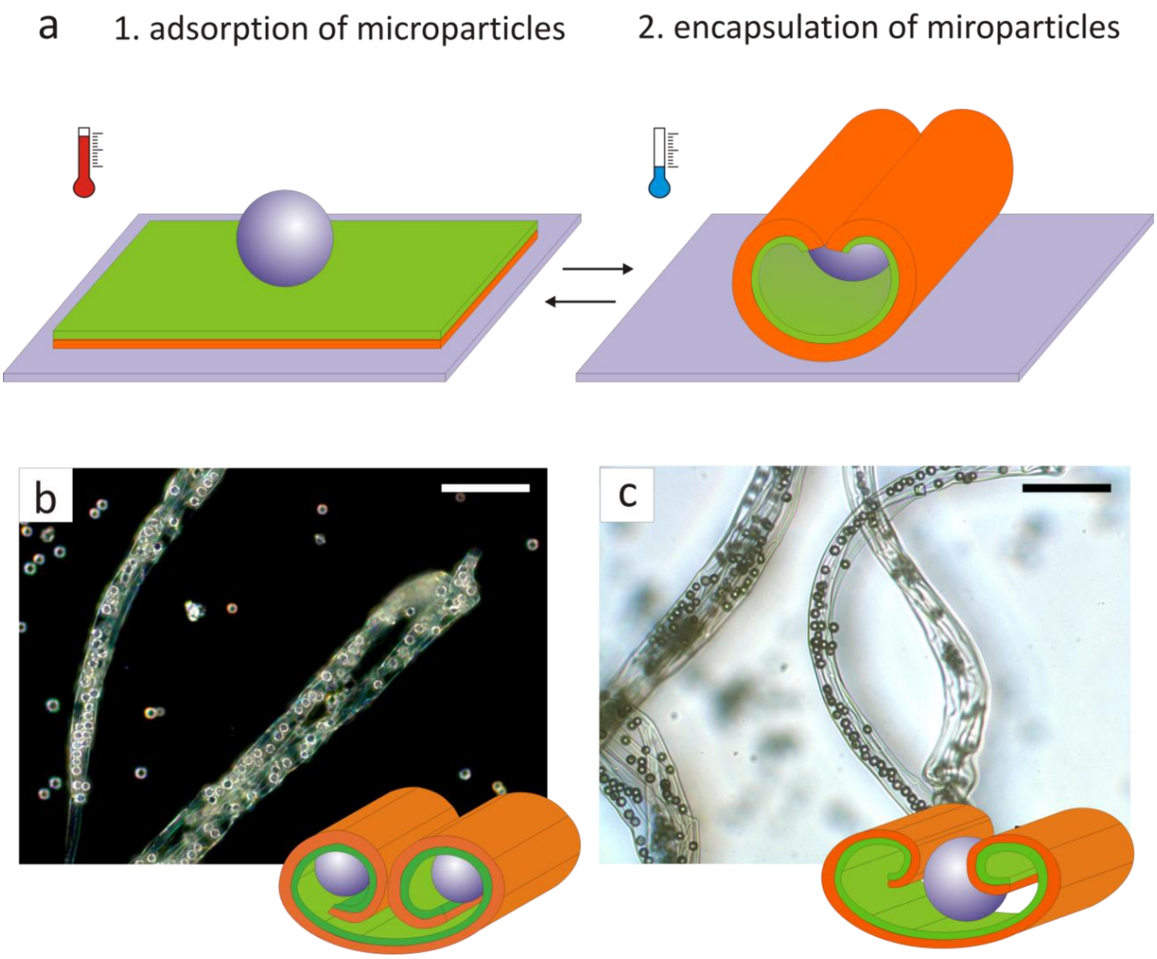
a
1. adsorption of microparticles
2. encapsulation of miroparticles
b
c

Figure 4.8 | Encapsulation of the microparticles inside self-rolled tubes: (a) scheme of encapsulation; (b) microscopic image and scheme of the particles encapsulated inside the rolled tube; (c) microscopic image and scheme of the particles entrapped between two tubes of the twin-tube. Scale bar is 100 µm.

Depending on the inner diameter of the tube two mechanisms of particle entrapment were observed. When the diameter of the forming tubes was comparable with the size of the particles and larger, particles were encapsulated inside the rolls (Figure 4.8b). When the inner diameter of the tubes was smaller than the size of the particles, particles were mainly entrapped between the twin-tubes (Figure 4.8c). The latter scenario was generally undesired, since this type of entrapment cannot be considered an encapsulation.

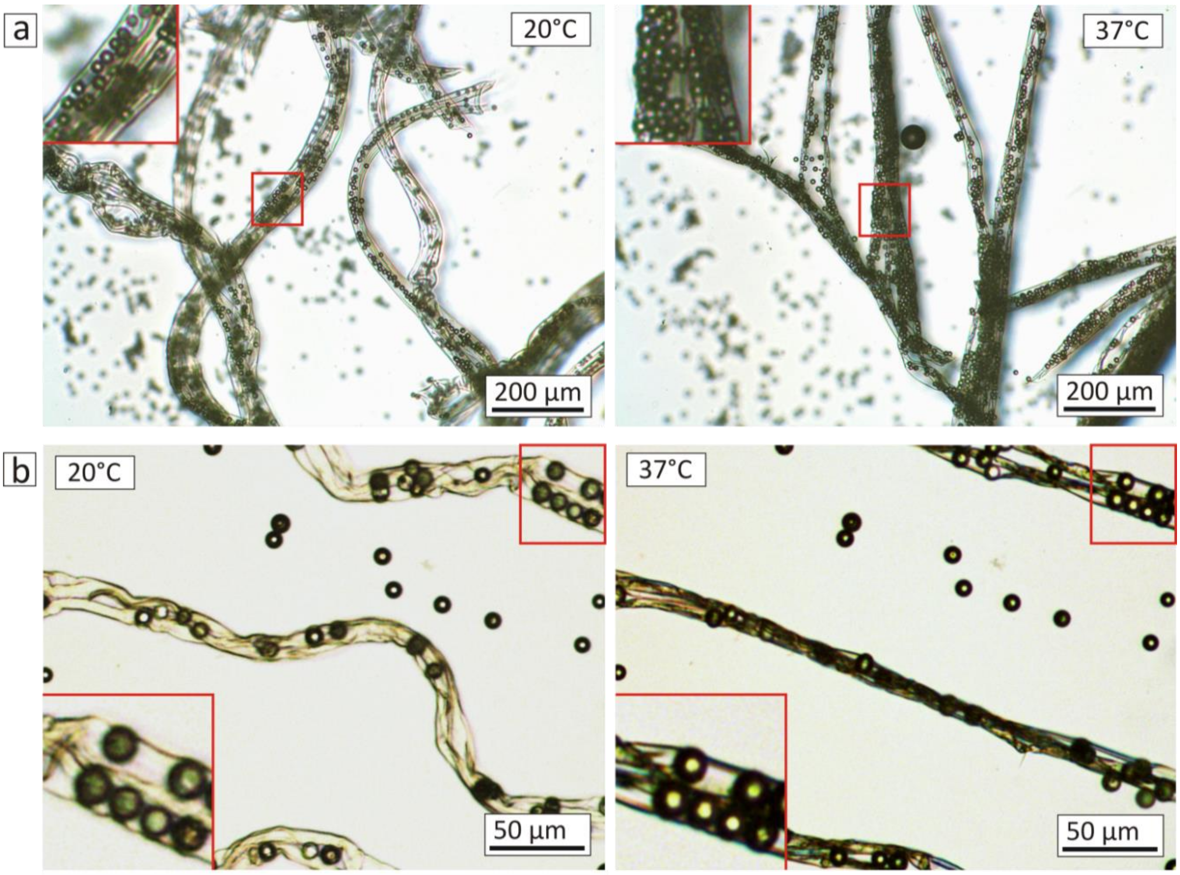

Figure 4.9 | Possibility to release encapsulated particles from PNIPAM-based tubes: (a) when self-rolled tubes are formed by one revolution, particles encapsulated inside the tubes can be released upon temperature increase above LCST; (b) when tubes are formed by multiple revolutions, encapsulated particles cannot be released and are squeezed inside the tubes.

Particles encapsulated inside one-revolution rolls were able to leave the microtubes at the temperature above LCST, when the thermoresponsive polymer was collapsed and tubes were unrolled (Figure 4.9a). On the other hand, particles encapsulated inside the rolls, produced by multiple revolutions, could not be released at elevated temperature due to inability of such microtubes to unroll, and remained entrapped inside the microtubes (Figure 4.9b). Since used glass particles were hard, no deformation occurred upon squeezing. Related videos can be found in online supplementary information of Ref[161].

4.1.3.7 Design strategy to produce PNIPAM-based self-rolled tubes with desired properties

Based on the described investigations of PNIPAM/PCL and PNIPAM/PMMA bilayers, we offer a design strategy which can help to choose parameters of the bilayer as well as pattern dimensions in order to produce self-rolled microtubes with desired properties (Figure 4.10).

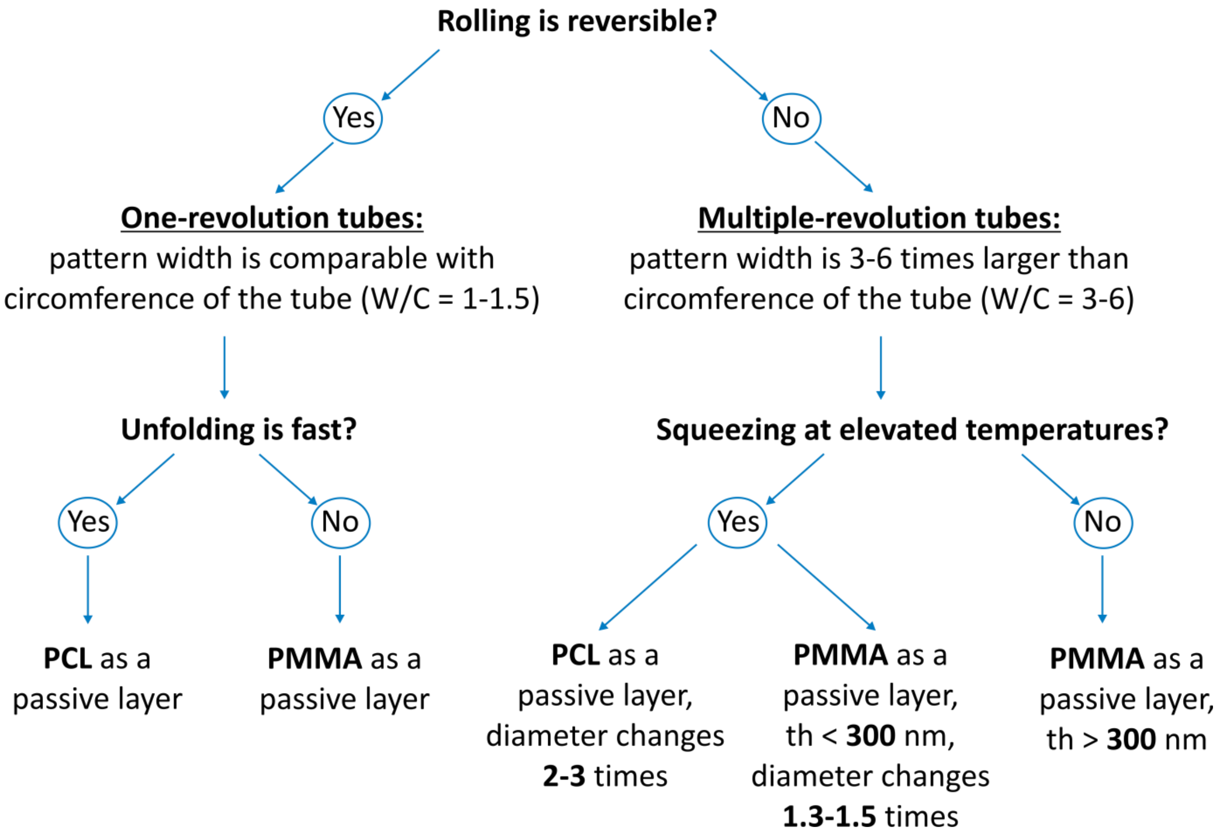
Rolling is reversible?
Yes
No
One-revolution tubes:
pattern width is comparable with circomference of the tube (W/C = 1-1.5)
Multiple-revolution tubes:
pattern width is 3-6 times larger than circomference of the tube (W/C = 3-6)
Unfolding is fast?
Squeezing at elevated temperatures?
Yes
No
Yes
No
PCL as a passive layer
PMMA as a passive layer
PCL as a passive layer, diameter changes 2-3 times
PMMA as a passive layer, th < 300 nm, diameter changes 1.3-1.5 times
PMMA as a passive layer, th > 300 nm

Figure 4.10 | Design strategy to obtain self-rolled tubes with desired properties.

4.1.3.8 Encapsulation of HeLa cells

The design strategy presented above was used to perform reversible and irreversible encapsulation of mammalian cells. For this p(NIPAM-BA)/p(MMA-BA) bilayers were used. Prior to cell encapsulation, samples with patterned bilayers were placed for several hours in vacuum oven at the temperature of 50°C to remove the rests of the solvents.

The HeLa Kyoto GFP-tub H2B-mcherry cells were supplied by our collaborators Dr. S. Sanchez and B. Koch from Leibniz Institute for Solid State and Materials Research, Dresden (IFW Dresden). These cells possess fluorescently tagged histone, H2B-mcherry (red fluorescence), and mEGFP-α-tubullin (green fluorescence) that allow visualization of nuclei and cytoskeleton respectively and permit evaluation of cell viability without performing a staining procedure. Cells were prepared in the following way: HeLa Kyoto GFP-tub H2B-mcherry cells were grown as a monolayer in DMEM+GlutaMAX^{TM} (gibco) supplemented with 10 % fetal bovine serum (FBS, Sigma-Aldrich), 100 units per milliliter (U/ml) of penicillin, 100 µg/ml streptomycin (gibco), 1 % NEAA (gibco), 0.5 mg/ml geneticin (gibco) and 0.5 µg/ml Puromycin and were subcultued according to standard cell culture protocols. To create a cell suspension the cells were washed once with PBS (gibco), detached using a 0.25 % Trypsin-EDTA solution (Sigma) and resuspended in cell culture medium.

First, the adhesion behavior of the cells on the p(MMA-BA) layer was investigated. For this, cells were seeded from their dispersion in culture medium on the top of the photocrosslinked p(MMA-BA) layer, grafted to the glass substrate, that was fixed in a 6 cm Petri dish. The samples were then incubated at a temperature of 37 °C under 5 % CO_2 atmosphere and the growth of the cells was observed under microscope. It was found that after 8 h cells were still rounded and not adhered to the polymer which is obviously due to the lack of cell adhesion molecules on the surface of non-modified polymer (Figure 4.11a). However, after 24 h of incubation, cells started to adhere to the material surface that could be caused by adsorption of protein from FBS on the polymer (Figure 4.11b). After five days of cultivation, cell layer covered approximately 70 % of the sample area (Figure 4.11c). Cells demonstrated normal morphology and high-graded cell-cell interactions. These results represent undisturbed cell proliferation, migration and maturation, indicating that no toxic effects of the used material could be seen after this period and using this method. Faster cell adhesion could be achieved by functionalization of PMMA with fibronectine.

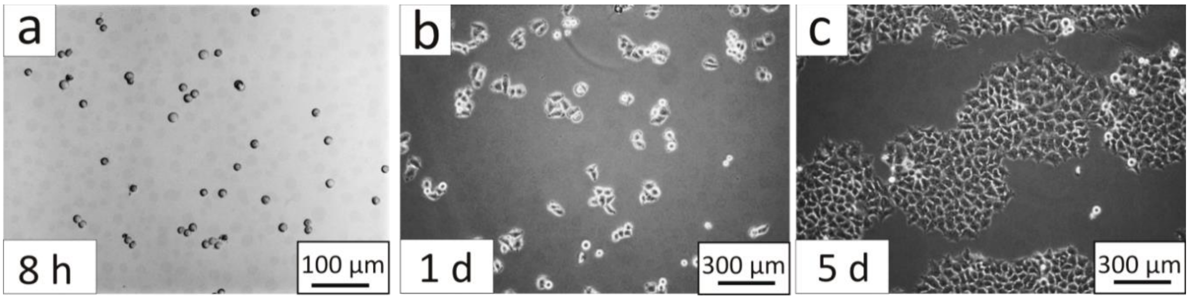

Figure 4.11 | Microscopic images of HeLa cells after (a) 8 h, (b) 24 h and (c) 5 days of growing on p(MMA-BA) film (made by Britta Koch, IFW Dresden).

HeLa cells were then encapsulated inside self-rolled p(NIPAM-BA)/p(MMA-BA) tubes of different diameters. For this, a patterned bilayer, prepared on a glass substrate, was fixed in a Petri dish. Cells were seeded from their dispersion in a culture media with concentration of around $1.5*10^5$ cells/ml. The sample was incubated for 10 - 20 min at 37 °C to allow cells to settle down on the top of the unfolded polymer bilayer film. Rolling of the tubes and simultaneous cell encapsulation was triggered by the decrease of the temperature down to 20 - 25 °C.

Contrary to the glass microparticles, cells can be squeezed. This led to the possibility to encapsulate HeLa cells inside the microtubes with diameters smaller than the diameter of rounded cells, which was 15 - 17 µm. So for example, encapsulation in tubes with diameter 8 µm resulted in both types of cell entrapment: between the rolls of the twin-tube (Figure 4.12a1) and inside the rolls of the formed tube (Figure 4.12a2). However, in the last case, severe and fast squeezing led to the apoptosis of the entrapped cells. Cells survived encapsulation when the diameter of the tubes was larger than 15 µm (Figure 4.12b-c). Obviously, the amount of the cells inside the tube can be regulated by varying the density of cell seeding.

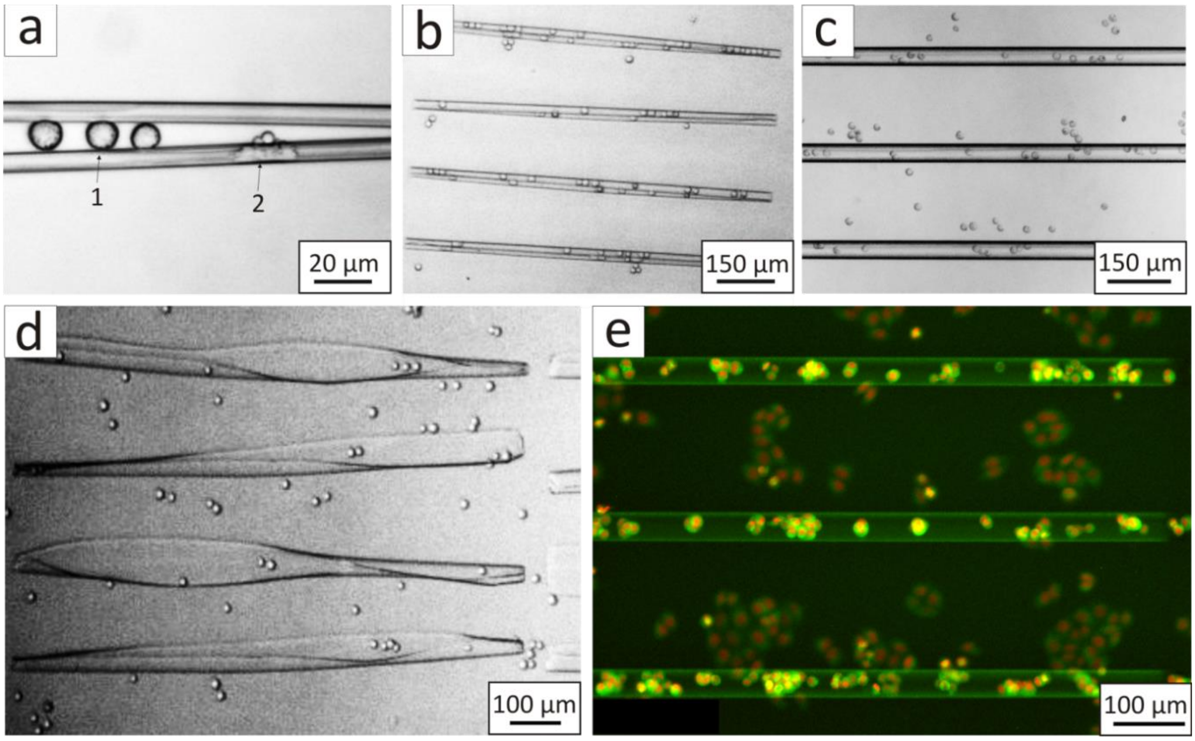

Figure 4.12 | Microscopic images of HeLa cells encapsulated in self-rolled polymer tubes. (a) Tube diameter 7 - 8 µm: cells entrapped between the rolls of twin-tube (1) and squeezed apoptotic cell entrapped inside the roll (2) ($th_{p(NIPAM-BA)}$ = 540 nm, $th_{p(MMA-BA)}$ = 60 nm, pattern size 90 µm x 948 µm, culture media, 25 °C); (b) cells encapsulated in tube with diameter 14 - 15 µm have a close contact with tube walls, some of the cells have slightly elongated shape ($th_{p(NIPAM-BA)}$ = 540 nm, $th_{p(MMA-BA)}$ = 80 nm, pattern size 90 µm x 948 µm, culture media, 25 °C); (c) freely located cells in tube with diameter 30 - 35 µm ($th_{p(NIPAM-BA)}$ = 1.2 µm, $th_{p(MMA-BA)}$ = 350 nm, pattern size 90 µm x 948 µm, culture media, 25 °C); (d) release of encapsulated cells upon increase of the temperature up to 37 °C ($th_{p(NIPAM-BA)}$ = 1.2 µm, $th_{p(MMA-BA)}$ = 300 nm, pattern size 90 µm x 948 µm, culture media, tube diameter at 25 °C 25 -30 µm); and (e) fluorescent image of HeLa cells, cultured inside self-rolled p(NIPAM-BA)/p(MMA-BA) microtubes for 24 h, where green fluorescence depicts cytoskeleton and red one – nuclei, indicating a good viability of encapsulated cells ($th_{p(NIPAM-BA)}$ = 1.2 µm, $th_{p(MMA-BA)}$ = 360 nm, pattern size 126 µm x 1327 µm, culture media, 37 °C) (together with Britta Koch, IFW Dresden).

When the polymer bilayer was designed in such a way that unrolling was possible, increase of the temperature up to 37 °C led to the unrolling of the tubes and release of encapsulated cells. Since the procedure took less than 1 h, cells were not adhered to the inner p(MMA-BA) wall of the tube and could freely leave unfolded bilayer (Figure 4.12d).

The possibility to cultivate encapsulated HeLa cells was investigated using irreversibly rolled tubes with 35 µm diameter (Figure 4.12e). After encapsulation that was performed within 10 - 15 min at 25 °C, samples were incubated at a temperature of 37 °C under 5 %

CO_2 atmosphere for 1 day. Cells which were not encapsulated were used as reference. Microscopic observation demonstrated that cells survived and proliferated both inside and outside of the tubes at least within 24 h. The reproduction behavior was equal in both cases: the number of cells increased fourfold and the cells at different stages of the cell cycle could be detected. HeLa cells demonstrated normal morphology, however, while cells outside were adhered to a substrate and grew flat, cells in the tube formed spheroid-like agglomerates. Due to the volume restriction, the cell density in the tubes was much higher than on the substrate. Nevertheless, within the observed interval of time no saturation of the growth rate was observed. These observations indicate that cells were not damaged during the encapsulation procedure and could obtain sufficient amount of nutrition within the tube.

4.1.3.9 Self-rolled tubes with porous walls

Inner walls of self-rolled polymer tubes, described above, consist of hydrophobic polymer and thus are water impermeable. Therefore the exchange of the media inside the tube occurs only through its open ends. This spatially inhomogeneous diffusion can be used for example to create 3D chemical patterning, when drug encapsulated inside the tube is inhomogeneously released from the open ends[162]. On the other hand, when tubes are used for cell culture scaffolding, the limitation of media permeability can lead to the lack of nutrition and accumulation of waste in the middle part of the tube. It can be especially essential when cells in confinement are investigated, and the diameter of the tube is comparable with the size of the cells. Media exchange may be also hindered when a big amount of cells is encapsulated, reducing the possibility for free diffusion inside the tube. In such situations, design of the tubes with porous walls, allowing the diffusion of the media through the bilayer, is required.

Here, the first results on the fabrication of polymer self-rolled tubes with porous walls are demonstrated. Preparation of the bilayers was done through a standard fabrication procedure by application of a specially designed photomask. After development, non-crosslinked round-shaped areas within the rectangular bilayer pattern formed pores through the whole depth of the film. The diameter of the pores was 7 - 10 µm and their location is shown in Figure 4.13a. One can expect that the introduction of perforating pores within the film may influence swelling and rolling behavior of the bilayer film. Indeed, in this case swelling of an active layer started not only from the edges of the pattern, as it was discussed previously, but also from the edges of the pores (Figure 4.13b). However, since the number of pores was considerably small, activation was still inhomogeneous and more intensive from the perimeter of the pattern. For the investigated pattern size (300 µm x 1800 µm) and W/C ratios (1; 3.5; 9), the long-side rolling scenario remained predominant (Figure 4.13c). At the same time, the introduction of pores, by all other parameters being equal, resulted in the increase of the inner diameter of the formed tubes, for example, from 13 µm for tubes without pores up to 27 µm for tubes with porous walls. This increase can be caused by the decrease of the bilayer rigidity.

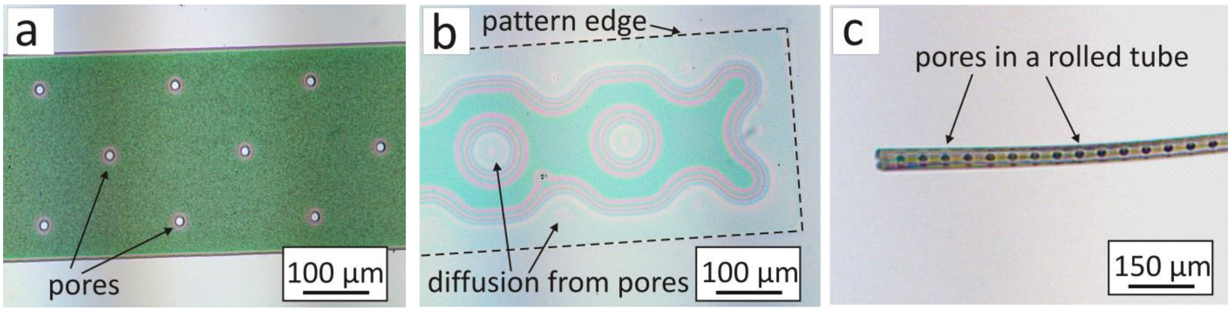

Figure 4.13 | Fabrication of self-rolled tubes with porous walls. Microscopic images: (a) Dry p(NIPAM-BA)/p(MMA-BA) bilayer film after UV-crosslinking and development: round-shaped pores, going through the whole thickness of the polymer film, are introduced within the rectangular pattern; (b) Interference colors indicate the propagation of the solvent diffusion front into an active layer of the p(NIPAM-BA)/p(MMA-BA) bilayer film both from the perimeter of the pattern and from the edges of the pores ($th_{p(NIPAM-BA)} = 500$ nm, $th_{p(MMA-BA)} = 300$ nm, pattern size 300 µm x 1800 µm, pores diameter 7 - 10 µm; PBS buffer 0.15 M, pH = 7.4); (c) Formed microtube with porous walls ($th_{p(NIPAM-BA)} = 600$ nm, $th_{p(MMA-BA)} = 160$ nm, pattern size 300 µm x 1800 µm, pores diameter 7 - 10 µm; tube diameter 10 µm).

Preliminary results have shown the possibility to produce polymer self-rolled tubes with porous walls using standard photolithographic procedure. However more detailed investigation of the influence of pores (their size, amount and location within the film) on the swelling and rolling behavior of the bilayer as well as on the diameter of formed tubes is needed.

4.1.3.10 Magneto-sensitive microtubes (manipulation in magnetic field)

Next, the possibility to manipulate microtubes using a magnetic field was tested. For this, superparamagnetic iron oxide (Fe_3O_4) nanoparticles coated with oleic acid[137] were admixed in the thermoresponsive p(NIPAM-BA) layer. Tubes were loaded with glass microparticles as described in section 4.1.3.6, and their water dispersion was placed into a 6 cm Petri dish (Figure 4.14a). It was found, that freely floating particle-loaded microtubes started to move in the direction of the external permanent magnet, placed at one side of Petri dish. The direction of the microtubes flow can be immediately switched by changing the position of the magnet, thus demonstrating the possibility to manipulate the microtubes using a magnetic field. Related video material can be found in the online supplementary information of Ref[161].

An alternative approach was reported by Sanchez and Mei *et al.*: they integrated a ferromagnetic (Fe) layer into the tube's wall in order to allow magnetic control over the motion direction of self-propelled catalytic microtubes[29].

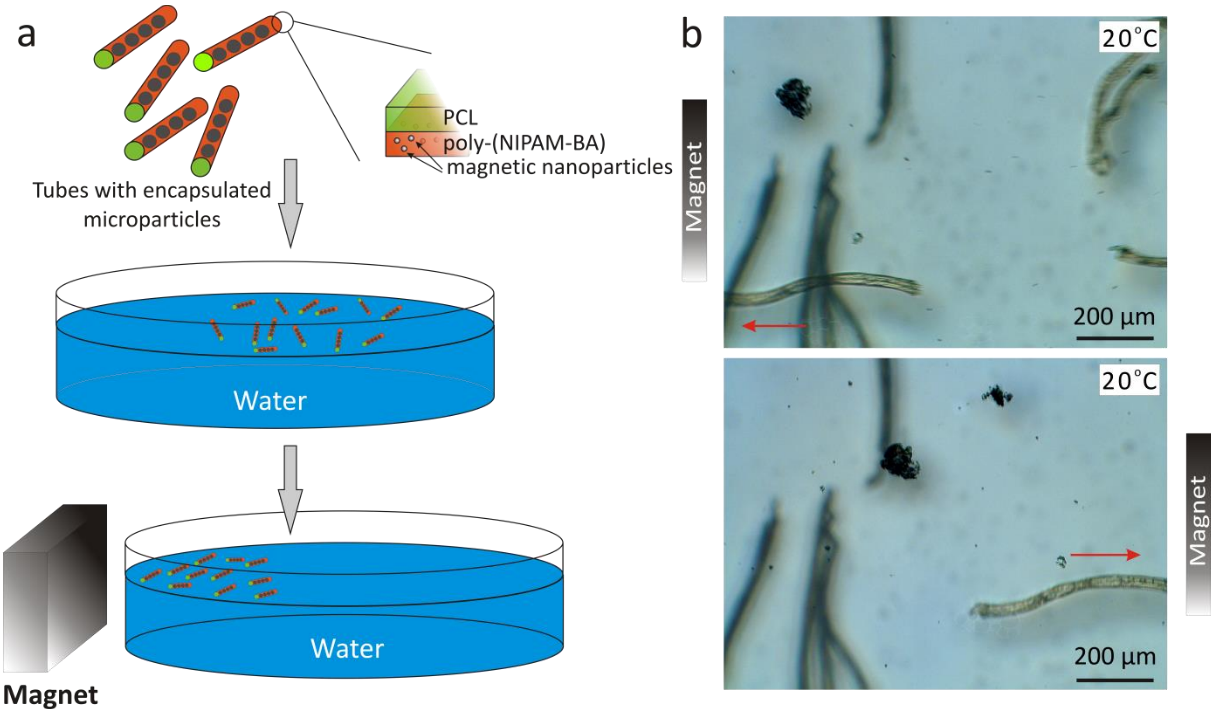

Figure 4.14 | Magneto-sensitive microtubes. (a) Scheme of the experiment. (b) Microscopy snapshots of microparticle-loaded microtubes containing superparamagnetic iron oxide nanoparticles flow into the applied magnetic field. Arrows show the direction of flow.

4.1.4 Conclusions

In this chapter, the fabrication of thermoresponsive self-rolled tubes was described. Rolling occurred within 1 - 10 min due to reversible swelling of PNIPAM-co-polymer at the temperature below LCST. As a passive layer biocompatible p(MMA-BA) or biocompatible and biodegradable polycaprolactone were used.

It was demonstrated that tube formation can be both reversible and irreversible depending on the morphology of the tubes. Tubes formed by one revolution unroll at the temperature above the LCST of PNIPAM, while tubes formed by multiple revolutions are not able to unroll and either keep a constant inner diameter or shrink upon increase of the temperature. Both rolling and unrolling and therefore capture and release take place in conditions close to physiological ones (in physiological buffer environment and at temperature in the range of 20 - 37 °C).

Controlled capture of micro-sized objects using PNIPAM-based self-rolled tubes was demonstrated on the example of glass microparticles and mammalian (HeLa) cells. Cells encapsulated in irreversibly formed tubes grew well at least within 1 day of incubation, showing suitability of such tubes for cell scaffolding. Reversible tubes were capable of triggered release of entrapped cells and microparticles. Moreover, incorporation of magnetic nanoparticles in the thermoresponsive layer provided sensitivity of the microtubes to a magnetic field. This could be used for controlled cell delivery.

The main advantages of reported p(NIPAM-BA)/p(MMA-BA) and p(NIPAM-BA)/PCL tubes in comparison to other self-folding systems reported to be applicable for cell encapsulation[34, 36, 65] are (1) the improved biocompatibility and biodegradability, (2) the possibility to release encapsulated objects as well as (3) the ability to manipulate them using magnetic field.

4.2 Solvent-responsive bilayer systems based on polysuccinimide

4.2.1 Objectives

In the previous chapter, thermo-responsive PNIPAM/PCL and PNIPAM/PMMA systems were discussed. These systems can be successfully used for capture and release of micrometer sized objects in response to the change of temperature in the physiological range between 25 °C and 37 °C. However, due to non-biodegradability and poor biocompatibility of poly(N-isopropylacrylamide), tubes based on this polymer can hardly be used for the fabrication of tissue engineering scaffolds. In this chapter, the fabrication of fully biodegradable solvent-responsive self-rolled tubes is reported. The tubes are based on cross-linked polysuccinimide/polycaprolactone bilayers. These polymers are biocompatible, biodegradable, produced industrially, and were already approved for biomedical purposes[18, 163, 164]. Both polycaprolactone and polysuccinimide are hydrophobic and intrinsically water-insoluble. Polysuccinimide, however, is able to hydrolyze in physiological buffer environment at room temperature, yielding water-swellable biodegradable polyaspartic acid[165]. Swelling of polyaspartic acid leads to the rolling of tubes and encapsulation of yeast cells.

4.2.2 Experimental part

Materials. As an active polymer polysuccinimide (PSI), synthesized by acid-catalyzed thermal polycondensation of L-aspartic acid (Chapter 3.2.4), was used. The passive layer consisted of polycaprolactone (PCL) (M_n = 70 000 - 90 000 g/mol).

Fabrication of the polymer bilayers and self-rolled tubes. Thin films (70 - 400 nm) of PSI containing 1 wt. % of 4-hydroxybenzophenone with respect to the weight of dry polymer were deposited on a silicon wafer from DMF solution. Next, thin films (70 - 500 nm) of PCL containing 5 wt. % of 4-hydroxybenzophenone were spin-coated from toluene solution, on the top of PSI film. Parameters of film preparation are listed in the Table 3.1. The solution concentration for polymer deposition was 4 - 14 % for PSI and 2 - 5 % for PCL. The benzophenone derivatives that generate free radicals upon irradiation with UV light[166] have already been applied for photocrosslinking of biodegradable biomaterials[167]. The polymer bilayers were patterned using photolithography through a mask with pattern sizes of 200 µm x 1600 µm or 300 µm x 1800 µm. Detailed conditions of photolithography are given in Chapter 3.3.2. After illumination with UV light, the non-crosslinked polymers were removed by sequential rinsing in chloroform and DMF where PCL and PSI are respectively soluble. To avoid cytotoxicity, the rest of the DMF was removed by rinsing in a large amount of ethanol. The crosslinked polymers are expected to be biodegradable, since they still contain the carbon oxygen and carbon nitrogen bonds of the original polymers.

The self-rolling tubes were fabricated by long-time exposure (24 h) of the patterned bilayer in PBS (0.15 M, pH = 7.4).

Experiments with yeast cells. Yeast cells encapsulated inside the tube were incubated in Dulbecco's modified Eagle's medium: Nutrient Mixture F-12. All experiments with yeast cells were carried out at 25 °C.

4.2.3 Results and discussions

4.2.3.1 Swelling of PSI thin films in an aqueous environment

First the swelling of photocrosslinked PSI thin film in physiological buffer (PBS 0.15 M, pH = 7.4) at T = 25°C was investigated using null-ellipsometry (Chapter 3.1.1). Since pH of culture media is often very close to pH of PBS, the swelling behavior of PSI is expected to be similar in both cases. Polysuccinimide is hydrophobic and an intrinsically water-insoluble polymer, but in physiological environment, it hydrolyzes slowly, yielding water-swellable biodegradable polyaspartic acid[168]:

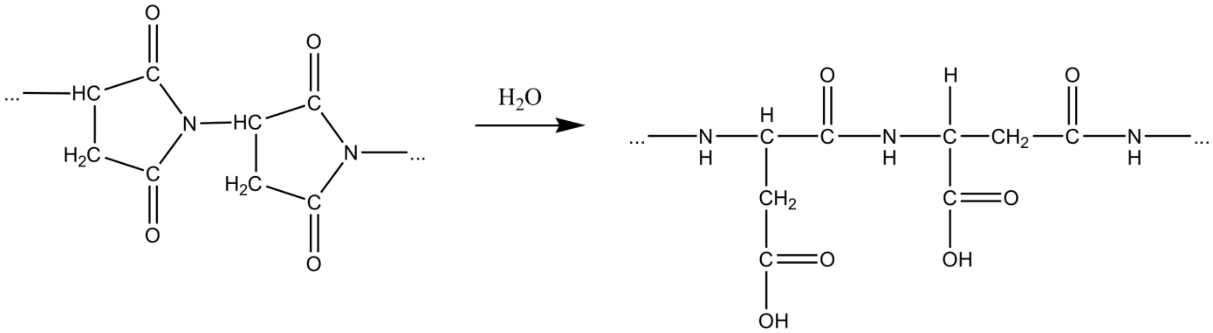

It was found that the thickness of PSI film, deposited on APS-modified silica wafer, increased by approximately 8 - 10 times (from 35 nm to 283 nm) after 24 hours of incubation in PBS buffer. This swelling was obviously due to the formation of polyaspartic acid during a heterogeneous hydrolysis reaction. Considering the fact that the PSI layer is homogenously crosslinked, the final degree of swelling (Formula 3.2) of the thicker layers is expected to be similar: 8 - 10.

The swelling of the PSI film had a step-like character (Figure 4.15a). The thickness of the polymer layer increased slightly during the first period (0 - 9 h) and strong swelling started after 8 - 9 h of incubation in the buffer. The swelling was completed after 24 h. The observed step-like swelling curve is typical for autocatalytic reactions and is most probably due to diffusion-limited penetration of water in the hydrophobic PSI layer. In the beginning, water starts to diffuse slowly into the hydrophobic PSI layer hydrolyzing it. As soon as a threshold amount of succinimide groups is hydrolyzed, the PSI layer starts to swell to a higher degree due to repulsion between the formed negatively charged carboxylic groups. As a result, the diffusion of water in the polymer layer increases. That leads to a faster hydrolysis of the remaining succinimide groups. Obviously, such swelling behavior is spontaneous and irreversible.

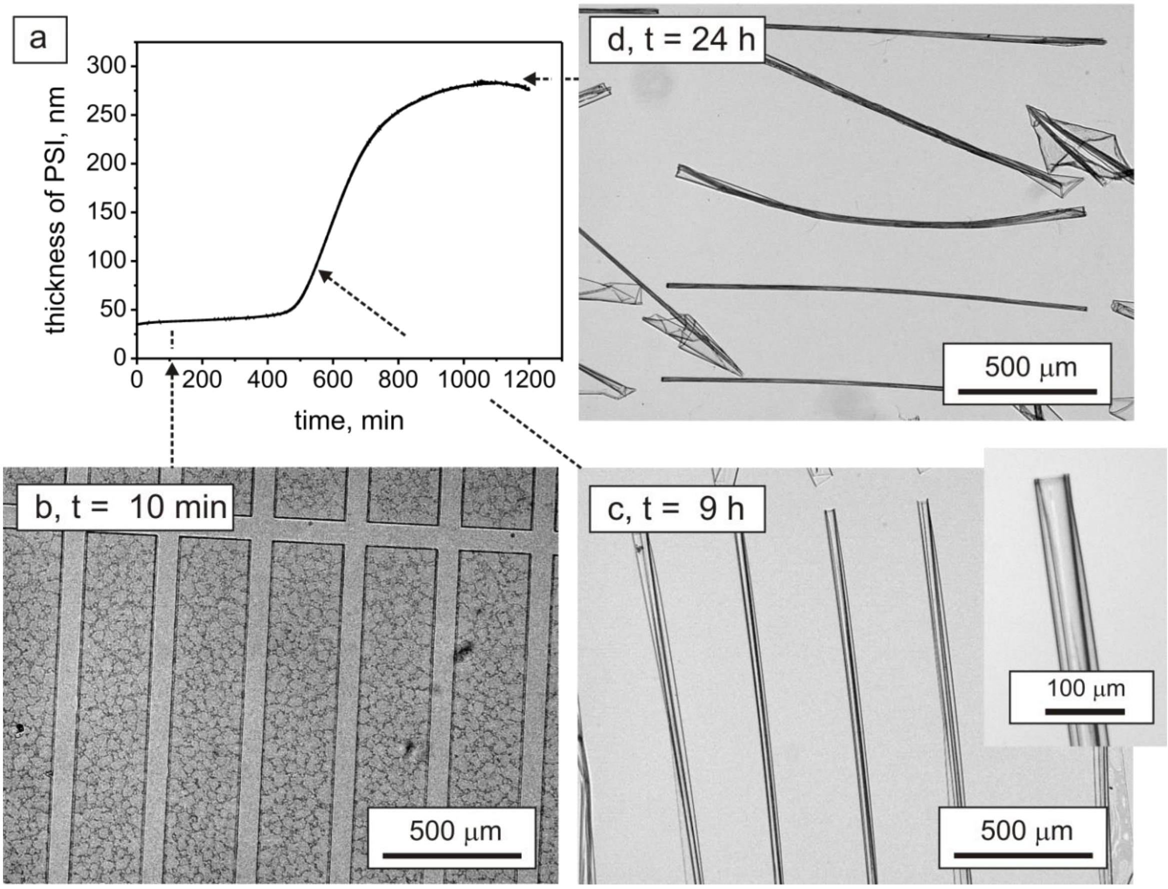

Figure 4.15 | (a) Swelling of photocrosslinked polysuccinimide film (thickness in a dry state 35 nm) in PBS buffer (0.15 M, pH = 7.4) at T = 25°C. Morphologies of self-rolling tubes (th(PSI) = 200 nm; th(PCL) = 86 nm, pattern 300 μm x 1800 μm) on the different stages of rolling: (b) after 10 min of incubation – unfolded film; (c) after 9 h of incubation – incompletely rolled tubes (d = 55 μm); (d) after 24 h of incubation – completed tubes (d = 25 μm).

4.2.3.2 Formation of the tubes

Next, the formation of solvent-responsive self-rolled polymer tubes in aqueous environment was investigated. Polymer bilayers were prepared on a silicon substrate using sequential deposition of PSI and PCL, followed by photolithographic patterning.

Produced PSI/PCL bilayers were incubated in PBS (I = 0.15 M, pH = 7.4). The bilayers, which appeared patchy due to the crystalline PCL, remained unchanged during the first 9 h at T = 25°C (Figure 4.15b). The rolling started after 9 h of incubation, which corresponds to the beginning of swelling of PSI thin film, and incompletely rolled tubes (d = 55 μm, Figure 4.15c) were formed. Further incubation led to a shrinkage of the tubes and a decrease of their diameter (d = 25 µm, Figure 4.15d). The formed tubes could be easily detached from the silicon substrate due to the swelling of the polyaspartic acid (hydrolyzed PSI). The decrease of the tube diameter with time is due to increasing of the swelling degree of the PSI layer and is in qualitative agreement with the Timoshenko equation[7]. According to the Timoshenko equation, higher stress in the film, which is proportional to the swelling degree, leads to a smaller diameter of the tubes (see Formula 2.1). The step-like rolling behavior of PSI/PCL bilayer correlates very well with the step-like character of swelling of the PSI layer. Since swelling of PSI is due to hydrolysis and therefore irreversible, the tube formation is also irreversible.

The delayed hydrolysis of PSI films, and therefore delayed rolling, can be considered as an advantage because cells might have enough time to adhere to the surface of the polymer bilayer and spread before the tube is formed.

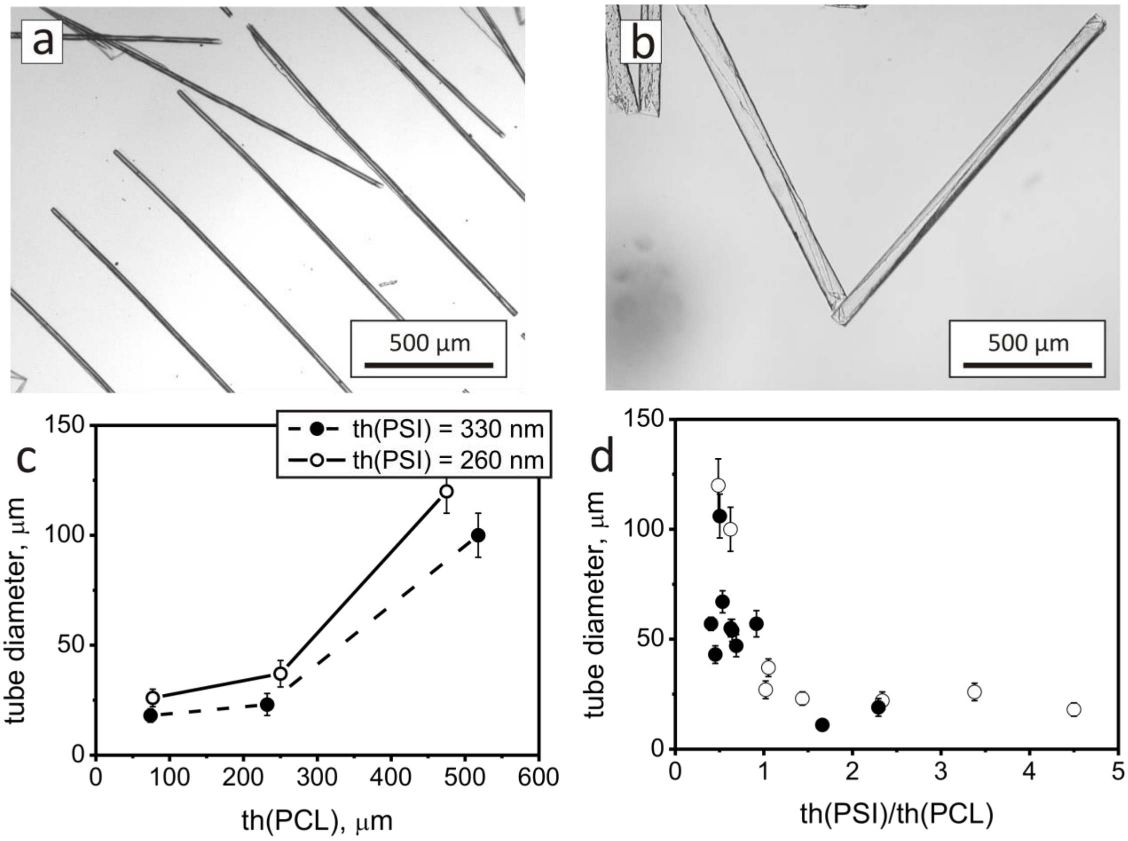

Figure 4.16 | Examples of microtubes with different diameters of (a) 22 µm or (b) 100 µm. (c) The dependence of tube diameters on the thickness of PCL and (d) the th(PSI)/th(PCL) ratio. The empty circles in (d) correspond to samples prepared by dipcoating without further treatment, solid circles correspond to PSI/PCL films annealed at 60 °C and cooled down to -196 °C.

It was found that the rolling of thick bilayers often results in peeling of the polymer films, which might be caused by the crystallinity of the PCL layer. To prevent the formation of large PCL crystallites, polymer bilayers were heated up to 60 °C to melt the

PCL and then quickly cooled down using liquid nitrogen T = -196 °C. This thermal treatment resulted in a decrease of the crystallite size from tens of micrometers to less than a micrometer (see Chapter 3.3.1) and improved the rolling in many cases.

4.2.3.3 Diameter of self-rolled tubes

The effect of the thickness of the polymer layers on the diameter of the formed tubes was then investigated. It was found that the tubes diameter increased with the increase of thickness of the PCL layer as well as with the decrease of the thickness of the PSI layer (Figure 4.16a-c). These results were obtained for tubes after 24 h of rolling when no further change of the tube diameter over time was observed. Moreover, PSI/PCL bilayers prepared with and without thermal treatment demonstrated similar dependence of the tube diameter on the ratio between thicknesses of the polymers layers (Figure 4.16d). In general, the smaller the ratio of the thickness of the PSI layer to the thickness of PCL layer (r = th(PSI) / th(PCL)), the larger the diameter of the formed tubes was (Figure 3d). Since strain in the film is related to the difference between the thickness of the PSI in swollen and dry states, these findings are in a qualitatively agreement with the Timoshenko equation as well[7]. Based on these observations, the possibilities to fabricate tubes with a diameter more than 50 µm was explored both by the decrease of the thickness of the PSI layer (th(PSI) = 67 nm; th(PCL) = 132 nm; r = 0.5) and by the increase of thickness of the PCL layer (th(PSI) = 260 nm; th(PCL) = 473 nm; r = 0.54). Notably, tubes were formed only in the second case, since a thin PSI layer was too soft and did not produced bending force big enough to cause rolling. The tubes of a diameter ranging from 10 µm up to more than 100 µm could be fabricated. Tubes with the size 100 µm or larger are particularly promising for the design of porous scaffolds[169].

4.2.3.4 Rolling direction and tubes morphology

Contrary to the previously discussed PNIPAM/PCL and PNIPAM/PMMA systems (Chapter 4.1.3.4), which demonstrated predominately long-side rolling, PSI/PCL bilayers were able to roll in different directions. For patterns with L/W ratio of 6, three cases were distinguished: long-side rolling, diagonal rolling and short-side rolling (Figure 4.17a-c). The probability to roll in each of these directions depended on the ratio of the final diameter of the tubes to the size of the pattern (pattern width/circumference ratio, W/C). The bilayer rolled in all directions equally if tubes with the smallest diameter were formed (W/C = 5). The increase of the diameter led to the formation of tubes with predominately long-side rolling. The decrease of W/C value to 4 resulted in the increase of the fraction of long-side rolled tubes to 60 %. When the pattern width was comparable with the tube circumference (W/C ~ 1), the fraction of long-side rolled tubes increased up to 70 %. In the last case, almost no short-side rolling was observed. However, fraction of diagonal rolling was equal for all investigated aspect ratios (approximately 25 - 30 %).

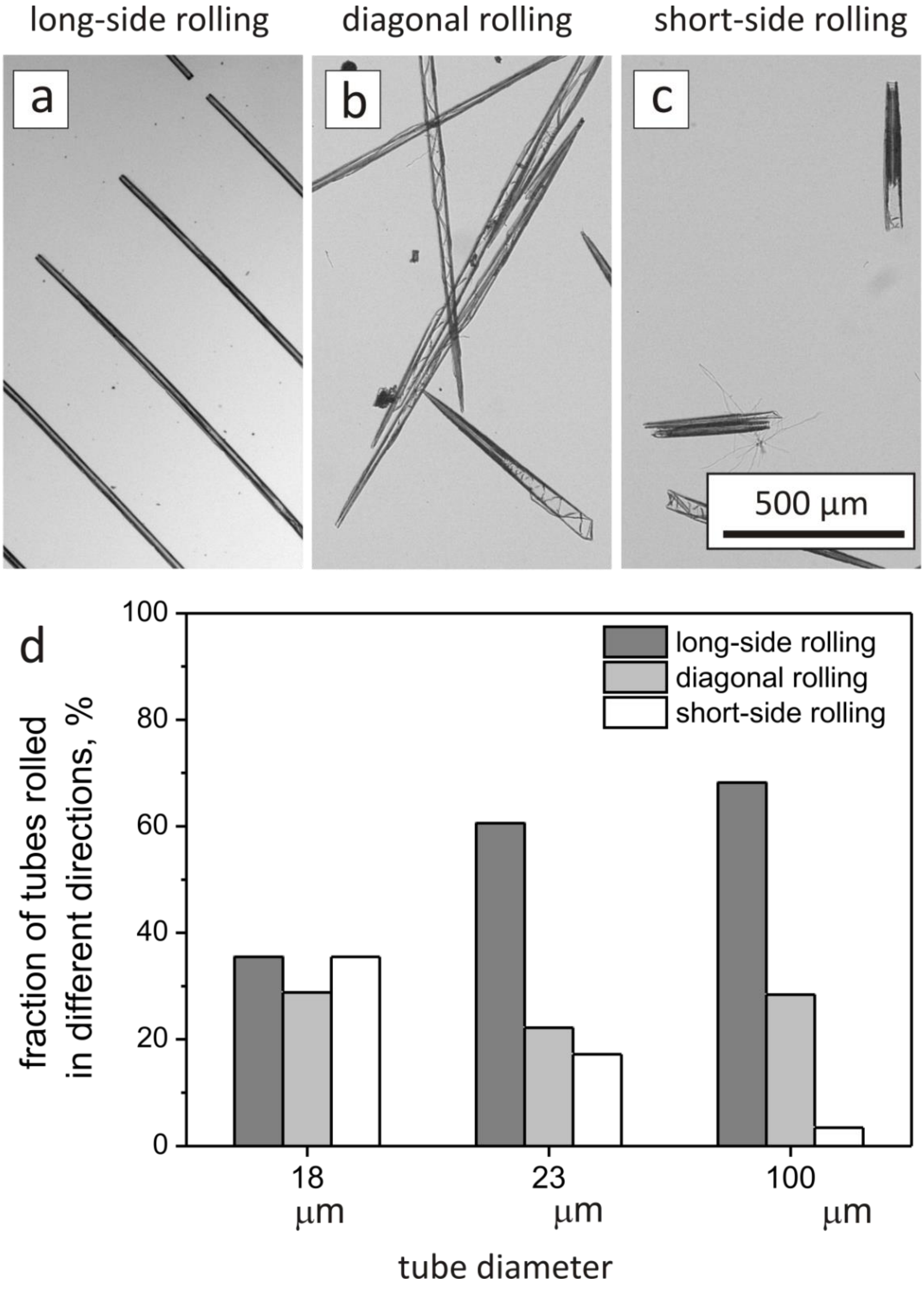

Figure 4.17 | Different morphologies of tubes formed of rolled PSI/PCL bilayers: (a) long-side rolling; (b) diagonal rolling; (c) short side rolling. (d) Fraction of the microtubes rolled in different directions depending on the tube diameter (pattern 300 µm x 1800 µm). Approximately 50 microtubes were analyzed in each case.

To explain the obtained results, the following scenario of rolling was proposed. Water starts to hydrolyze PSI and diffuse inside an active layer along the perimeter of the pattern. The bilayer loses its contact with the substrate at the point where adhesion to the substrate is the smallest and starts to roll. Due to the step-like character of PSI swelling, there is quite a long period of time, when rolling is not completed and tubes of much larger diameters than the final one are formed. During this step the diffusion of the solvent is not limited by a substrate any longer and there is still a possibility for the tube to change direction of its rolling. Therefore, activation of PSI/PCL bilayer can be considered as inhomogeneous at the initial step of rolling and as homogeneous at the latter steps. This mechanism can also explain the fact, that predominantly single-tubes were formed even when W/C ratio was big enough. Here, initially rolled single-tubes with big diameter gradually shrank during PSI hydrolysis to form multiple-turned single-tubes with smaller final diameter.

4.2.3.5 Yeast cell encapsulation

Finally, the possibility to encapsulate yeast cells using fully biodegradable PSI/PCL tubes was tested (Figure 4.18a). For that, patterned PSI/PCL bilayer was placed into PBS buffer (0.15 M, pH = 7.4) with suspended bakery yeast cells. Due to delayed rolling, yeast cells settled down on the top of the unfolded bilayer within the first hours (Figure 4.18b). After 27 h of incubation, the PSI/PCL bilayer formed tubes with diameters of 80 - 100 µm with encapsulated yeast cells (Figure 4.18c). The number of cells remained approximately constant in PBS. One microtube with encapsulated yeast cells was transferred into the nutrition media (Figure 4.18d) and further incubated for 14 h. Incubation in nutrition media led to proliferation and division of the yeast cells that tripled their number (Figure 4.18e). This was an indication of nontoxicity and availability of free space for new cells as well as on the permeability of the tubes for nutrition. The movie of cell growth inside the tube can be found in the supplementary materials of Ref[170].

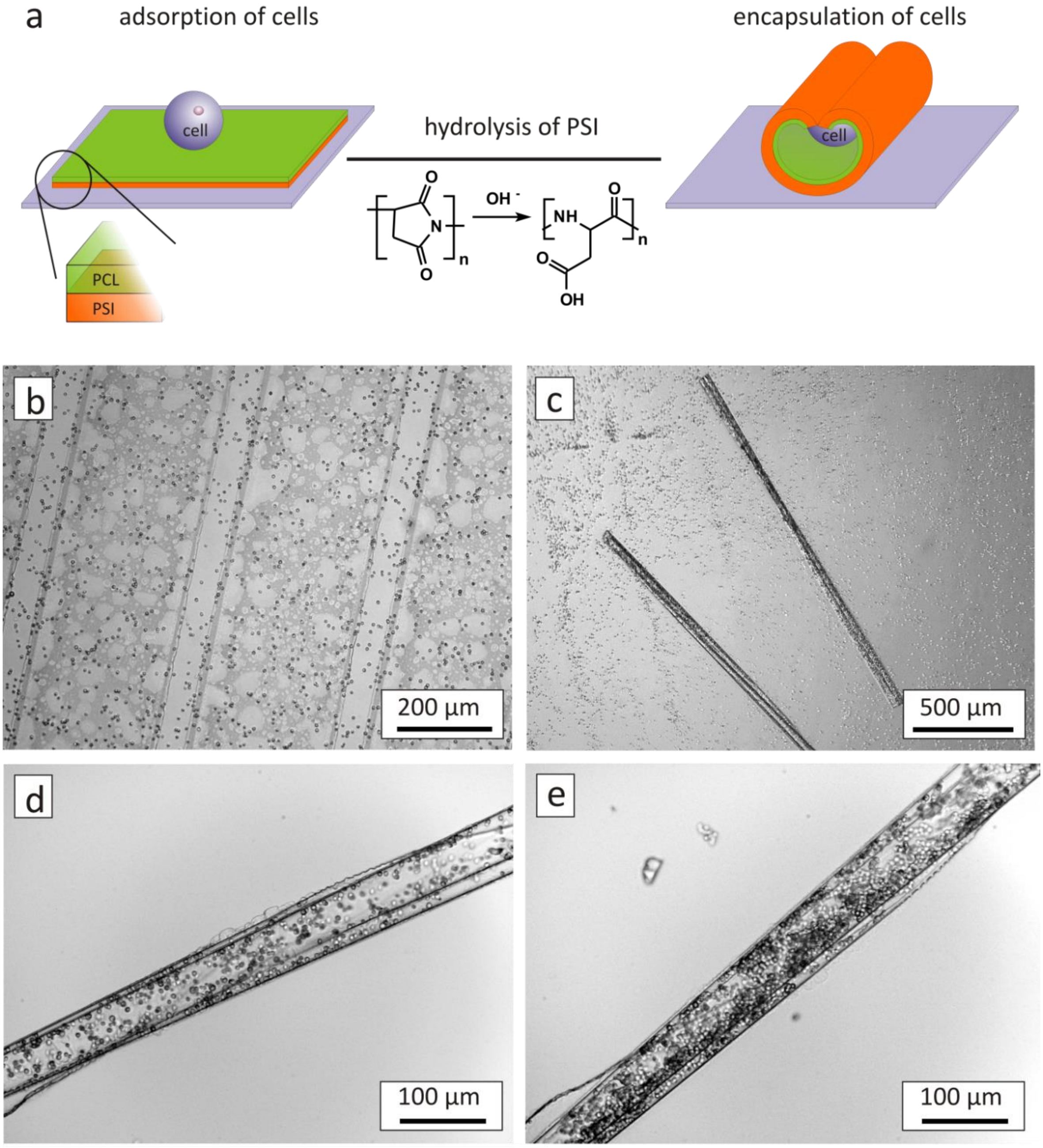

Figure 4.18 | Encapsulation of yeast cells inside PSI/PCL self-rolling tubes. (a) Scheme of the encapsulation. Microscopic images: (b) yeast cells settled down on the top of unfolded PSI/PCL patterned bilayer after 1 h of incubation in PBS buffer (0.15 M, pH = 7.4) at T = 25°C; (c) rolled tubes with encapsulated yeast cells after 24 h of incubation; (d) rolled tube with yeast cells inside directly after transfer form PBS buffer into the nutrition media and (e) after 14 h of incubation in the nutrition media.

4.2.4 Conclusions

In this chapter, the fabrication of fully biodegradable solvent-responsive self-rolled tubes was demonstrated. The approach is based on the use of polymer bilayers where both components are water-insoluble polymers: polysuccinimide and polycaprolactone. Polysuccinimide is able to slowly hydrolyze in a physiological buffer environment resulting in water-swellable polyaspartic acid, that leads to self-rolling of the polymer bilayer and the irreversible formation of the microtubes within 24 h of incubation in PBS buffer (0.15 M, pH = 7.4). It was demonstrated that PSI/PCL bilayers can be used for parallel encapsulation of yeast cells inside microtubes during rolling process. Encapsulated cells were shown to be able to divide inside the tube, placed in nutrition media. Since the used polymers are biocompatible, biodegradable, produced industrially and are approved for biomedical purposes[163-165], the proposed approach is of practical interest for controlled cell encapsulation and the design of scaffolds for tissue engineering.

However, there are several limitations to be considered. Polysuccinimide is insoluble in the most of organic solvents, except DMF and DMSO. In the present work, PSI deposition was performed from DMF, which is highly toxic. Although the solvent was carefully removed by heating the film at 170 °C and washing in a big amount of ethanol, for further cell experiments, it is necessary to prove that no traces of DMF remain in the polymer film. The preliminary tests (not shown) demonstrated that mammalian cells adhered to the PSI film and could proliferate, however more investigations have to be done in this respect. Another possibility would be to use DMSO as a solvent for PSI film deposition. Although DMSO is also toxic at the physiological temperatures, but in contrast to DMF it is routinely used in cell culturing as a cryoprotectant, added to cell media to reduce ice formation and prevent cell death during the freezing process.

4.3 Thermo-responsive bilayer systems based on gelatin

4.3.1 Objectives

Previously, we discussed a design of fully biodegradable self-rolled tubes based on polysuccinimide/polycaprolactone bilayers, which roll due to slow hydrolysis of polysuccinimide in physiological buffer. The rolling of PSI-based bilayers is determined by kinetics of hydrolysis and can be hardly controlled by external signals. Therefore, development of fully biodegradable self-folding polymer films, whose folding can be triggered by an external signal, is strongly desirable. The pH and UV light are less favorable signals to trigger encapsulation of the cells inside the tubes. UV light may cause damaged of DNA due to dimerization of thymine fragments, while even small pH changes affect cell membrane potential. On the other hand, since cells can tolerate variations in temperature in the range between 4 °C and 37 °C, temperature appears to be the most suitable stimulus to trigger folding.

In this chapter, a simple and cheap approach for fabrication of fully biodegradable tubes, whose rolling can be triggered by temperature, is reported. The tubes are based on the use of natural biodegradable polymer – gelatin – as an active component. As a passive polymer biodegradable[18] polycaprolactone was used. Gelatin forms hydrogels upon cooling from an aqueous solution, due to helix-formation and association of the helices. These physically crosslinked hydrogels have a sol-gel transition temperature[171]. Chemically crosslinked gelatin undergoes one-way swelling in aqueous environment, wherein the degree of swelling strongly depends on the temperature. The use of gelatin as a thermo-responsive component is highly attractive since the polymer is cheap and produced in huge quantity by hydrolysis of collagen. Due to biocompatibility and biodegradability gelatin is offered for application in tissue engineering, therapeutic angiogenesis, gene therapy, and drug delivery[172, 173]. Moreover, gelatin allows design of both (i) self-folding polymer films, which are unfolded in aqueous environment at room temperature, but irreversibly fold at 37 °C, and (ii) films, which fold at room temperature (22 °C) and irreversible unfold at 37 °C.

Two approaches for the design of thermo-responsive gelatin-based self-folding films are discussed in this chapter. The first approach utilizes non-crosslinked gelatin/polycarolatone bilayers, while in the second approach both components of the bilayer are crosslinked using UV-light.

4.3.2 Experimental part

Materials. Gelatin from porcine skin, gel strength 300 g Bloom, Type A was used as an active polymer. Passive layer consisted of polycaprolactone (M_n = 70 000 - 90 000 g/mol).

Fabrication of polymer bilayers. For the preparation of crosslinked gelatin/polycaprolactone bilayers, polymers were deposited on a silicon wafer as described in Table 3.1. The thickness of layers varied in the range of 440 - 940 nm for gelatin (deposited from 7 - 10 % water solution, with addition of Pen/Strep solution up to concentration 100 U/ml penicillin, 100 µg/ml streptomycin) and 260-1300 nm for PCL (deposited from 3 - 9 % toluene solution). Since both polymers are intrinsically not photosensitive, photosensitive compounds, which generate radicals upon UV irradiation, were admixed to the polymer solutions. Polycaprolactone solution contained 5 wt.% of 4-hydroxybenzophenone with respect to the weight of dry polymer. Water-soluble derivative of diazostilbene – 4,4′-diazido-2,2′-stilbenedisulfonic acid disodium salt tetrahydrate (DAz) – was added to gelatin solution in amount of 12 wt.% with respect to the weight of dry polymer. Patterning of the bilayers was performed by simultaneous irradiation with UV light of 254 nm (for BPhOH activation) and 354 nm (for DAz activation) through a photomasks with typical pattern size of 190 µm x 1650 µm and 300 µm x 1800 µm (Chapter 3.3.2). Non-crosslinked polycaprolactone was removed by washing in chloroform, while non-crosslinked gelatin was subsequently removed by very fast washing in warm water (37 - 40 °C), followed by immediate drying.

4.3.3 Results and discussions

4.3.3.1 Folding of non-crosslinked bilayer

First, swelling properties of non-crosslinked gelatin films deposited on a substrate were investigated. Exposure of thin gelatin film to PBS buffer (0.15 M, pH = 7.4) at room temperature (T = 22 °C) led to its swelling from 20 nm (as measured in a dry state) up to 120 nm. Increase of the temperature up to 37 °C resulted in a sharp increase of the film thickness followed by its abrupt decrease (Figure 4.19a). Obviously, gelatin swelled moderately in cold water, still staying in a gel form, while an increase of the temperature resulted in a stronger swelling of the film, accompanied by polymer dissolution[171]. The residual thickness of gelatin film was 50 nm in a swollen state at 37 °C and 6 nm after drying, which was found to be independent of the initial thickness of gelatin (either it was 50 nm or 2 µm). This residual layer most probably originates from adsorption of gelatin on the charged silica wafer. Thick gelatin films demonstrated similar temperature-dependent swelling behavior.

A non-crosslinked gelatin/polycarolactone bilayer was fabricated by deposition of a 45 µm layer of polycaprolactone on an 150 µm thick layer of gelatin. The sample was annealed at 60 °C for 30 s in order to melt polycaprolactone, fuse it to gelatin layer and make the bilayer more stable. Immersion of the sample in water at 20 °C led to slow bending of the film and the formation of the tube with an inner diameter of 7 mm (Figure 4.19b). An increase of temperature up to 37 °C led to unfolding of the film, caused by dissolution of gelatin. Finally, the unfolded PCL film was left. Since thickness and Young's modulus of the gelatin layer in each moment is unknown, a quantitative description of folding-unfolding behavior using Timoshenko equation is hardly possible.

Therefore, non-crosslinked gelatin/PCL system undergoes folding in aqueous media at low temperature and unfolding at higher temperature (Figure 4.19c). Since both polymers are not photosensitive, pattering of bilayer using photolithography is not possible, and desired shapes can be prepared by cutting.

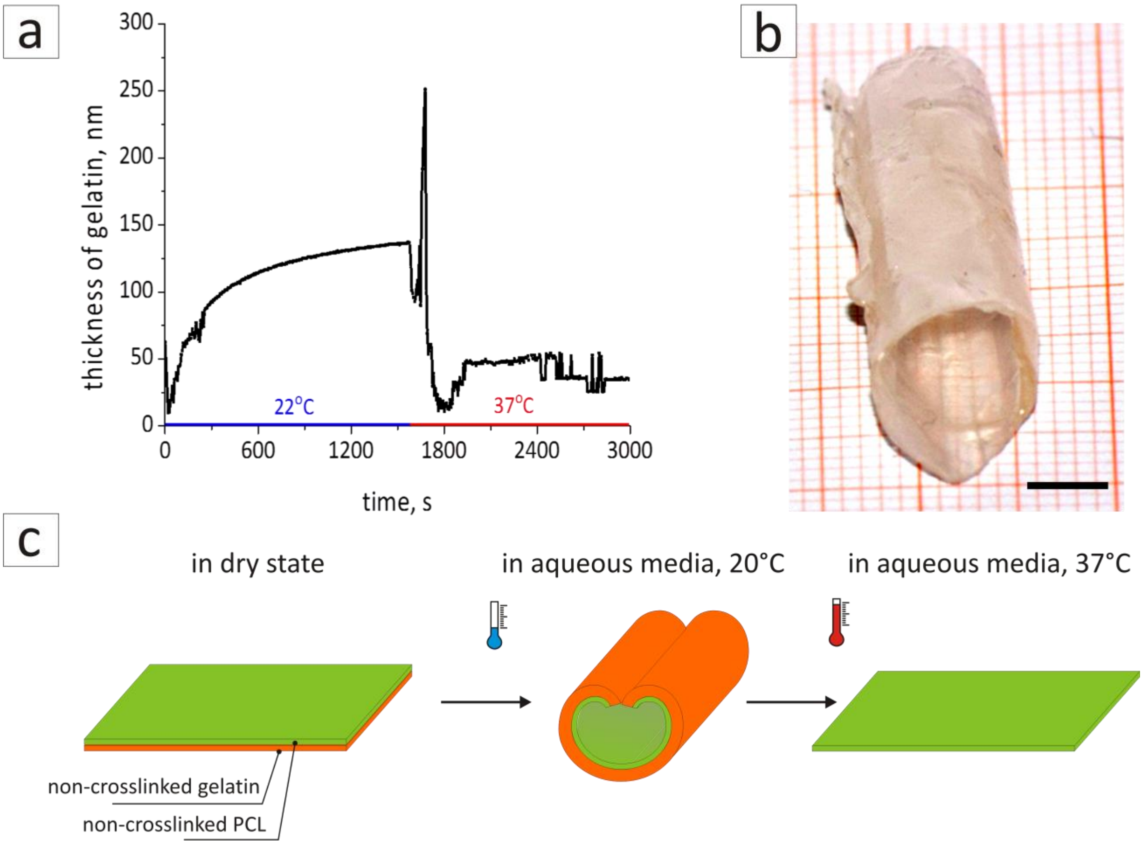

Figure 4.19 | Non-crosslinked gelatin/polycaprolactone system: (a) swelling and dissolving of non-crosslinked gelatin film (thickness in a dry state 20 nm) in PBS buffer (0.15 M, pH = 7.4) first at T = 22 °C (0-1500 s) and then at T = 37°C (1500-3000 s). (b) Photographic image of the tube, based on non-crosslinked gelatin/PCL bilayer and rolled in water at 20 °C (th(gelatin) = 45 µm; th(PCL) = 150 µm, d = 6 mm), scale bar is 4 mm; and (c) scheme of the self-rolling experiment.

4.3.3.2 Folding of crosslinked gelatin/polycaprolactone bilayer

Swelling of photocrosslinked gelatin depended strongly on the temperature. Contrary to polysuccinimide, swelling of crosslinked gelatin started immediately after immersion in physiological buffer and was considerably faster. So, the swelling degree increased significantly within the first 10 - 30 min and achieved its maximum value in 1 - 2 h. The thickness of the gelatin layer increased by approximately factor 5 during swelling in PBS buffer at room temperature (T = 24°C). That is comparable to the character of swelling of non-crosslinked gelatin. An increase of the temperature up to 37°C resulted in a swelling degree of 8 (Figure 4.20a). The thickness of the swollen polymer layer remained constant after cooling down, signifying irreversibility of thermo-triggered swelling of the crosslinked gelatin layer.

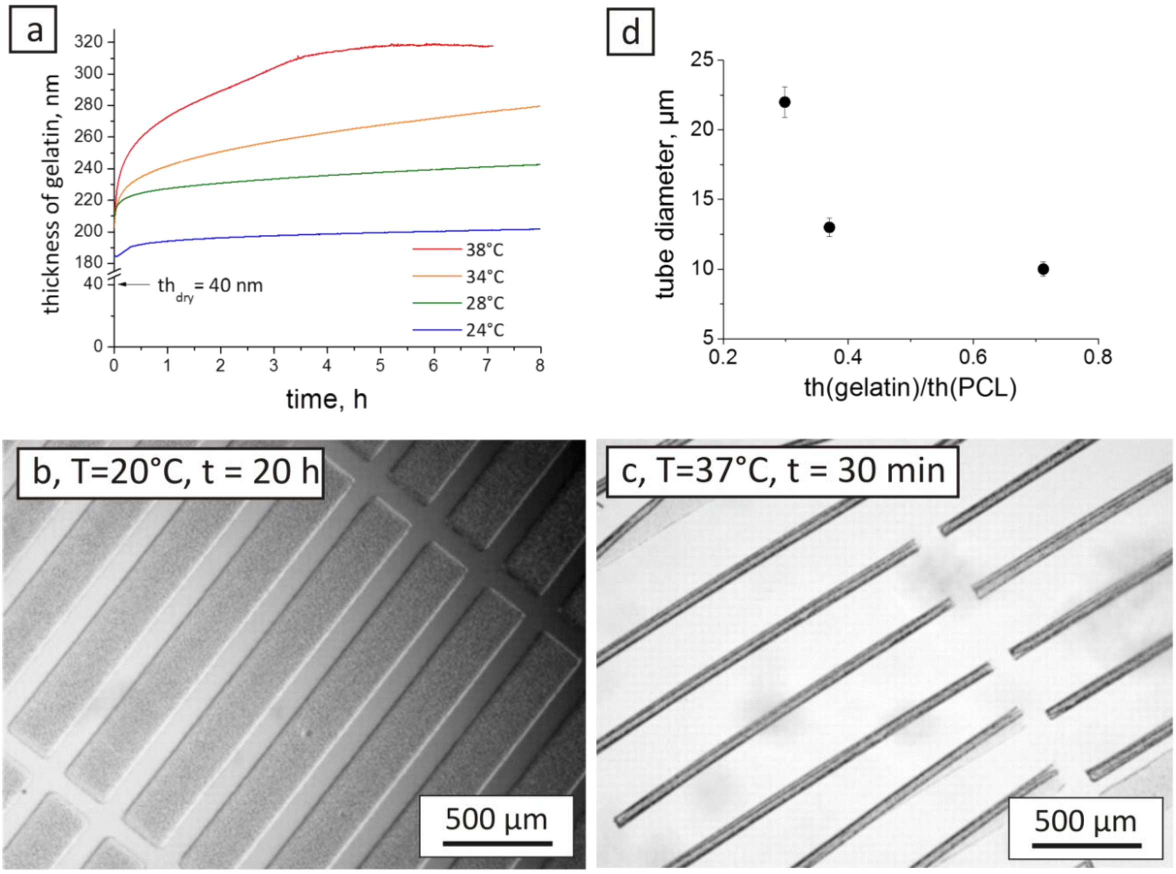

Figure 4.20 | Crosslinked gelatin/polycaprolactone system: (a) swelling of photocrosslinked gelatin films (thickness in a dry state 40 nm) in PBS buffer (0.15 M, pH = 7.4) at different temperatures (measured by Evgeni Sperling) and morphologies of self-rolling tubes (th(gelatin) = 400 nm; th(PCL) = 1340 nm, pattern 190 µm x 1650 µm) at different temperatures on different stages of rolling: (b) after 20 h of incubation at 24 °C no rolling is observed; (c) after 30 min of incubation at 37 °C tubes are formed, d_{inn}=18 µm. (d) Dependence of the tube diameter on the thickness ratio th(gelatin)/th(PCL).

Immersion of the crosslinked and photopatterned gelatin/polycaprolactone bilayer in PBS buffer (0.15 M, pH = 7.4) at room temperature (24 °C) did not affect the bilayer, and it remained undeformed after 20 h of incubation (Figure 4.20b). Increase of the temperature up to 37 °C led to fast rolling of the bilayer and formation of the tubes within 20 - 30 min (Figure 4.20c). On one hand, an increase of the temperature led to a stronger swelling of gelatin that, according to the Timoshenko equation (2.1), shall result in the decrease of radius of curvature, i.e. rolling. On the other hand, basing on the swelling curves, one can expect that tubes must also be formed at room temperature and their diameter shall decrease at 37 °C. Obviously, the reason why rolling started only at 37 °C, but was not observed at room temperature, was non-completed development of the gelatin layer after photolithography. Since the rinsing with warm water during development was very fast, not all non-crosslinked gelatin could be removed. As it was shown in the previous section, although non-crosslinked gelatin swells at room temperature, it stays in a gel form. Gelatin gel between photolithographicaly produced bilayer patterns hindered rolling at room temperature, while an increase of the temperature and following incubation resulted in a complete dissolution of the non-crosslinked gelatin film that allowed rolling of the bilayer. Similarly to the previously investigated systems, the diameter of gelatin/polycaprolactone tubes formed at elevated temperature depended on the ratio between the thicknesses of the polymers (Figure 4.20d).

4.3.4 Conclusions

In this chapter, we demonstrated the fabrication of biocompatible and fully biodegradable thermo-responsive self-rolled tubes, based on gelatin/polycaprolactone bilayers. Use of gelatin as an active component allowed the design of both reversible (one cycle) and irreversible bilayer structures. Non-crosslinked gelatin/PCL films, which can be fabricated by cutting, folded upon exposure in aqueous media at room temperature (24 °C) and irreversible unfolded when the temperature was increased up to 37 °C. Contrary, UV-photocrosslinked gelatin/PCL bilayers did not bend in aqueous media at room temperature. Irreversible folding occurred at an elevated temperature and was finished within 30 min – 1 h. Such complex thermoresponsive behavior cannot be achieved by the use of polymers with LCST behavior. The latter can only allow fabrication of self-folding films, which are unfolded at elevated temperature and fold upon cooling.

Since in both cases folding occurs in conditions close to physiological (temperature range of 24 - 37° C, physiological buffer environment), gelatin-based self-folding films could be applied for reversible as well as for irreversible encapsulation of cells.

ASSEMBLIES OF SELF-ROLLED POLYMER TUBES

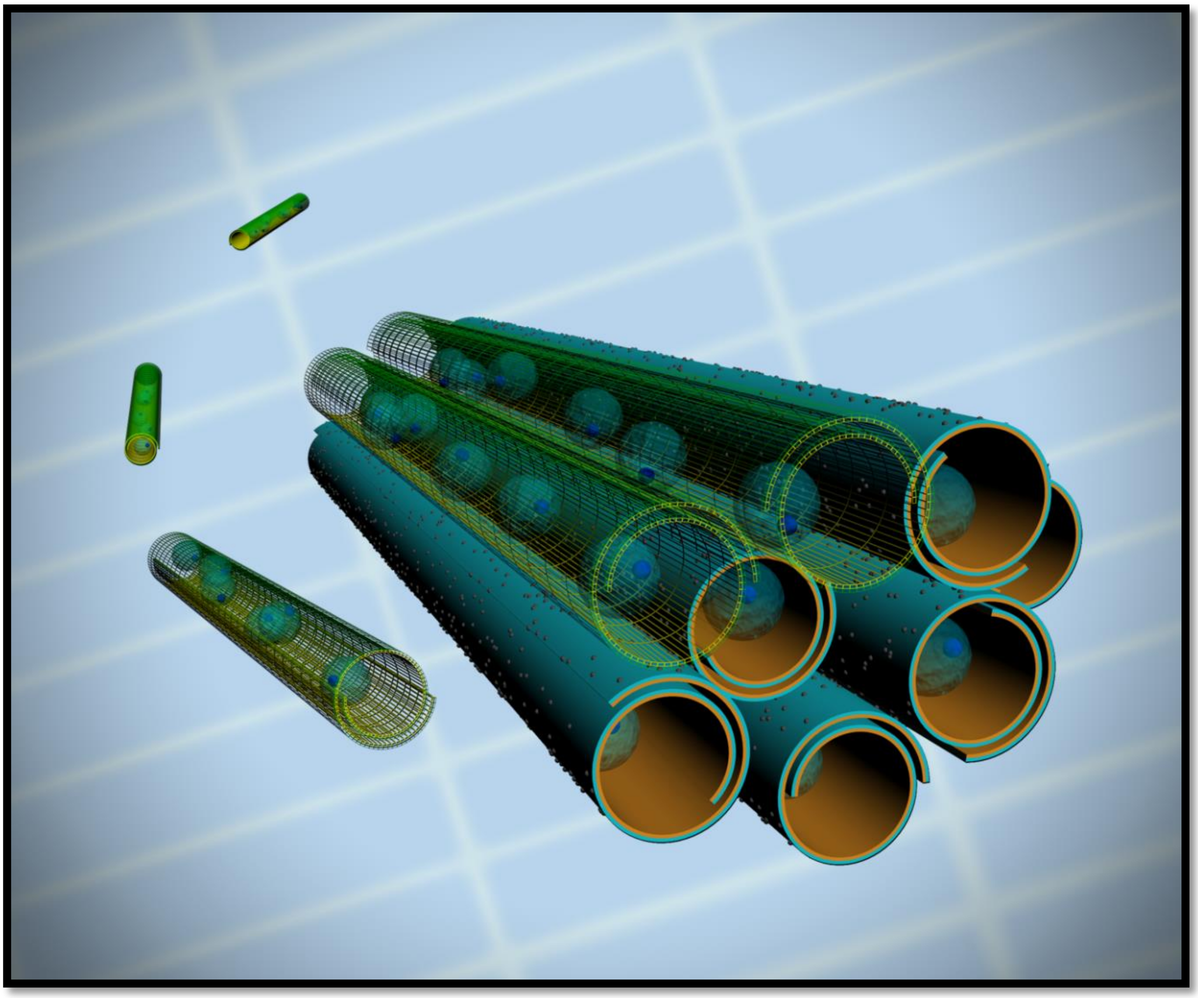

4.4 Self-assembly of self-rolled polymer tubes into a 3D constructs with aligned pores

4.4.1 Objectives

Materials with uniaxially aligned/oriented pores have a huge potential for a number of applications including the design of self-healing materials[174, 175], functional ceramic[176], membranes for separation and sensing[177], photonic crystals[178-180], catalyst support[181], lightweight materials[182], vibration-damping materials[182], heat insulating materials[183] photovoltaic applications[184], microanalytics[185], and tissue engineering[13]. Among a variety of possible applications, tissue engineering is one of the most attractive fields. Many kinds of tissues such as bones[13], vascular tissue[11, 12], cardiac tissue[14-16], nerve[186, 187] have either tubular or uniaxially aligned porous structure. In order to mimic specific structural environment, tubular scaffolds were fabricated using phase separation technique[11, 12, 188], polymer fiber templating[14, 186, 187], directed foaming[189], directional freezing[12, 190-193], prototyping[16], uniaxial stretching of porous materials[194], or using of natural porous materials such as wood[176]. In these approaches the separate tubes or scaffold with tubular structure are first fabricated and then filled with living cells. Use of this “post-filling” strategy often suffers from non-homogenous cell seeding inside the porous scaffold due to slow cell migration.

Self-folding polymer films offer a very elegant solution of the problem of non-homogenous distribution of cells inside the pores[22, 84]. The polymer nature of the tubes is particularly attractive for biotechnological applications due to their sensitivity to stimuli in physiological range, potential biocompatibility and biodegradability[62, 161, 170]. The main advantage of self-folding films is that they can be filled with cells before self-assembly and formation of tubes (folding) that provides the desired homogeneity of filling[62, 84, 170]. Moreover, self-rolled tubes are able to provide structural anisotropy.

The approach presented in this chapter consists in the fabrication of self-rolled tubes filled with cells and their self-assembly in a complex 3D construct with uniaxially aligned pores homogenously filled with cells (Figure 4.21). The approach is based on the use of microtubes formed by stimuli-induced rolling of polymer bilayers consisting of hydrophobic and stimuli-responsive hydrophilic polymers. As a first step, cells can be encapsulated inside the tubes during their rolling. For the proof of principle, yeast cells were chosen for encapsulation. As a second step, the formed self-rolled tubes can be assembled in an uniaxial tubular scaffold, which is homogeneously filled with cells. Moreover, the approach allows the design of a porous material with the pores having different properties.

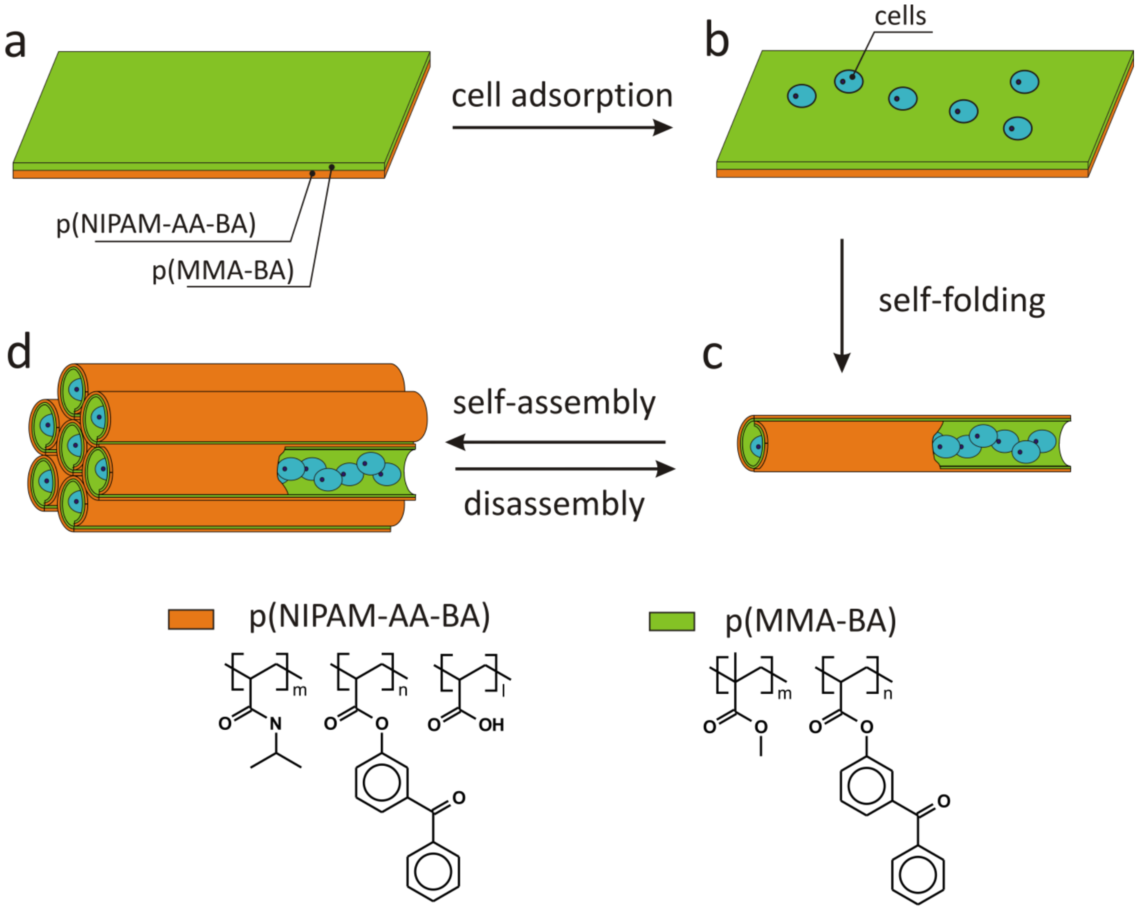

Figure 4.21 | Fabrication of tubular self-assembling structures filled with cells using self-rolled tubes. (a) Unfolded patterned bilayer consisting of two polymers: red represents hydrophilic p(NIPAM-AA-BA) and green represents hydrophobic p(MMA-BA); (b) cells are adsorbed on the top of an unfolded bilayer; (c) cells are encapsulated inside the rolled film; and (d) self-rolled tubes are assembled together forming a porous construct homogenously filled with cells.

4.4.2 Experimental part

Materials. As a responsive layer, a random copolymer of NIPAM, AA and BA p(NIPAM-AA(4.8 mol.%)-BA(1.6 mol.%)) was used. Additional admixing of 10 wt. % of 4-hydroxybenzophenone to a p(NIPAM-AA(4.5 mol.%)-BA(1.5 mol.%)) allowed us to increase the degree of hydrogel crosslinking. The LCST of copolymer in deionized water and PBS buffer (0.15 M, pH = 7.4) was 33 °C and 40 °C respectively. The swelling behavior of the polymer was discussed in Chapter 4.1.3.1. For the preparation of a passive layer, a random copolymer of MMA and BA p(MMA-BA(1.6 mol.%)) was used.

Two types of positively charged silica particles (SP) were used for tubes assembly experiments. In the first type, 1 µm large SiO_2 particles were covered with grafted 60 nm thick polyelectrolyte brush layer of poly((2-dimethylamino)ethyl methacrylate) (PDMAEMA) – SP-PDMAEMA. In the second type, PDMAEMA was quaternized using iodomethane (Q-PDMAEMA) – SP-Q-PDMAEMA. Synthesis of used polymers and particles was described in Chapter 3.2.5.

Fabrication of polymer bilayers and self-rolled tubes. All bilayer films were produced on silica wafer substrate using automatic dip-coating with parameters described in the Table 3.1. The typical solution concentration was 8 - 10 % for PINPAM- and 5 - 7 % for PMMA-copolymers. Thickness of active and passive layers varied in the range of 600 - 760 nm and 200 - 300 nm respectively. Photolithography was performed as described in Chapter 3.3.2 with standard masks giving pattern size of 200 µm x 1600 µm or 300 µm x 1800 µm. The tubes were fabricated by exposure of patterned bilayers in PBS (0.15 M, pH 7.4) at room temperature followed by fast rolling within 5 - 10 minutes.

Preparation of fluorescent tubes. To prepare fluorescent tubes for confocal microscopy a standard procedure was used. To achieve fluorescence, small amount of either red emitting (CdSe) or green emitting ($CdSe/Cd_{1-x}Zn_xSe_{1-y}S_y/ZnS$) quantum dots, provided by Christian Waurisch, Stephen G. Hickey and Alexander Eychmüller, TU Dresden (Figure 3.6) was admixed into the p(MMA-BA) toluene solution, used for the polymer film deposition. The amount of added QDs was chosen to obtain equal intensity of fluorescence.

Tube aggregates preparation and alignment. Tube dispersion was prepared by washing off the rolled tubes from the substrate with a small amount (2 - 3 ml) of water or PBS buffer into a glass vial. To assemble the tubes, water dispersion of PDMAEMA-covered SiO_2 particles (85 mg/l) was added to the tube dispersion. The amount of added particles was calculated with respect to 25 - 30 % saturation of the tubes surface with particles in assumption of hexagonal close packing and complete adsorption of all added particles on the tubes surface. The water dispersion of tubes and oppositely charged particles was carefully shaken for 10 - 15 min that resulted in tube agglomerate formation. Tubes in aggregates were aligned by pulling out from water with a needle.

Experiments with yeast cells. To adsorb yeast cells, patterned polymer bilayers were exposed in water dispersion of the cells for 20 min at room temperature. Next, the excess of water was removed and replaced with PBS buffer (0.15 M, pH = 7.4) that resulted in the rolling of the tubes and encapsulation of the cells within 30 min – 1 hour. Tubes with encapsulated cells were agglomerated using the procedure described above. Agglomerates with encapsulated yeast cells were incubated in Alpha medium w/o nucleosides (Biochrom AG) at 25 °C for 24 hours.

4.4.3 Results and discussions

4.4.3.1 Assembling and alignment of microtubes in aqueous solution

First, the possibility to assemble and align microtubes in aqueous solution was investigated. The tubes' self-assembly was observed during drying of the water droplet, on the water-air interface and in the flow when dispersion of tubes in water passed through a long and narrow glass capillary (Figure 4.22).

Liquid droplet evaporation on a solid surface was reported to lead to an alignment of nanofibers[195], carbon nanotubes[196] and nanorods[197]. For microtubes, which were prefabricated on a wafer, drying of the droplet led to the detachment of the microtubes from the substrate, followed by formation of aggregates. Due to the type of polymer bilayer patterning, the tubes were initially located parallel to each other after folding. The capillary flow in the drying droplet often pulled tubes together without changing their orientation and therefore alignment of the tubes in agglomerates was achieved. However, the number of tubes assembled together was rare more than ten (Figure 4.22a). For the next experiments, a big amount of tubes was first produced. In one experiment, tubes were washed from the substrate into a glass vial. Shaking of the dispersion led to the increase of the tubes amount at the water-air interface, where tubes formed 2D clusters (Figure 4.22b). In the third experiment, assembly in the flow was investigated while tubes' dispersion was placed in a glass capillary and forced to flow in one direction. Tubes first oriented in the flow parallel to the walls of the capillary, and in case when the path was long enough to allow tubes to come into a contact with each other, agglomerates formation was detected (Figure 4.22c). In last two cases, the orientation of the tubes in agglomerates was also predominantly parallel. Apparently, self-assembly of self-rolled tubes is close to nematic liquid crystalline phase formation and is expected to depend on the tubes aspect ratio (ratio of length to diameter). In the present work, the tube length varied in the range between 1600 µm and 2000 µm, the aspect ratio was always more than 40.

Though in all attempts described above, relatively good alignment of the tubes was achieved, the size of aggregates was small. Moreover, the agglomerates were mechanically unstable and could spontaneously disassemble. In one of the common approaches, to obtain mechanically stable aggregates post-assembly photocrosslinking can be used to fix the structures[4, 198]. Other assembly strategies involve chemical patterning of the components so that they can interact with each other and form stable structures in a fluidic medium. Such interactions of molecular linkers can be due to chemical[199] or hydrogen[200] bonding, protein recognition[201], DNA recognition[202], antibody-antigen recognition[203] or metallic complexation[204].

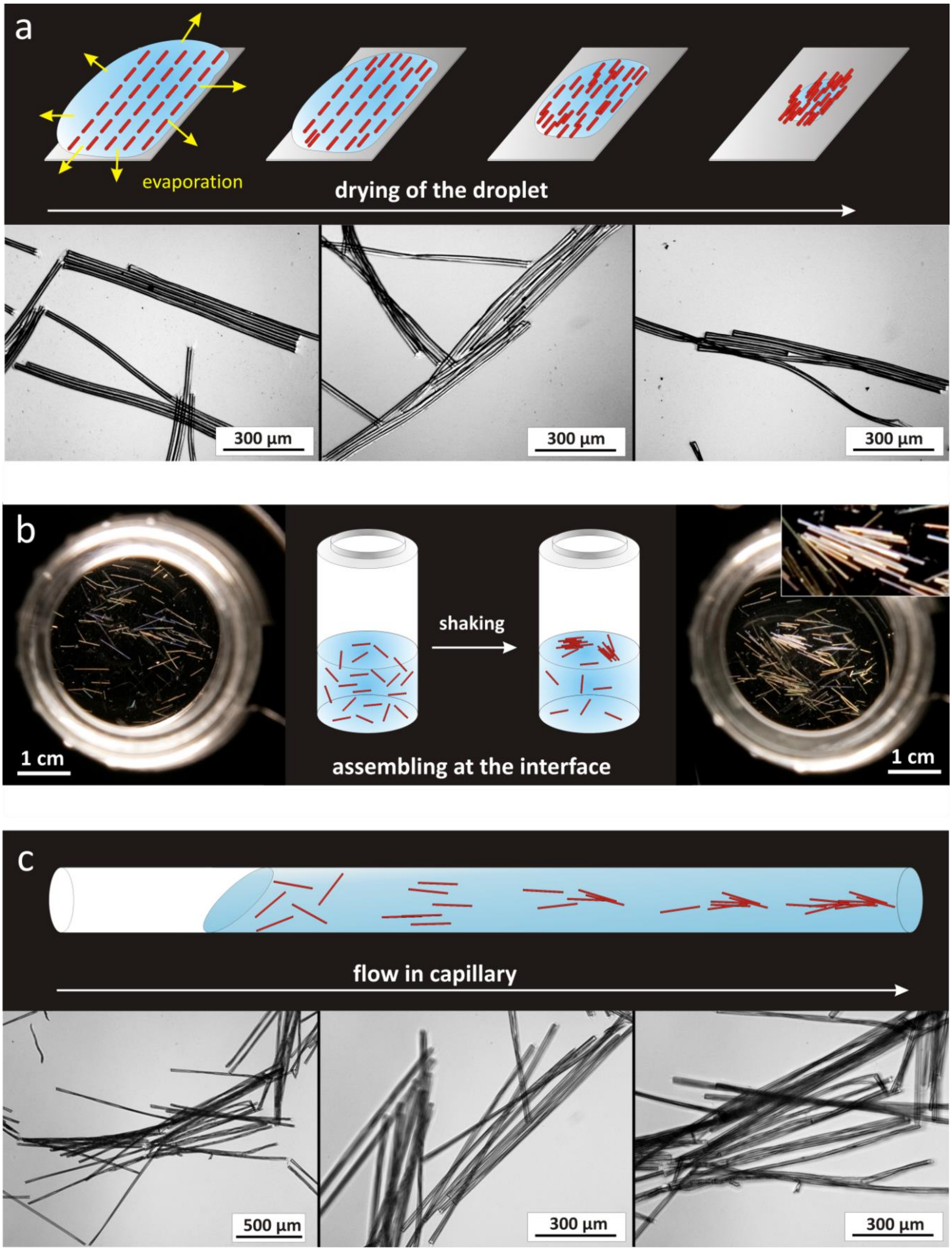
a
evaporation
drying of the droplet
300 µm
300 µm
300 µm
b
1 cm
shaking
assembling at the interface
1 cm
c
flow in capillary
500 µm
300 µm
300 µm

Figure 4.22 | Assembling and alignment of the tubes in water. (a) Alignment by droplet evaporation: scheme and microscopy images; (b) nematic cluster formation at the water-air interface: scheme and photographic images of the glass vial from above; (c) tubes alignment in a capillary flow: scheme and microscopy images.

The approach presented in this work suggests fixation of self-rolled tubes in agglomerates using microparticles, which are able to interact with external walls of the tubes, gluing tubes together. In order to demonstrate a proof of the principle, self-rolled polymer tubes possessing negatively charged groups on the external wall were used. In this case ion-ion interaction with positively charged particles is possible.

The bilayer for tubes fabrication consisted of a hydrophilic stimuli-responsive poly(N-isopropylacrylamide-co-acylic acid-co-benzophenoneacylate) (p(NIPAM-AA-BA)) bottom layer and a hydrophobic poly(methylmethacrylate-co-benzophenoneacylate) (p(MMA-BA)) top layer. The random copolymer p(NIPAM-AA-BA) demonstrated pH-dependent swelling in aqueous environment. So, the swelling degree of the polymer in deionized water (pH = 5.5) was 1.5 times less than that in PBS buffer (0.15 M, pH = 7.4) (see Chapter 4.1.3.1). Moreover, in DI water swelling was slower, than in buffer, and correspondingly the bilayer remained undeformed for considerable time – approximately 1 h. The transition temperature and the swelling/rolling rate increased with the increase of ionic strength and pH of the aqueous solution due to boosted dissociation of acrylic acid ($pK_a = 4.5$). For example, transfer of the bilayer into PBS buffer led to very quick rolling and formation of tubes occurred in 5 - 10 minutes. After rolling, tubes could be released from the substrate and washed off with water or PBS into a glass vial where they chaotically flowed without forming aggregates. The surface of the tubes was negatively charged due to dissociation of the carboxylic groups in the p(NIPAM-AA-BA) hydrogel layer.

Two types of positively charged particles were used to investigate a possibility of tubes assembly. In first the type, 1 µm large SiO_2 particles were covered with grafted 60 nm thick polyelectrolyte brush layer of poly((2-dimethylamino)ethyl methacrylate) (PDMAEMA). In the second type, PDMAEMA was quaternized using iodomethane (Q-PDMAEMA).

First, interaction of the particles with self-rolled tubes was examined. For that, dispersion of the particles was added to dispersion of the tubes, and resulting mixture was carefully shaken for several minutes. Next, tubes were taken out from the dispersion, dried and investigated using SEM. Formation of polyelectrolyte complex between amino groups of the particles (PDMAEMA or Q-PDMAEMA polymer shell) and carboxylic groups of the external walls of the tubes (p(NIPAM-AA-BA) hydrogel) led to an attachment of the particles on the tubes. Moreover, particles were rather penetrated into a p(NIPAM-AA-BA) hydrogel, than externally attached to the tubes surface (Figure 4.23b-f). The depth of penetration (DP), calculated as shown in Figure 4.23a-b, depended on the particle type. For PDMAEMA covered particles the depth of penetration into a p(NIPAM-AA-BA) hydrogel was 50 %, meaning that half of the particle was dipped into the external wall of the tube and half of it stayed exposed to the surrounding (Figure 4.23c). At the same time, quaternized particles SP-Q-PDMAEMA were almost fully dipped into tube walls with 95 - 100 % penetration (Figure 4.23d). This behavior can be explained by the difference in charge density on the particles surface. Indeed, PDMAEMA contains only tertiary amino groups; the charge density is lower than for quaternized polymer, resulting in a weaker interaction with the negatively charged hydrogel. Another factor that influenced the depth of particle penetration was the degree of hydrogel crosslinking. Admixing of 10 wt.% (in relation to the mass of dry polymer) of 4-hydroxybenzophenone to a p(NIPAM-AA-BA) resulted in an increase of the polymer crosslinking and led to a corresponding decrease of particles penetration: 30 % for PDMAEMA (Figure 4.23e) and 75 % for Q-PDMAEMA covered particles (Figure 4.23f).

For spherical particles, their projection on a surface, on which they are arranged, gives an array of circles and corresponds to surface coverage. The distribution of the particles on the tubes surface was random and homogeneous, when diluted dispersion was used. The surface coverage increased as the amount of added particles increased (Figure 4.24a). Addition of excess particles led to a saturation of the tube surface with particles. In this case, observed arrangement of the particles was close to a hexagonal packing, where each particle was surrounded by 6 other particles (Figure 4.24b). Hexagonal close packing provides a highest density of the circles arrangement in two-dimensional space and therefore the largest surface coverage, which can be calculated geometrically as a ratio of occupied area to the total area of the surface. Since the centers of three circles in contact form an equilateral triangle, the maximal surface coverage by one layer of hard spheres (F_{max}) can be calculated as ratio of ½ circle area A_{circle} to the area of triangle $A_{triangle}$ (Figure 4.24c). Therefore, the largest coverage of the tubes surface with particles is 91 %.

The particles form positively charged “patches” on the negatively charged tube walls. The area of the positive “patches” depends on the surface coverage as well as on the depth of particle penetration into the hydrogel. Indeed, even if hexagonal close packing of the particles is achieved, penetration of the particles deep into the hydrogel reduces effective surface of the particles, which is exposed to the surrounding and available for interaction with other tubes. “Effective surface coverage” can be therefore calculated as a projection of the exposed part of the particles on the tube surface. Obviously, the maximum of “effective coverage” (91 %) can be achieved when the depth of particles penetration is less than 50 %. In this case, tubes can be considered as positively charged, as only about 10 % of original negatively charged tube walls are present.

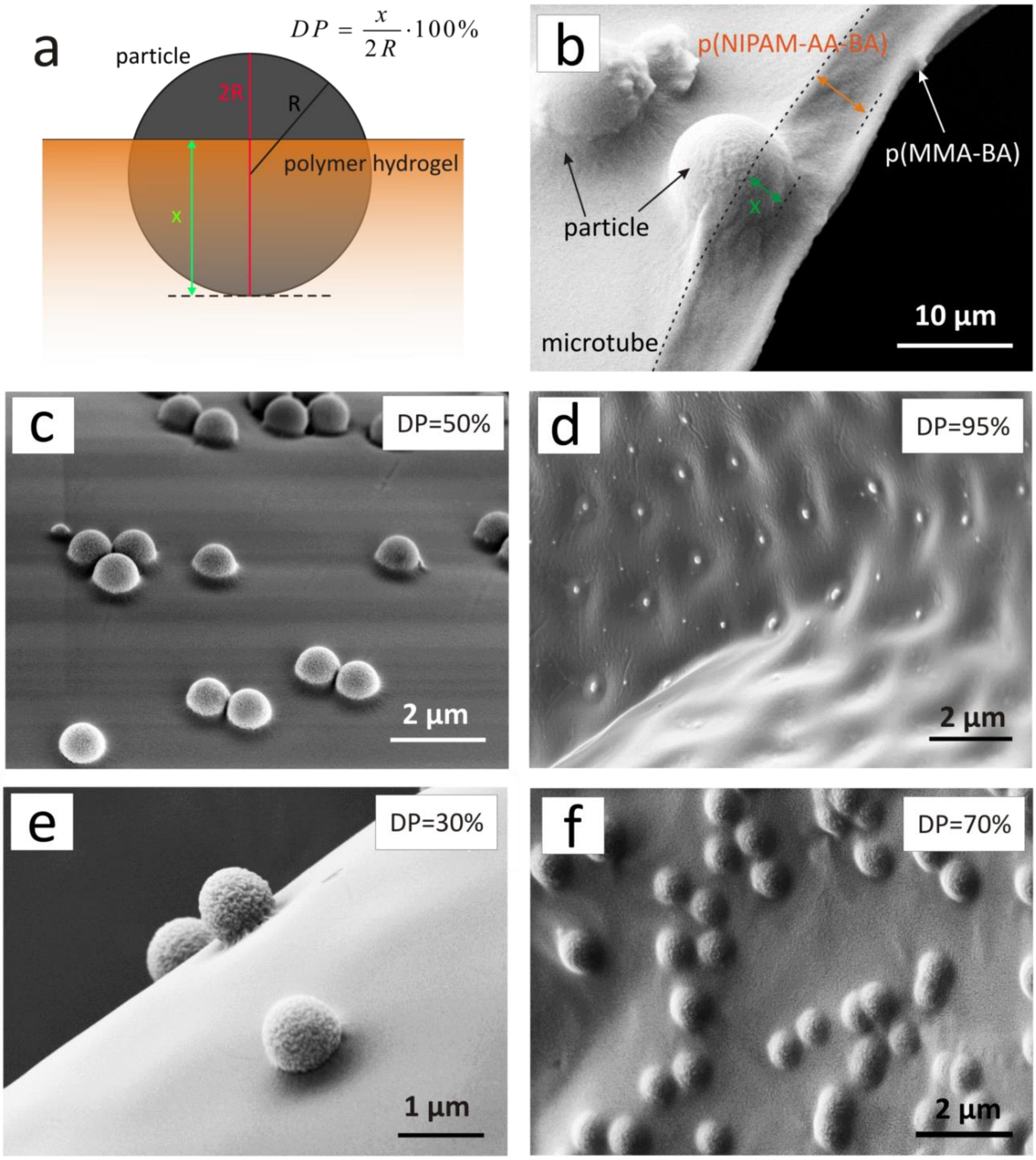
a
$DP = \frac{x}{2R} \cdot 100\%$
particle
2R
R
polymer hydrogel
x
b
p(NIPAM-AA-BA)
p(MMA-BA)
particle
x
microtube
10 µm
c
DP=50%
2 µm
d
DP=95%
2 µm
e
DP=30%
1 µm
f
DP=70%
2 µm

Figure 4.23 | Interaction of positively charged particles with negatively charged external walls of self-rolled microtubes. Schematic illustration (a) and SEM image (b) of the particle immersed into a hydrogel formed by a layer of responsive polymer and calculation of the depth of particle penetration (DP). SEM images show the parts of self-rolled tube surfaces and illustrate the difference of DP depending on particles type and on the hydrogel crosslinking degree: (c) SP-PDMAEMA on p(NIPAM-AA-BA) hydrogel; (d) SP-Q-PDMAEMA on p(NIPAM-AA-BA) hydrogel; (e) SP-PDMAEMA on p(NIPAM-AA-BA) hydrogel with higher crosslinking degree (additional BPhOH); (f) SP-Q-PDMAEMA on p(NIPAM-AA-BA) hydrogel with higher crosslinking degree (additional BPhOH).

The depth of particle penetration into a polymer hydrogel was almost equal for interaction that took place in water and in PBS buffer, meaning that at equal tubes and particles concentrations, the effective recharged area of the tubes was the same for both solutions. Once particles came in contact with p(NIPAM-AA-BA) hydrogel, cooperative interaction of the functional groups of the polymers provided strong attachment of the particles and mechanically stable surface coverage. Particles stayed attached even after tubes were dried. To examine the effect of solvent exchange, several tubes were removed from the particle-tube dispersion and compared with the tubes extracted after washing. For that, the dispersion was left for several minutes to let the tubes settle down, the medium was exchanged and the tubes redispersed in water. The washing procedure was repeated several times. Analysis of SEM images of the tubes before and after washing gave the same surface coverage: the particles were not detached from the tubes during redispersion and shaking. The same results were obtained for redispersion in PBS buffer. Hence, in the range of used conditions (ionic strength and pH), interpolyelectrolyte interactions are strong enough, and particles are stable attached to the tube walls.

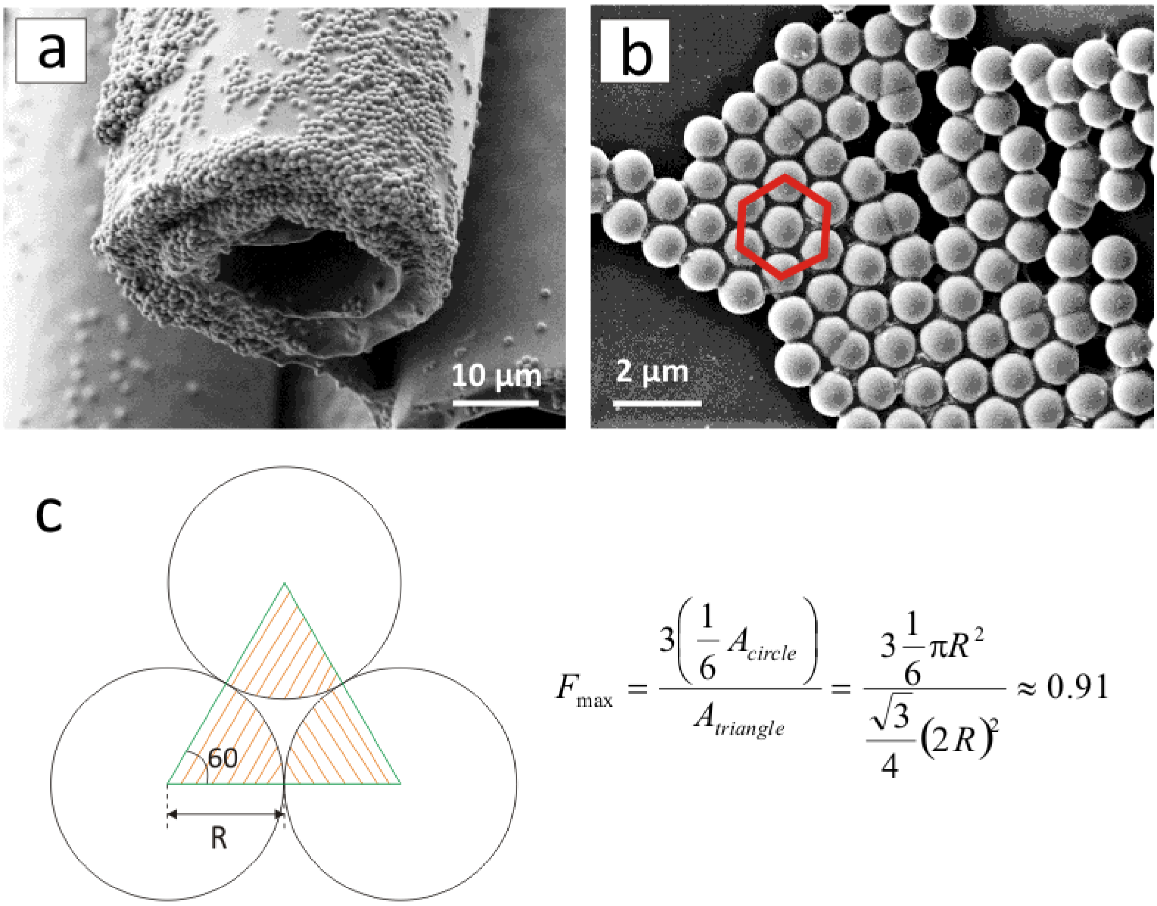

$$F_{\max} = \frac{3\left(\frac{1}{6}A_{circle}\right)}{A_{triangle}} = \frac{3\frac{1}{6}\pi R^2}{\frac{\sqrt{3}}{4}(2R)^2} \approx 0.91$$

Figure 4.24 | Arrangement of the particles on the surface of self-rolled microtubes: (a) saturation of the microtube surface with particles; (b) hexagonal packing of the particles on the surface of a self-rolled tube; (c) calculation of surface coverage for hexagonal close packing of hard spheres

The positive charged particle-formed “patches” on the wall of one tube can interact with the negative charged wall of a second tube (Figure 4.25), resulting in tubes agglomeration. However, there has been no significant interaction between individual tubes dispersed in PBS buffer, while in water aggregates were formed. This effect is obviously due to ionic strength that leads to a screening of the charges of carboxylic and amino groups and terminates tube interactions in buffer.

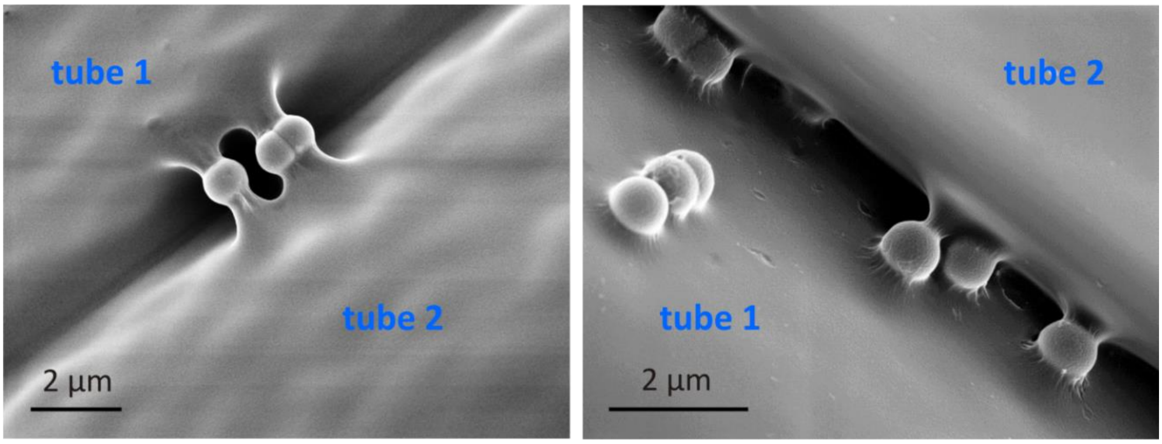

Figure 4.25 | Particles simultaneously interact with two microtubes, fixing them together.

The best aggregation rate in water tube-particle dispersion was observed, when PDMAEMA covered particles were used and p(NIPAM-AA-BA) hydrogel contained additionally admixed crosslinker (BPhOH). Indeed, in this case the particles on the tube walls are most exposed to a surrounding and therefore most available for further interaction, still being strongly attached to the tube. In all experiments discussed below this system has been used.

Based on the observations described above, the following procedure for tubes self-assembly was developed. Tubes were first fabricated (Figure 4.26a) and rinsed with deionized water into a glass vial (Figure 4.26b). A small amount of water dispersion of PDMAEMA covered SiO_2 particles was added to a dispersion of tubes (Figure 4.26c). The amount of particles was taken in respect to 25 - 30 % coverage of outer surface of the tubes. The resulting particle-tube dispersion was carefully shaken that led to fast (10-20 min) aggregation of the tubes due to formation of polyelectrolyte complex between charged groups on the particles and on the tube surfaces (Figure 4.26d). Additional alignment of the tubes was possible when an agglomerate was pulled off the dispersion with a needle (Figure 4.26e). Photographs of microtubes self-assembly in water are shown in Figure 4.27a-d. On the other hand, injection of excess particles (amount of particles is more than required to cover all tubes) did not lead to aggregation of tubes. In the first case, the surface of the tubes is not saturated with the particles and tubes have “patchy” surface consisting of areas with negative charge (polymer surface) and areas with positive charge (particles). As a result of interactions between positive and negative patches, tubes adhere to each other. In the second case, the tube surface is saturated with positively charged particles, which leads to charge inversion of the tube surface. Positively charged tubes covered with particles repel each other due to electrostatic interaction and are unable to assemble. However, in this case, assembly is possible when negatively charged tubes which are not covered with particles are added.

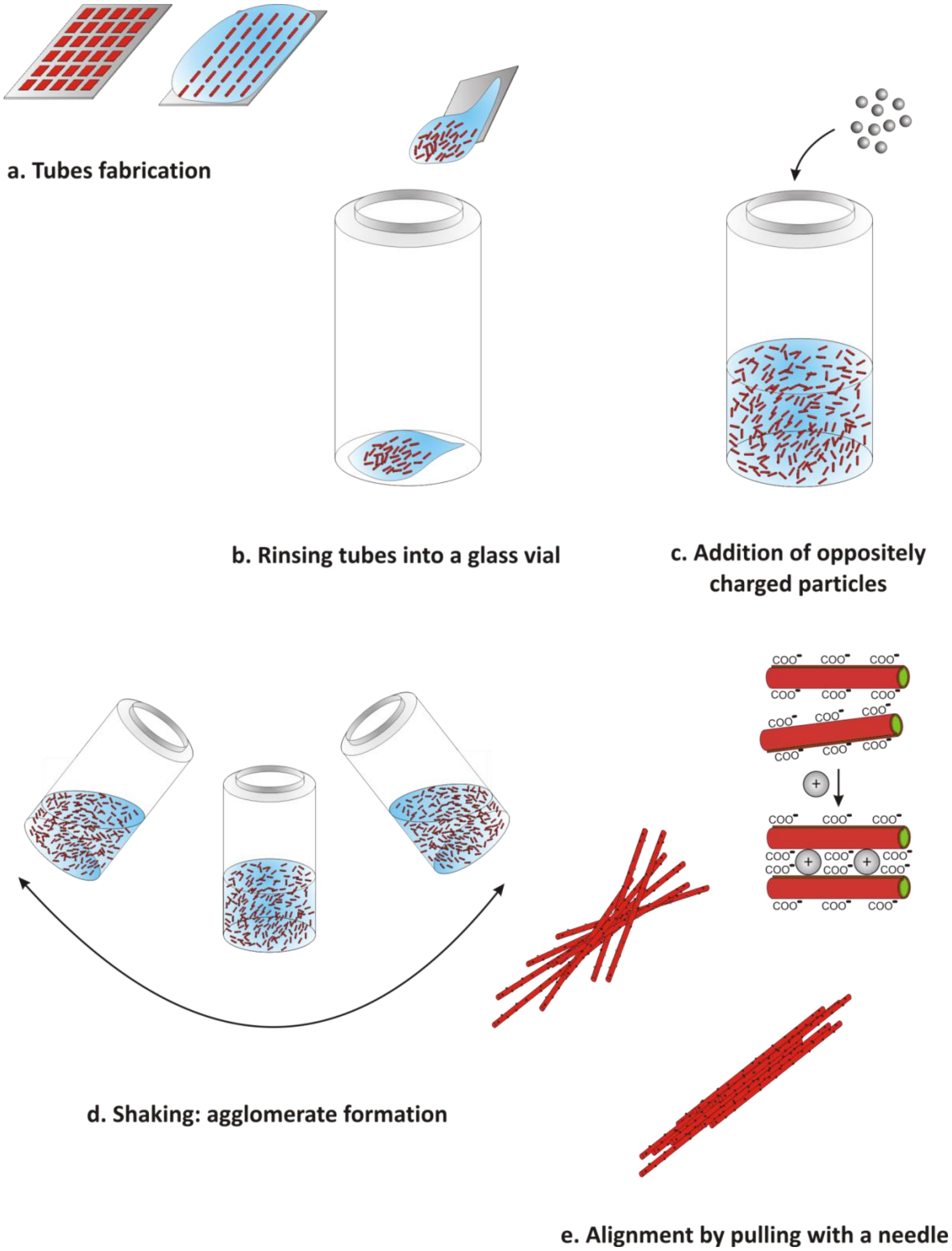
a. Tubes fabrication
b. Rinsing tubes into a glass vial
c. Addition of oppositely charged particles
COO⁻ COO⁻ COO⁻
COO⁻ COO⁻ COO⁻
COO⁻ COO⁻ COO⁻
COO⁻ COO⁻ COO⁻
+
COO⁻ COO⁻ COO⁻
COO⁻ + COO⁻ + COO⁻
COO⁻ COO⁻ COO⁻
COO⁻ COO⁻ COO⁻
d. Shaking: agglomerate formation
e. Alignment by pulling with a needle

Figure 4.26 | Scheme of tube assembly with fixation of 3D structure, followed by alignment. (a) Tubes are fabricated on the substrate; (b) fabricated tubes are rinsed with water from the substrate into a glass vial; (c) water dispersion of oppositely charged particles is added to the tubes dispersion; (d) shaking of the mixture for 10-15 min, followed by tubes agglomeration; (e) tubes are aligned by pulling with a needle.

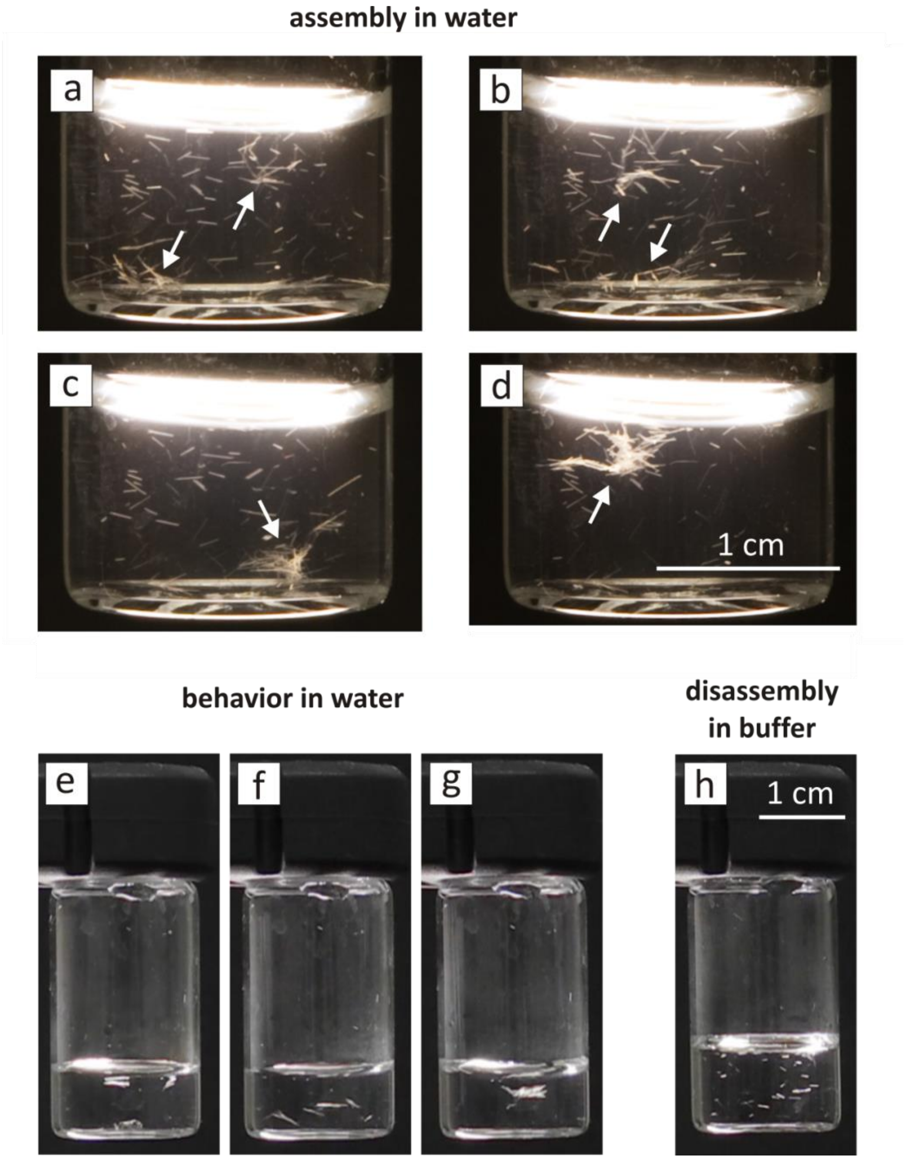

Figure 4.27 | Self-assembly of self-rolled tubes: (a-d) optical photographs of microtubes during self-assembly (c = 180 tubes per ml); (e-g) optical photographs of microtube aggregates in water after shaking (c = 90 tubes per ml); and (h) optical photographs of the disassembly of microtube aggregates in PBS buffer (I=0.15, pH 7.4).

Formed aggregates are mechanically stable in Millipore water. Upon intensive shaking they can break apart into smaller aggregates, which, however, re-assemble again (Figure 4.27e-g). The aggregates are less stable in saline buffer environment. For example, fresh aggregates easily break apart into small ones after transfer in PBS 0.15 M pH = 7.4 buffer (Figure 4.27h). Obviously, the increase of ionic strength leads to screening of the charges of carboxylic and amino groups that results in weakening of the bonds between the tubes and disassembly. Small agglomerates, which stay stable in saline buffer, have a well aligned structure. Transfer of the tubes obtained by disassembly of aggregates back in deionized water leads to restoration of electrostatic interactions and re-agglomeration of the tubes (not shown). The self-rolled tubes, thus, demonstrate an ability of reversible stimuli-controlled assembly-disassembly.

Next, the self-assembly of the tubes was modeled. The tubes are linked by multiple non-covalent bonds formed between the tube surface and brush layer on the particles. While a small number of non-covalent bonds is relatively weak and can be easily broken, the probability to break many non-covalent bonds is small. Two different scenarios of aggregation can be proposed by considering the assembly of three tubes (Figure 4.28). All three tubes are separate at the beginning (Figure 4.28a). Let us consider that the green tube sticks to the blue one (Figure 4.28b), and finally the red tube sticks to the aggregate of blue and green (Figure 4.28c). Since the contact area between the green and the blue tubes is not large, they can rotate with a characteristic rotational time t_1. As soon as both tubes align with each other, the contact area between them will increase and further rotation will be suppressed. On the other hand, the time that is needed for the red tube to reach the aggregate shall be denoted by t_2. If $t_1 >> t_2$ the green and blue tubes will not have enough time to align. In this case, the red tube will stick to both tubes and stabilize the disordered structure by forming additional bonds. In the opposite case for $t_1 << t_2$, the green and the blue tube will be able to orient parallel to each other before the red tube sticks to them. This scenario can easily be extended to a larger number of tubes. The rotational time (t_1) for a thin rigid rod scales with the third power of the length of the rod, i.e. $t_1 \sim l^3$[205]. The translational time (t_2) is given by the diffusion of the rod over the average distance between two rods, $\xi \sim c^{-1/3}$, where c denotes the concentration of tubes/rods. The diffusion coefficient for the translational diffusion of the rod can be assumed to scale as $D \sim 1/l$[205]. The typical distance over which the tubes can diffuse during time t_1 is thus given by $\xi \sim l$. Therefore, one can expect that if the distance between the tubes is much larger than their own length, the formation of more ordered agglomerates is expected. The characteristic concentration scales accordingly as $c^* \sim 1/l^3$. The distance between the tubes illustrated in Figure 4.27a-d, as calculated from their concentration (c = 180 tubes per ml), is approximately d = 1.8 mm, which is comparable to their length l = 1.6 mm. Therefore, one can expect formation of both ordered and unordered agglomerates in this case. The tubes in the aggregates, which were obtained from more (c = 250 tubes per ml, Figure 4.29c-e) and less (c = 90 tubes per ml, Figure 4.27e-g) concentrated dispersions, are less and more ordered, respectively.

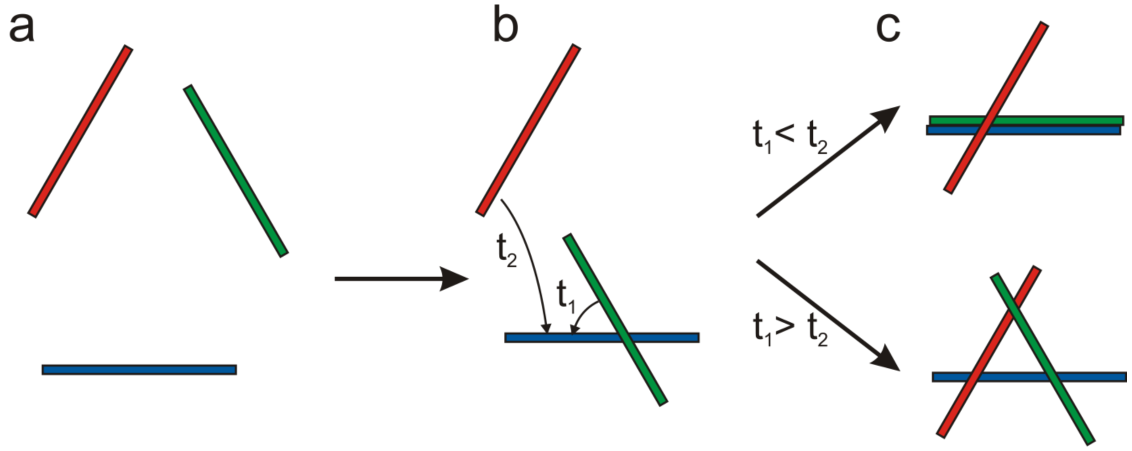

Figure 4.28 | Scheme of the agglomeration of 3 tubes in dispersion. All three tubes are separate in the first moment. The green tube sticks to the blue one and, finally, the red tube sticks to the aggregate of blue and green ones. t_1 and t_2 are the times needed for rotation of the green tube and diffusion of the red tube, respectively.

The tubes strongly align in one direction when a force is applied. This, for example, occurs when the aggregates are pulled out from the water with a needle (Figure 4.29). Moreover, aggregates where tubes are aligned are more stable comparing to that ones where the tubes are disordered: the aligned aggregates do not break apart in PBS buffer. The character of tube orientation corresponds to orientation in nematic liquid crystals – tubes are oriented in one direction while their centers of mass are unordered. The two-dimensional degree of tube orientation (S) was estimated using equation 4.1[206]. It was found that orientation degree in the sample illustrated in Figure 4.29f-h (c = 50 tubes per ml) is extremely high, $S = 0.98$. Tubes in the sample illustrated in Figure 4.29c-e, which was obtained by assembly at higher concentration of microtubes (c = 250 tubes per ml), have an apparently lower orientation degree.

$$S = \frac{\left\langle 3(\cos\theta)^2 - 1 \right\rangle}{2} \qquad (4.1)$$

The porosity of the formed aggregates was estimated by considering the inner diameter of the tubes, wall thickness as well as packing density of the tubes. The inner diameter (d_{inn}) varied in the range of 10 - 100 µm, the thickness (d_{wall}) of swollen wall was approximately 1 - 5 µm depending on the thickness of polymer layers. The maximal packing density of cylinders was ca. 0.91. The porosity (P, ratio of pore volume to total volume), which was estimated using equation 4.2, varied in the range P = 76 % - 90 %.

$$P = \frac{(0.5d_{inn})^2}{0.91(0.5d_{inn} + d_{wall})^2} \qquad (4.2)$$

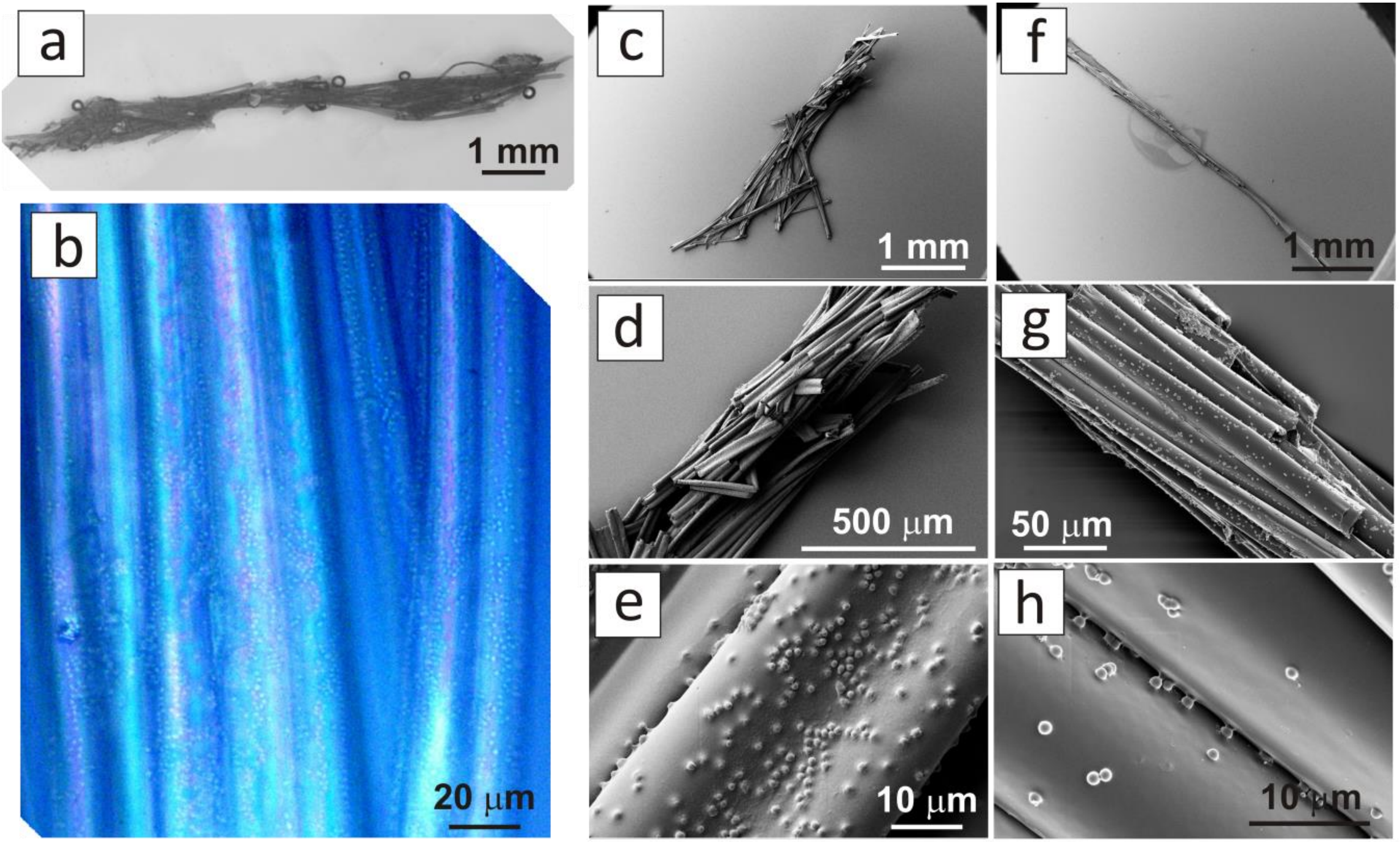
a
1 mm
b
20 μm
c
1 mm
d
500 μm
e
10 μm
f
1 mm
g
50 μm
h
10 μm

Figure 4.29 | Aligned self-assembled self-rolled tubes. (a and b) Optical microscopy, (c-h) scanning electron microscopy images of two aggregats (c-e and f-h) formed by self-rolled tubes crosslinked by positively charged particles and aligned by pulling out from water with a needle.

4.4.3.2 Complex structures consisting of two types of microtubes

The used assembling approach allows us to fabricate complex porous architectures consisting of microtubes with different properties. To distinguish the tubes, they were labeled with red and green fluorescent QDs admixed to the PMMA layer (“red” and “green” tubes). The possibility to form “mixed” and “core-shell” structures was examined.

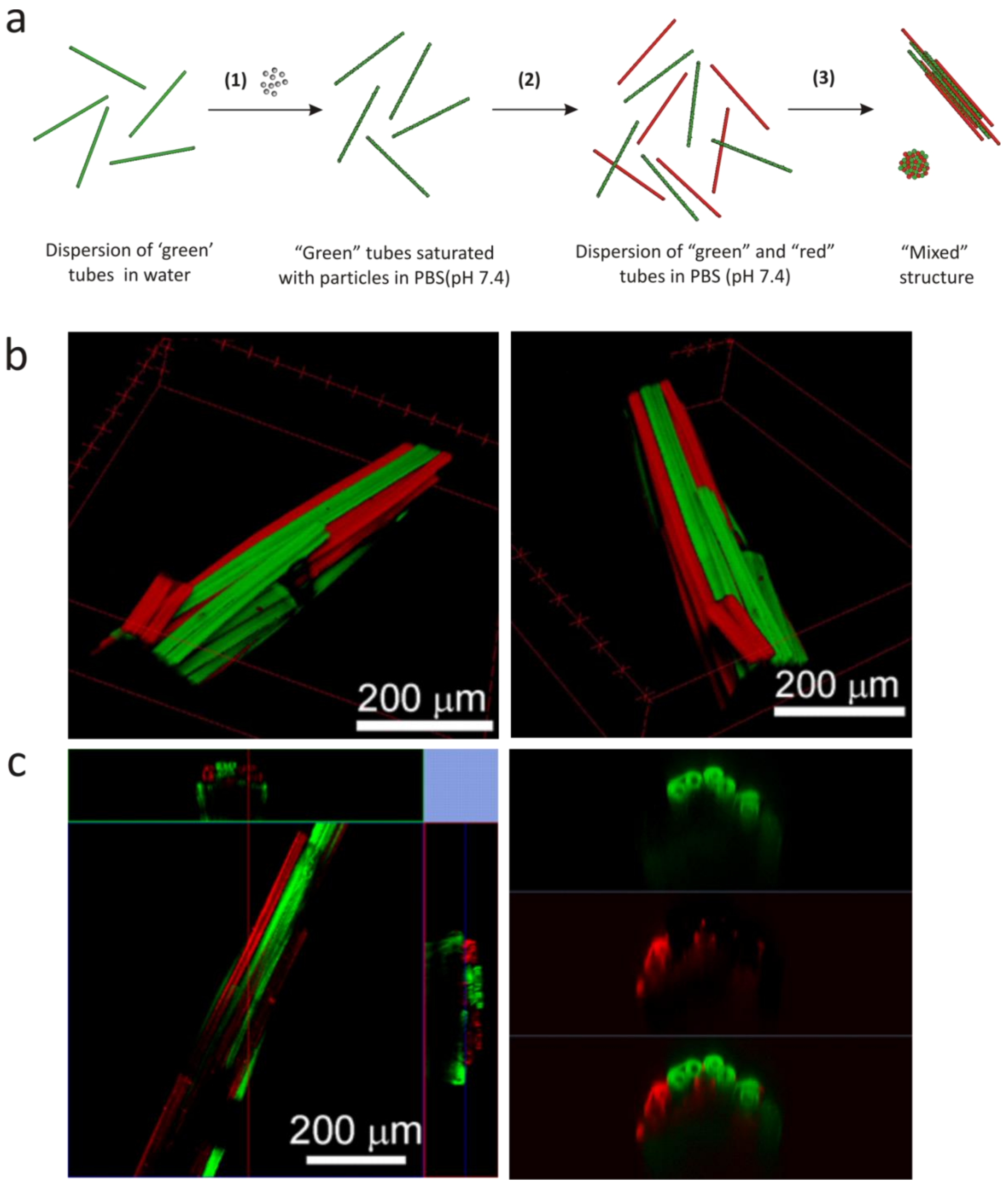
a
(1)
(2)
(3)
Dispersion of ‘green’ tubes in water
“Green” tubes saturated with particles in PBS(pH 7.4)
Dispersion of “green” and “red” tubes in PBS (pH 7.4)
“Mixed” structure
b
200 μm
200 μm
c
200 μm

Figure 4.30 | “Mixed” porous microtube scaffold. (a) Scheme of assembling experiment: (1) addition of the excess of oppositely charged particles to a dispersion of “green” tubes in PBS (pH 7.4), (2) “green” tubes saturated with particles and not agglomerated are added to a dispersion of “red” tubes in PBS, (3) exchange of PBS to water, followed by assembly of the microtubes into a “mixed” structure; (b) confocal microscopy images of a “mixed” porous scaffold, where “green” tubes are first coated by PDMAEMA particles and then assembled together with “red” ones, 3D reconstruction; (c) confocal microscopy optical section through the “mixed” microtubes porous scaffold (left); Z cross-section: green channel, red channel and mixed image (right).

In the first experiment, schematically depicted in Figure 4.30a, "green" tubes were mixed with excess of PDMAEMA-coated particles in PBS buffer which terminates aggregation, and incubated together for 30 min. The particle-coated but not agglomerated green tubes were added to the dispersion of "red" ones and solvent was replaced by water to allow the agglomeration. As a result, an agglomerate consisting of randomly distributed red and green tubes was formed that can be seen from a 3D reconstruction and from the optical sections provided by confocal microscopy investigation (Figure 4.30b-c).

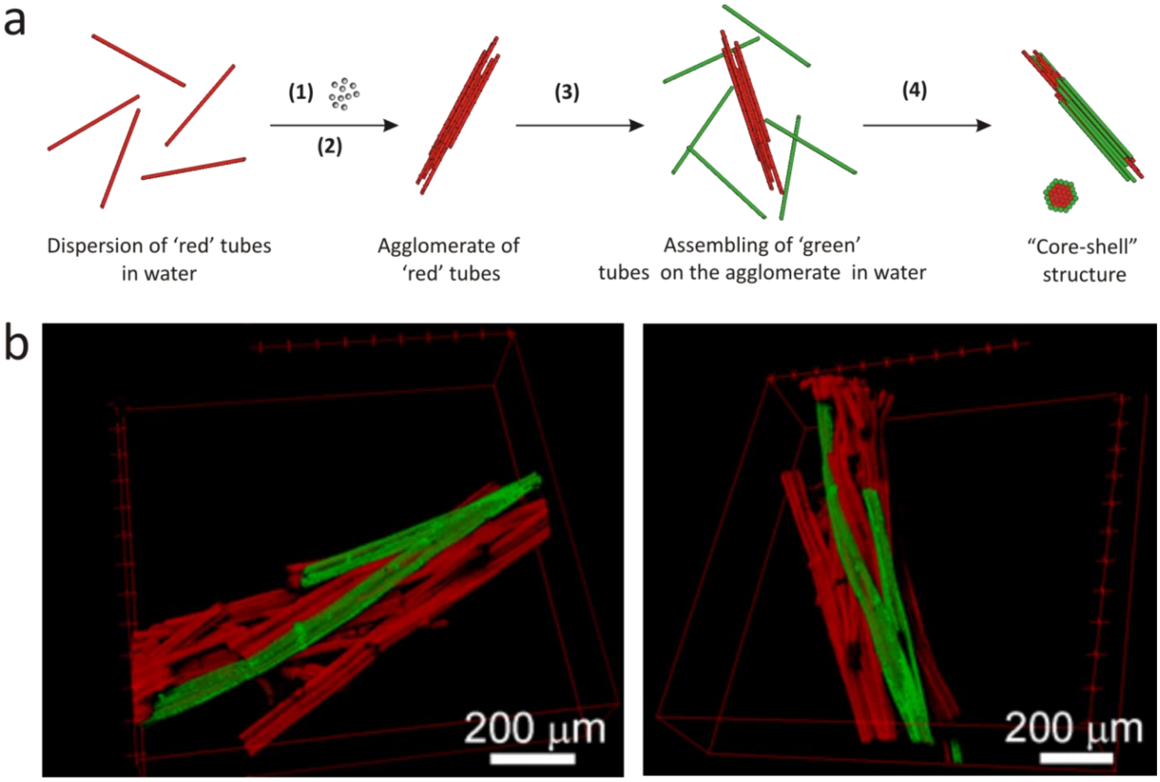
a
(1)
(2)
(3)
(4)
Dispersion of 'red' tubes in water
Agglomerate of 'red' tubes
Assembling of 'green' tubes on the agglomerate in water
"Core-shell" structure
b
200 µm
200 µm

Figure 4.31 | "Core-shell" porous microtube scaffold. (a) Scheme of assembling experiment: (1) addition of the oppositely charged particles to a water dispersion of "red" tubes and formation of agglomerate, (2) alignment by pulling with a needle, (3) addition of preassembled agglomerate of "red" tubes to a water dispersion of "green" tubes, (4) assembling of "green" tubes on the "red" agglomerate in water and formation of "core-shell" microtubes structure; (b) confocal microscopy images of "core-shell" porous scaffold, where green tubes are immobilized on assembly of red ones, 3D reconstruction.

In the second experiment, schematically represented in Figure 4.31a, "red" tubes were assembled by crosslinking with colloidal particles in water and additionally aligned by pulling with a needle. The formed aggregate of uniaxially aligned tubes was immersed in a water dispersion of "green" tubes. The negatively charged "green" tubes stuck to the positively charged particles patches presented on the aggregate of "red" tubes starting to form a "core-shell" structure (Figure 4.31b). The fact, that the "shell" of green tubes is not completed in the sample presented in Figure 4.31b is apparently due to low concentration of “green” tubes in dispersion. To increase the probability for free tubes to come into a contact with the agglomerate and therefore to achieve a completely closed “shell” structure, either the time of immersion of preassembled agglomerate in the “green” tubes dispersion or the concentration of the latter should be increased.

4.4.3.3 Fabrication of porous self-assembled tubular constructs filled with yeast cells

Finally, the possibility to fabricate a porous self-assembled construct where tubular pores are filled with cells was explored. For this, yeast cells were adsorbed from water dispersion on the top of patterned unfolded p(NIPAM-AA-BA)/p(MMA-BA) bilayers at room temperature. At these conditions, rolling was very slow providing enough time for cells to adsorb on the surface (Figure 4.32a). After the yeast cells were settled down from their aqueous dispersion, water was replaced with PBS buffer to stimulate rolling of the tubes and encapsulation of the yeast cells (Figure 4.32b). The tubes filled with cells were washed off from the substrate with several milliliters of water into a glass vial (Figure 4.32c).

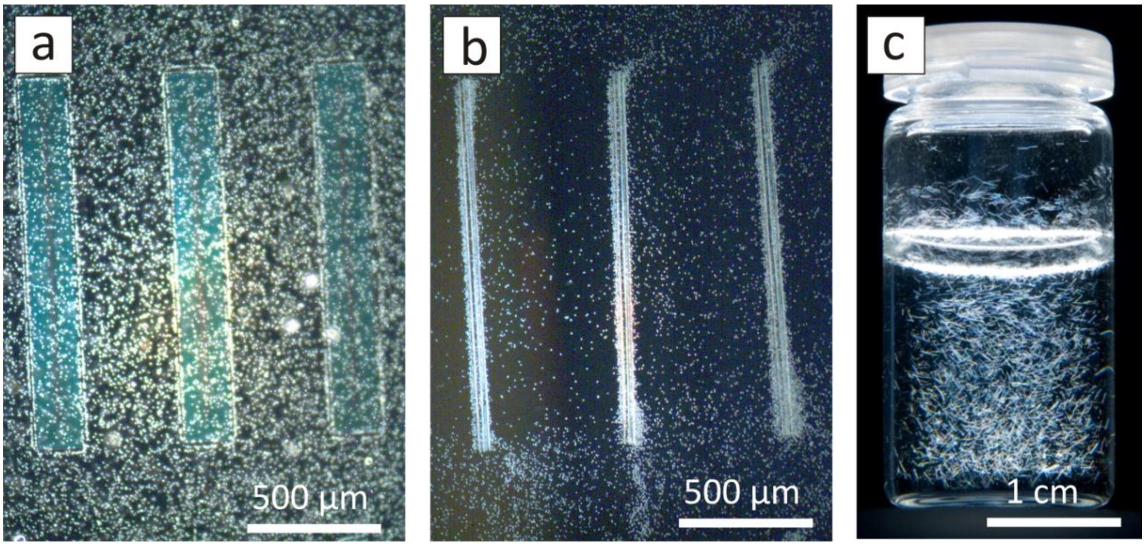

Figure 4.32 | Polymer bilayers at different stages of processing: (a) dark field microscopy image after yeast cells were adsorbed on the patterned bilayer (in water, at room temperature); (b) dark field microscopy image after tube rolling and encapsulation of the cells (in PBS pH 7.4 buffer, at RT); and (c) photograph of aqueous dispersion of self-rolled tubes.

Afterwards, tubes were assembled into agglomerates by shaking them together with a small amount of PDMAEMA coated particles. The yeast cells stayed encapsulated inside the tubes during assembly. The assembled tubes were aligned by pulling them out from water with a needle (similar to the previous experiments, Figure 4.33a), transferred into the culture medium and incubated there for 24 h at room temperature. The number of cells inside the tubes increased significantly indicating free diffusion of nutrition molecules into the tubes (Figure 4.33b) at least until the tube is completely filled with yeast cells. In this experiment, fabricated tubes had a small inner diameter (d_{inn} = 20 µm) which is very close to the size of the yeast cells (d = 5 µm), in order to demonstrate the advantage of used approach. Obviously, postfilling of narrow tubes, which are disconnected from the tubular network, with cells is almost impossible due to the slow migration of cells into the narrow tubes. Indeed, some tubes, which were occasionally not filled with cells during tube formation, remained empty after incubation in the cell culture medium. For example, tube 1 (Figure 4.33a) was empty after cell encapsulation and it remained empty after 24 h of incubation in the cell culture medium. In contrast, tube 2, which was initially partly filled with yeast cells, is completely filled with yeast cells after incubation. In this experiment, yeast cells were used for demonstration of the proof of the concept. It was demonstrated that the number of cells increases with time and cells receive enough nutrition, which might be an issue in narrow tubes. As it was demonstrated in Chapter 4.1.3.8 mammalian cells can also be encapsulated inside self-rolled tubes, which potentially allows fabrication of 3D scaffolds for tissue engineering.

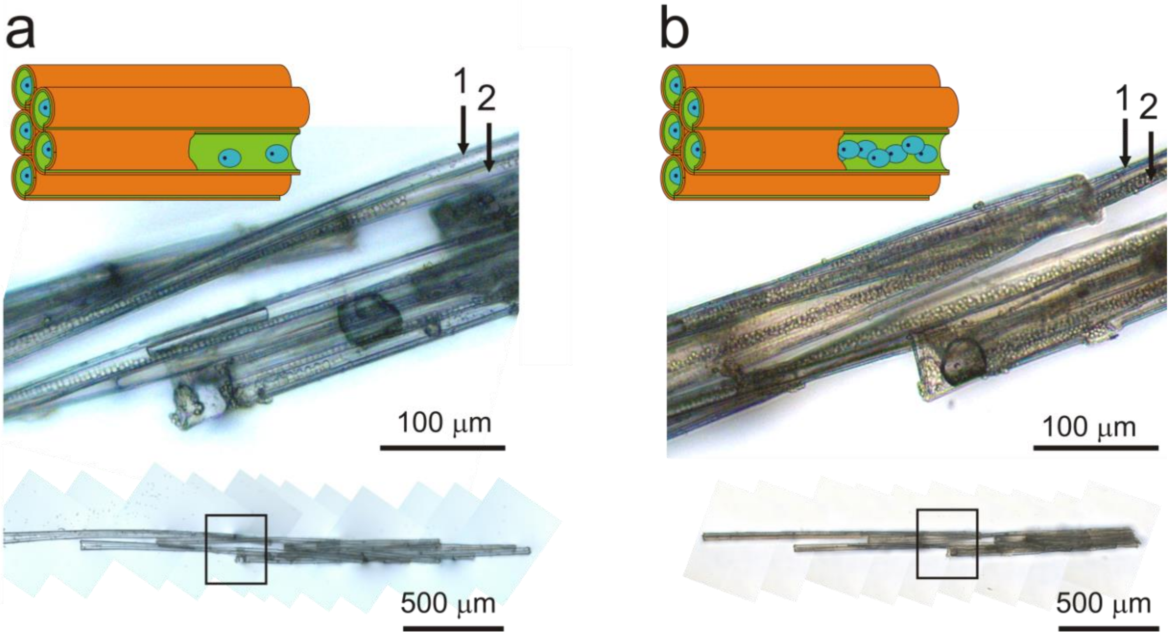

Figure 4.33 | Porous 3D construct obtained by self-assembly of self-rolled tubes filled with yeast cells: (a) directly after self-assembly; (b) after 1 day of incubation in the cell culture medium. The images in the lower panel are the microscopy snapshots of the whole cell-filled agglomerate. The images in the middle panel are the magnifications of the areas restricted by rectangles. Tubes 1 and 2 are empty and partially filled with yeast cells, respectively right after assembly. Tube 1 remains empty after incubation in the cell culture medium. Tube 2 is completely filled with cells after incubation in the cell culture medium.

4.4.4 Conclusions

A novel approach for the fabrication of self-assembled porous scaffolds with uniaxial tubular pores has been developed. The approach is based on the use of microtubes formed by stimuli-induced rolling of rectangular bilayers consisting of hydrophobic and stimuli-responsive hydrophilic polymers. Any micrometer objects, for example yeast cells, can be encapsulated inside the tubes during their rolling. The self-rolled tubes filled with the yeast cells can be easily assembled in an uniaxial tubular scaffold homogeneously filled with the cells. The main advantage of this approach is the possibility to homogenously fill the pores with any kind of matter – inorganic, organic or living. Moreover, the approach allows the design of porous material with complex architectures formed by tubes of different sorts.

The developed approach is versatile and very simple. Indeed, the preparation of polymer films does not require expensive equipment und is easy to perform. The polymers, used for a proof of the concept, are not biodegradable. On the other hand since the approach is generic, a variety of polymers with different properties such as biodegradability can be used, which allows the design of novel materials with advanced properties for biomedical purposes.

5 Summary and outlook

The aim of this thesis was to demonstrate a proof of the concept, offering to use self-rolled polymer tubes for a variety of bioapplications. The concept includes fabrication of biocompatible/biodegradable self-rolled tubes, which are sensitive to stimuli at physiological conditions and can be loaded with cells during the rolling process. As a second step, cell-loaded microtubes can be assembled into a 3D construct with uniaxially aligned pores, homogeneously filled with cells. This chapter summarizes obtained results.

Polymer bilayers foldable in physiological conditions

Three polymer systems were designed and investigated in the present work in order to allow triggered folding of the bilayer.

In the first system poly(N-isopropylacrylamide) (PNIPAM) was used as an active component and hydrophobic polycaprolactone (PCL) or polymethylmethacrylate (PMMA) as a passive one. In an aqueous environment PNIPAM homopolymer reversibly changes its solubility at the Low Critical Solution Temperature (LCST) of 32 - 33 °C, changing from a hydrophilic state below this temperature to a hydrophobic state above it. Bilayer films are able to self-roll and unroll due to swelling and collapse of PNIPAM at low and elevated temperatures, respectively.

Characteristics of the system:

- Biocompatible; partially biodegradable (PNIPAM/PCL);
- Experimental conditions: physiological buffer; temperature range 20 - 37° C;
- Thermo-responsive, stimulus: temperature decreases below LCST of PNIPAM-co-polymer;
- Folding within 1 - 10 min;
- Reversibility: tube formation can be both reversible and irreversible depending on the tubes’ morphology. Tubes formed by one revolution unroll at the temperature above the LCST of PNIPAM, such folding and unfolding can be repeated many times. Tubes formed by multiple revolutions are not able to unroll and either keep constant inner diameter or shrink upon increase of the temperature.

The second designed system was based on polysuccinimide/polycaprolactone (PSI/PCL) bilayer. Both polymers are hydrophobic and intrinsically water-insoluble. Polysuccinimide, however, is able to hydrolyze in physiological buffer environment, yielding water-swellable biodegradable polyaspartic acid, which leads to rolling of the tubes.

Characteristics of the system:

- Fully biocompatible and biodegradable;
- Experimental conditions: physiological buffer; temperature range 25 - 37° C;

- Solvent-responsive, stimulus: hydrolysis of PSI;
- Folding within 24 h;
- Reversibility: irreversible, only folding is possible.

The third polymeric system consisted of natural biodegradable polymer gelatin as active layer and PCL as a passive one. Gelatin forms hydrogels upon cooling from an aqueous solution, due to helix-formation and association of the helices. These physically crosslinked hydrogels have a sol-gel transition temperature. Chemically crosslinked gelatin undergoes one-way swelling in aqueous environment, wherein the degree of swelling strongly depends on the temperature.

Characteristic of the system:

- Fully biocompatible and biodegradable;
- Experimental conditions: physiological buffer; temperature range 25 - 37° C;
- Thermo-responsive, stimulus: increased temperature 37 °C;
- Folding within 30 min - 1 h;
- Reversibility: reversible (one cycle) for non-crosslinked bilayer and irreversible (only folding is possible) for crosslinked bilayer.

For each designed system the direction of rolling, morphology of formed tubes, reversibility of rolling as well as possibility to vary tubes' diameters were investigated.

Encapsulation of particles and cells

The possibility to encapsulate micro objects inside self-rolled polymer tubes was demonstrated on the example of 10 µm sized silica particles, yeast cells and mammalian HeLa cells. At conditions when bilayer film is unfolded, particles or cells were deposited from their aqueous dispersion on the top of bilayer. An appropriate change of conditions triggers folding of the bilayer and results in encapsulation of particles or cells inside the tubes.

One way swelling of an active polymer allows irreversible encapsulation of cells in a way that tubes do not unroll and cells cannot escape. It was demonstrated that encapsulated cells can proliferate and divide inside the tubes for a long period of time. Since used polymers are optically transparent, encapsulated cells can be easily observed using optical and fluorescent microscopy. Reversible swelling demonstrated by the PNIPAM-based system provides the possibility to release encapsulated objects when temperature is increased above LCST of PNIPAM and tubes unroll. At the same time PNIPAM based tubes formed by multiple-revolution are unable to unroll, but rather shrink in diameter, which leads to the squeezing of encapsulated objects.

Assembly of the individual tubes

Using the PNIPAM/PMMA system it was demonstrated that in aqueous media microtubes possessing small amount of negatively charged groups on external walls self-assemble in the presence of oppositely charged microparticles that results in a formation of 3D constructs. In obtained aggregates tubes and therefore pores were well-aligned and the orientation degree was extremely high (up to 0.98). Porosity of the aggregates varied in the range of 76 - 90 %.

The possibility to encapsulate cells prior to tubes assembly was demonstrated on the example of yeast cells. The self-rolled tubes filled with the yeast cells are capable of controlled self-assembly and form a uniaxial tubular homogeneously filled scaffold. Moreover, the approach allows the design of porous materials with complex architectures formed by tubes of different sorts.

The results presented in this work demonstrate that the proposed approach is of practical interest for biotechnological applications. Self-rolled tubes can be filled with cells during their folding providing the desired homogeneity of filling. Individual tubes of different diameters could be used to investigate cell behavior in confinement in conditions of structural anisotropy as well as to mimic blood vessels. Due to their directionality tubes could be used to guide the growth of cells that is of interest for regeneration of neuronal tissue. Reversibly foldable films allow triggered capture and release of the cells that could be implemented for controlled cell delivery. In perspective, self-assembled 3D constructs with aligned pores could be used for bottom-up engineering of the scaffolds, mimicking such tissues as cortical bone and skeletal muscle, which are characterized by repeating longitudinal units. Such constructs can be also considered as a good alternative of traditional 2D flat cell culture.

Further investigations are, however, required in respect to the growth and viability of mammalian cells encapsulated within self-rolled polymer tubes with different diameters for a longer period of time. Moreover, the design of self-assembled tubular scaffolds was demonstrated on example of non-biodegradable PNIPAM-based microtubes. For potential application of this approach in tissue engineering it is necessary to demonstrate its applicability for fully biodegradable microtubes, such as gelatin-based ones.

List of abbreviations

2D	two-dimentional
3D	three-dimensional
Δ and ψ	ellipsometric angles
σ_{RMS}	root mean square roughness
AA	acrylic acid
AFM	atomic force microscopy
AIBN	2,2'-azobis(2-methylpropionitrile)
APS	(3-aminopropyl)triethoxysilane
BA	4-acryloylbenzophenone
BPhOH	4-hydroxybenzophenone
C	circumference of the first roll formed by the tube
CH_2Cl_2	dichloromethane
$CHCl_3$	chloroform
DAz	2,2'-stilbenedisulfonic acid disodium salt tetrahydrate
d_{inn}	inner diameter of the tube
DI water	deionized water
DMF	N,N-dimethylformamide
DP	depth of penetration of particles into a polymer hydrogel
EDTA	ethylenediaminetetraacetic acid
EtOH	ethanol
GPC	gel permission chromatography
L	length of the pattern
LCST	lower critical solution temperature
L/W ratio	ratio of pattern length to pattern width
MMA	methylmethacrylate
MSE	mean square error
n	refractive index
NIPAM	*N*-isopropylacrylamide
NMR	nuclear magnetic resonance
PAA	polyacrylic acid
PBS	phosphate buffered saline
PCL	polycaprolactone
PDI	polydispersity index
PDMS	polydimethylsiloxane
PEG	poly(ethylene glycol)
PMMA	polymethylmethacrylate
p(MMA-BA)	poly(methylmethacrylate-co-benzophenoneacylate), random

	copolymer
PNIPAM	poly(*N*-isopropyl acrylamide)
p(NIPAM-AA-BA)	poly(*N*-isopropylacrylamide-co-acylic acid-co-benzophenoneacylate), random copolymer
p(NIPAM-BA)	poly(*N*-isopropylacrylamide-co-benzophenoneacylate), random copolymer
PDMAEMA	poly(2-(dimethylamino)ethyl methacrylate)
PSI	polysuccinimide
QDs	quantum dots
Q-PDMAEMA	quaternized poly(2-(dimethylamino)ethyl methacrylate)
RMS	root mean square
RT	room temperature
SEM	scanning electron microscopy
SiO_2	silicon dioxide
SD	swelling degree
SP	silica particles
SP-PDMAEMA	silica particles with grafted brush layer of poly((2-dimethylamino)ethyl methacrylate)
SP-Q- PDMAEMA	silica particles with grafted brush layer of quaternized poly((2-dimethylamino)ethyl methacrylate)
T_m	melting temperature
THF	tetrahydrofuran
W	width of the pattern
W/C ratio	ratio of the pattern width to the circumference of the first roll of the tube

Table of figures

Figure 1.1 Scheme of the microtube-based scaffold formation 5

Figure 2.1 Different scenario of swelling of the hydrogels 13

Figure 2.2 Design of self-folding films 16

Figure 3.1 Simplified principle of null ellipsometry and scheme of ellipsometric experiment 37

Figure 3.2 Perception of a magnified virtual image in the microscope 40

Figure 3.3 Principle of the confocal microscopy 43

Figure 3.4 Atomic force microscopy 44

Figure 3.5 Illustration of AFM scratch test experiment 45

Figure 3.6 Quantum dots: absorbance and fluorescence spectra and TEM images 48

Figure 3.7 Scheme of chemisorption of 3-aminopropyltriethoxysilane on a silica surface 51

Figure 3.8 Scheme of patterned polymer bilayer film fabrication 53

Figure 3.9 Surface morphology of PCL thin films 57

Figure 3.10 Scheme of polymer UV light crosslinking using benzophenone derivatives 58

Figure 3.11 The defects of patterns due to development step 60

Figure 4.1 Swelling degree of PNIPAM-co-polymers in DI water and PBS buffer (0.15 M, pH = 7.4) at the temperature of 20°C and 37°C 70

Figure 4.2 Cyclic changes of swelling degree of PNIPAM-co-polymers 71

Figure 4.3 Scheme of temperature triggered formation PNIPAM-based self-rolled tube 71

Figure 4.4 Time-resolved microscopic images of PNIPAM-based tubes formation 72

Figure 4.5 Effect of the polymer layer thicknesses on the diameter of PNIPAM-based self-rolled tubes 74

Figure 4.6 Different morphologies of the tubes formed by rolling of PNIPAM/PMMA bilayers 76

Figure 4.7 Reversibility of PNIPAM-based tube formation 78

Figure 4.8 Encapsulation of the microparticles inside PNIPAM-based self-rolled tubes 79

Figure 4.9 Possibility to release encapsulated particles from PNIPAM-based tubes 80

Figure 4.10 Design strategy to obtain self-rolled tubes with desired properties 81
Figure 4.11 Microscopic images of HeLa cells growing on p(MMA-BA) film 82
Figure 4.12 Microscopic images of HeLa cells encapsulated in self-rolled polymer tubes 83
Figure 4.13 Fabrication of self-rolled tubes with porous walls 85
Figure 4.14 Magneto-sensitive PNIPAM-based microtubes 86
Figure 4.15 Swelling of photocrosslinked polysuccinimide film and self-rolling of PSI/PCL bilayers in PBS buffer at T = 25°C 90
Figure 4.16 Effect of the polymer layer thicknesses on the diameter of PSI/PCL self-rolled tubes 91
Figure 4.17 Different morphologies of tubes formed by the rolling of PSI/PCL bilayers 93
Figure 4.18 Encapsulation of yeast cells inside PSI/PCL self-rolling tubes 95
Figure 4.19 Non-crosslinked gelatin/polycaprolactone system 99
Figure 4.20 Crosslinked gelatin/polycaprolactone system 100
Figure 4.21 Scheme of fabrication of tubular self-assembling structures filled with cells using self-rolled tubes 106
Figure 4.22 Assembling and alignment of the tubes in water 109
Figure 4.23 Interaction of positively charged particles with negatively charged external walls of self-rolled microtubes 112
Figure 4.24 Arrangement of the particles on the surface of self-rolled microtubes 113
Figure 4.25 Particles simultaneously interact with two microtubes, fixing them together 114
Figure 4.26 Scheme of tube assembly with fixation of 3D structure, followed by alignment 115
Figure 4.27 Optical photographs of self-assembly of self-rolled tubes 116
Figure 4.28 Scheme of the agglomeration of 3 tubes in dispersion 118
Figure 4.29 Aligned self-assembled self-rolled tubes 119
Figure 4.30 “Mixed” porous microtube scaffold 120
Figure 4.31 “Core-shell” porous microtube scaffold 121
Figure 4.32 Polymer bilayers at different stages of processing 122
Figure 4.33 Porous 3D construct obtained by self-assembly of self-rolled tubes filled with yeast cells 123

References

[1] Hollister, S. J., *Adv Mater*, (2009) **21**, 3330.

[2] Khademhosseini, A.; Langer, R., *Biomaterials*, (2007) **28**, 5087.

[3] Zamanian, B.; Masaeli, M.; Nichol, J. W.; Khabiry, M.; Hancock, M. J.; Bae, H.; Khademhosseini, A., *Small*, (2010) **6**, 937.

[4] Du, Y.; Lo, E.; Ali, S.; Khademhosseini, A., *Proceedings of the National Academy of Sciences of the United States of America*, (2008) **105**, 9522.

[5] Luchnikov, V.; Sydorenko, O.; Stamm, M., *Advanced Materials*, (2005) **17**, 1177.

[6] Azam, A.; Laflin, K. E.; Jamal, M.; Fernandes, R.; Gracias, D. H., *Biomedical microdevices*, (2011) **13**, 51.

[7] Timoshenko, S., *J. Opt. Soc. Am. Rev. Sci. Instrum.*, (1925) **11**, 233.

[8] Solovev, A. A.; Mei, Y.; Bermudez Urena, E.; Huang, G.; Schmidt, O. G., *Small*, (2009) **5**, 1688.

[9] Smith, E. J.; Schulze, S.; Kiravittaya, S.; Mei, Y.; Sanchez, S.; Schmidt, O. G., *Nano letters*, (2011) **11**, 4037.

[10] Kumar, K.; Luchnikov, V.; Nandan, B.; Senkovskyy, V.; Stamm, M., *European Polymer Journal*, (2008) **44**, 4115.

[11] Hu, X. X.; Shen, H.; Yang, F.; Bei, J. Z.; Wang, S. G., *Biomaterials*, (2008) **29**, 3128.

[12] Ma, H. Y.; Hu, J. A.; Ma, P. X., *Advanced Functional Materials*, (2010) **20**, 2833.

[13] Yaszemski, M. J.; Payne, R. G.; Hayes, W. C.; Langer, R.; Mikos, A. G., *Biomaterials*, (1996) **17**, 175.

[14] Madden, L. R.; Mortisen, D. J.; Sussman, E. M.; Dupras, S. K.; Fugate, J. A.; Cuy, J. L.; Hauch, K. D.; Laflamme, M. A.; Murry, C. E.; Ratner, B. D., *Proceedings of the National Academy of Sciences of the United States of America*, (2010) **107**, 15211.

[15] Kenar, H.; Kose, G. T.; Toner, M.; Kaplan, D. L.; Hasirci, V., *Biomaterials*, (2011) **32**, 5320.

[16] Engelmayr, G. C.; Cheng, M. Y.; Bettinger, C. J.; Borenstein, J. T.; Langer, R.; Freed, L. E., *Nat. Mater.*, (2008) **7**, 1003.

[17] Smith, E. J.; Xi, W.; Makarov, D.; Monch, I.; Harazim, S.; Bolanos Quinones, V. A.; Schmidt, C. K.; Mei, Y.; Sanchez, S.; Schmidt, O. G., *Lab on a chip*, (2012) **12**, 1917.

[18] Nair, L. S.; Laurencin, C. T., *Progress in Polymer Science*, (2007) **32**, 762.

[19] Stuart, M. A. C.; Huck, W. T. S.; Genzer, J.; Mueller, M.; Ober, C.; Stamm, M.; Sukhorukov, G. B.; Szleifer, I.; Tsukruk, V. V.; Urban, M.; Winnik, F.; Zauscher, S.; Luzinov, I.; Minko, S., *Nat. Mater.*, (2010) **9**, 101.

[20] Kalaitzidou, K.; Crosby, A. J., *Applied Physics Letters*, (2008) **93**, 041910.

[21] Simpson, B.; Nunnery, G.; Tannenbaum, R.; Kalaitzidou, K., *Journal of Materials Chemistry*, (2010) **20**, 3496.

[22] Leong, T. G.; Zarafshar, A. M.; Gracias, D. H., *Small*, (2010) **6**, 792.

[23] Hawkes, E.; An, B.; Benbernou, N. M.; Tanaka, H.; Kim, S.; Demaine, E. D.; Rus, D.; Wood, R. J., *Proceedings of the National Academy of Sciences of the United States of America*, (2010) **107**, 12441.

[24] Smela, E.; Inganäs, O.; Lundström, I., *Science*, (1995) **268**, 1735.

[25] Jager, E. W. H.; Inganäs, O.; Lundström, I., *Science*, (2000) **288**, 2335.

[26] Bufon, C. C.; Gonzalez, J. D.; Thurmer, D. J.; Grimm, D.; Bauer, M.; Schmidt, O. G., *Nano letters*, (2010) **10**, 2506.

[27] Yang, L.; Wang, S.; Mao, J.; Deng, J.; Gao, Q.; Tang, Y.; Schmidt, O. G., *Adv Mater*, (2013) **25**, 1180.

[28] Ji, H. X.; Wu, X. L.; Fan, L. Z.; Krien, C.; Fiering, I.; Guo, Y. G.; Mei, Y.; Schmidt, O. G., *Adv Mater*, (2010) **22**, 4591.

[29] Solovev, A. A.; Sanchez, S.; Pumera, M.; Mei, Y. F.; Schmidt, O. G., *Advanced Functional Materials*, (2010) **20**, 2430.

[30] Mei, Y.; Solovev, A. A.; Sanchez, S.; Schmidt, O. G., *Chemical Society reviews*, (2011) **40**, 2109.

[31] Harazim, S. M.; Bolanos Quinones, V. A.; Kiravittaya, S.; Sanchez, S.; Schmidt, O. G., *Lab on a chip*, (2012) **12**, 2649.

[32] Huang, G. S.; Kiravittaya, S.; Bolaños Quiñones, V. A.; Ding, F.; Benyoucef, M.; Rastelli, A.; Mei, Y. F.; Schmidt, O. G., *Applied Physics Letters*, (2009) **94**, 141901.

[33] Huang, G.; Mei, Y.; Thurmer, D. J.; Coric, E.; Schmidt, O. G., *Lab on a chip*, (2009) **9**, 263.

[34] Bassik, N.; Brafman, A.; Zarafshar, A. M.; Jamal, M.; Luvsanjav, D.; Selaru, F. M.; Gracias, D. H., *J. Am. Chem. Soc.*, (2010) **132**, 16314.

[35] Fernandes, R.; Gracias, D. H., *Advanced drug delivery reviews*, (2012) **64**, 1579.

[36] Leong, T. G.; Randall, C. L.; Benson, B. R.; Zarafshar, A. M.; Gracias, D. H., *Lab on a chip*, (2008) **8**, 1621.

[37] Randall, C. L.; Kalinin, Y. V.; Jamal, M.; Manohar, T.; Gracias, D. H., *Lab on a chip*, (2011) **11**, 127.

[38] Randall, C. L.; Kalinin, Y. V.; Jamal, M.; Shah, A.; Gracias, D. H., *Nanomedicine : nanotechnology, biology, and medicine*, (2011) **7**, 686.

[39] Jamal, M.; Bassik, N.; Cho, J. H.; Randall, C. L.; Gracias, D. H., *Biomaterials*, (2010) **31**, 1683.

[40] Prinz, V. Y.; Seleznev, V. A.; Gutakovsky, A. K.; Chehovskiy, A. V.; Preobrazhenskii, V. V.; Putyato, M. A.; Gavrilova, T. A., *Physica E*, (2000) **6**, 828.

[41] Py, C.; Reverdy, P.; Doppler, L.; Bico, J.; Roman, B.; Baroud, C., *Physical Review Letters*, (2007) **98**,

[42] Behl, M.; Lendlein, A., *Materials Today*, (2007) **10**, 20.

[43] Bassik, N.; Abebe, B. T.; Laflin, K. E.; Gracias, D. H., *Polymer*, (2010) **51**, 6093.

[44] Bhattacharya, S.; Eckert, F.; Boyko, V.; Pich, A., *Small*, (2007) **3**, 650.

[45] Ulijn, R.; Bibi, N.; Jayawarna, V.; Thornton, P.; Todd, S.; Mart, R.; Smith, A.; Gough, J., *Materials Today*, (2007) **10**, 40.

[46] Kwon, G. H.; Choi, Y. Y.; Park, J. Y.; Woo, D. H.; Lee, K. B.; Kim, J. H.; Lee, S. H., *Lab on a chip*, (2010) **10**, 1604.

[47] Holmes, D. P.; Roché, M.; Sinha, T.; Stone, H. A., *Soft Matter*, (2011) **7**, 5188.

[48] Yu, C.; Duan, Z.; Yuan, P.; Li, Y.; Su, Y.; Zhang, X.; Pan, Y.; Dai, L. L.; Nuzzo, R. G.; Huang, Y.; Jiang, H.; Rogers, J. A., *Adv Mater*, (2013) **25**, 1541.

[49] Mansfield, E. H., *Proceedings of the Royal Society of London Series a-Mathematical and Physical Sciences*, (1962) **268**, 316.

[50] Mansfield, E. H., *Proceedings of the Royal Society of London Series a-Mathematical and Physical Sciences*, (1965) **288**, 396.

[51] Alben, S.; Balakrisnan, B.; Smela, E., *Nano letters*, (2011) **11**, 2280.

[52] Chun, I. S.; Challa, A.; Derickson, B.; Hsia, K. J.; Li, X., *Nano letters*, (2010) **10**, 3927.

[53] Cendula, P.; Kiravittaya, S.; Monch, I.; Schumann, J.; Schmidt, O. G., *Nano letters*, (2011) **11**, 236.

[54] Kim, J.; Hanna, J. A.; Hayward, R. C.; Santangelo, C. D., *Soft Matter*, (2012) **8**, 2375.

[55] Kim, J.; Hanna, J. A.; Byun, M.; Santangelo, C. D.; Hayward, R. C., *Science*, (2012) **335**, 1201.

[56] Jamal, M.; Zarafshar, A. M.; Gracias, D. H., *Nature communications*, (2011) **2**, 527.

[57] Klein, Y.; Efrati, E.; Sharon, E., *Science*, (2007) **315**, 1116.

[58] Konotop, I. Y.; Nasimova, I. R.; Tamm, M. V.; Rambidi, N. G.; Khokhlov, A. R., *Soft Matter*, (2010) **6**, 1632.

[59] Randhawa, J. S.; Leong, T. G.; Bassik, N.; Benson, B. R.; Jochmans, M. T.; Gracias, D. H., *J. Am. Chem. Soc.*, (2008) **130**, 17238.

[60] Smith, E. J.; Makarov, D.; Schmidt, O. G., *Soft Matter*, (2011) **7**, 11309.

[61] Kumar, K.; Nandan, B.; Luchnikov, V.; Gowd, E. B.; Stamm, M., *Langmuir : the ACS journal of surfaces and colloids*, (2009) **25**, 7667.

[62] Stoychev, G.; Puretskiy, N.; Ionov, L., *Soft Matter*, (2011) **7**, 3277.

[63] He, H.; Guan, J.; Lee, J. L., *Journal of controlled release : official journal of the Controlled Release Society*, (2006) **110**, 339.

[64] Shim, T. S.; Kim, S. H.; Heo, C. J.; Jeon, H. C.; Yang, S. M., *Angew Chem Int Ed Engl*, (2012) **51**, 1420.

[65] Leong, T. G.; Randall, C. L.; Benson, B. R.; Bassik, N.; Stern, G. M.; Gracias, D. H., *Proceedings of the National Academy of Sciences of the United States of America*, (2009) **106**, 703.

[66] Kumar, K.; Nandan, B.; Luchnikov, V.; Simon, F.; Vyalikh, A.; Scheler, U.; Stamm, M., *Chemistry of Materials*, (2009) **21**, 4282.

[67] Stoychev, G.; Turcaud, S.; Dunlop, J. W. C.; Ionov, L., *Advanced Functional Materials*, (2013) **23**, 2295.

[68] Guan, J.; He, H.; Lee, L. J.; Hansford, D. J., *Small*, (2007) **3**, 412.

[69] Guan, J.; He, H.; Hansford, D. J.; Lee, L. J., *The Journal of Physical Chemistry B*, (2005) **109**, 23134.

[70] Behl, M.; Razzaq, M. Y.; Lendlein, A., *Adv Mater*, (2010) **22**, 3388.

[71] Pedron, S.; van Lierop, S.; Horstman, P.; Penterman, R.; Broer, D. J.; Peeters, E., *Advanced Functional Materials*, (2011) **21**, 1624.

[72] Kelby, T. S.; Wang, M.; Huck, W. T. S., *Advanced Functional Materials*, (2011) **21**, 652.

[73] Luchnikov, V.; Kumar, K.; Stamm, M., *Journal of Micromechanics and Microengineering*, (2008) **18**, 035041.

[74] Jeong, K.-U.; Jang, J.-H.; Kim, D.-Y.; Nah, C.; Lee, J. H.; Lee, M.-H.; Sun, H.-J.; Wang, C.-L.; Cheng, S. Z. D.; Thomas, E. L., *Journal of Materials Chemistry*, (2011) **21**, 6824.

[75] Li, W.; Huang, G.; Yan, H.; Wang, J.; Yu, Y.; Hu, X.; Wu, X.; Mei, Y., *Soft Matter*, (2012) **8**, 7103.

[76] Feinberg, A. W.; Feigel, A.; Shevkoplyas, S. S.; Sheehy, S.; Whitesides, G. M.; Parker, K. K., *Science*, (2007) **317**, 1366.

[77] Alford, P. W.; Feinberg, A. W.; Sheehy, S. P.; Parker, K. K., *Biomaterials*, (2010) **31**, 3613.

[78] Yu, Y. L.; Nakano, M.; Ikeda, T., *Nature*, (2003) **425**, 145.

[79] Techawanitchai, P.; Ebara, M.; Idota, N.; Asoh, T.-A.; Kikuchi, A.; Aoyagi, T., *Soft Matter*, (2012) **8**, 2844.

[80] Liu, Y.; Boyles, J. K.; Genzer, J.; Dickey, M. D., *Soft Matter*, (2012) **8**, 1764.

[81] Zhang, X.; Pint, C. L.; Lee, M. H.; Schubert, B. E.; Jamshidi, A.; Takei, K.; Ko, H.; Gillies, A.; Bardhan, R.; Urban, J. J.; Wu, M.; Fearing, R.; Javey, A., *Nano letters*, (2011) **11**, 3239.

[82] Laflin, K. E.; Morris, C. J.; Muqeem, T.; Gracias, D. H., *Applied Physics Letters*, (2012) **101**, 131901.

[83] Ryu, J.; D'Amato, M.; Cui, X.; Long, K. N.; Jerry Qi, H.; Dunn, M. L., *Applied Physics Letters*, (2012) **100**, 161908.

[84] Ionov, L., *Soft Matter*, (2011) **7**, 6786.

[85] Ghaemmaghami, A. M.; Hancock, M. J.; Harrington, H.; Kaji, H.; Khademhosseini, A., *Drug discovery today*, (2012) **17**, 173.

[86] Revzin, A.; Rajagopalan, P.; Tilles, A. W.; Berthiaume, F. O.; Yarmush, M. L.; Toner, M., *Langmuir : the ACS journal of surfaces and colloids*, (2004) **20**, 2999.

[87] Kim, H.; Cohen, R. E.; Hammond, P. T.; Irvine, D. J., *Advanced Functional Materials*, (2006) **16**, 1313.

[88] Murua, A.; Portero, A.; Orive, G.; Hernandez, R. M.; de Castro, M.; Pedraz, J. L., *Journal of controlled release : official journal of the Controlled Release Society*, (2008) **132**, 76.

[89] Hernandez, R. M.; Orive, G.; Murua, A.; Pedraz, J. L., *Advanced drug delivery reviews*, (2010) **62**, 711.

[90] Kelm, J. M.; Fussenegger, M., *Advanced drug delivery reviews*, (2010) **62**, 753.

[91] Wilson, J. T.; Chaikof, E. L., *Advanced drug delivery reviews*, (2008) **60**, 124.

[92] Teramura, Y.; Iwata, H., *Soft Matter*, (2010) **6**, 1081.

[93] Peppas, N. A.; Hilt, J. Z.; Khademhosseini, A.; Langer, R., *Advanced Materials*, (2006) **18**, 1345.

[94] Brigham, M. D.; Bick, A.; Lo, E.; Bendali, A.; Burdick, J. A.; Khademhosseini, A., *Tissue Eng. Part A*, (2009) **15**, 1645.

[95] Velasco, D.; Tumarkin, E.; Kumacheva, E., *Small*, (2012) **8**, 1633.

[96] Tumarkin, E.; Kumacheva, E., *Chemical Society reviews*, (2009) **38**, 2161.

[97] Xu, S.; Nie, Z.; Seo, M.; Lewis, P.; Kumacheva, E.; Stone, H. A.; Garstecki, P.; Weibel, D. B.; Gitlin, I.; Whitesides, G. M., *Angew Chem Int Ed Engl*, (2005) **44**, 724.

[98] Burdick, J. A.; Khademhosseini, A.; Langer, R., *Langmuir : the ACS journal of surfaces and colloids*, (2004) **20**, 5153.

[99] Zhang, H.; Tumarkin, E.; Peerani, R.; Nie, Z.; Sullan, R. M. A.; Walker, G. C.; Kumacheva, E., *J. Am. Chem. Soc.*, (2006) **128**, 12205.

[100] Roh, K. H.; Martin, D. C.; Lahann, J., *Nat. Mater.*, (2005) **4**, 759.

[101] Yeh, J.; Ling, Y.; Karp, J. M.; Gantz, J.; Chandawarkar, A.; Eng, G.; Blumling, J., 3rd; Langer, R.; Khademhosseini, A., *Biomaterials*, (2006) **27**, 5391.

[102] Khademhosseini, A.; Eng, G.; Yeh, J.; Fukuda, J.; Blumling, J., 3rd; Langer, R.; Burdick, J. A., *Journal of biomedical materials research. Part A*, (2006) **79**, 522.

[103] Fukuda, J.; Khademhosseini, A.; Yeo, Y.; Yang, X.; Yeh, J.; Eng, G.; Blumling, J.; Wang, C. F.; Kohane, D. S.; Langer, R., *Biomaterials*, (2006) **27**, 5259.

[104] Khademhosseini, A.; Yeh, J.; Jon, S.; Eng, G.; Suh, K. Y.; Burdick, J. A.; Langer, R., *Lab on a chip*, (2004) **4**, 425.

[105] Franzesi, G. T.; Ni, B.; Ling, Y. B.; Khademhosseini, A., *J. Am. Chem. Soc.*, (2006) **128**, 15064.

[106] Tekin, H.; Sanchez, J. G.; Landeros, C.; Dubbin, K.; Langer, R.; Khademhosseini, A., *Adv Mater*, (2012) **24**, 5543.

[107] Du, Y.; Ghodousi, M.; Qi, H.; Haas, N.; Xiao, W.; Khademhosseini, A., *Biotechnology and bioengineering*, (2011) **108**, 1693.

[108] Panda, P.; Ali, S.; Lo, E.; Chung, B. G.; Hatton, T. A.; Khademhosseini, A.; Doyle, P. S., *Lab on a chip*, (2008) **8**, 1056.

[109] Yuan, B.; Jin, Y.; Sun, Y.; Wang, D.; Sun, J.; Wang, Z.; Zhang, W.; Jiang, X., *Advanced Materials*, (2012) **24**, 890.

[110] Kuribayashi-Shigetomi, K.; Onoe, H.; Takeuchi, S., *PLoS One*, (2012) **7**,

[111] McGuigan, A. P.; Sefton, M. V., *Proceedings of the National Academy of Sciences of the United States of America*, (2006) **103**, 11461.

[112] Chung, S. E.; Park, W.; Shin, S.; Lee, S. A.; Kwon, S., *Nat Mater*, (2008) **7**, 581.

[113] Bruzewicz, D. A.; McGuigan, A. P.; Whitesides, G. M., *Lab on a chip*, (2008) **8**, 663.

[114] Shi, Z.; Chen, N.; Du, Y.; Khademhosseini, A.; Alber, M., *Physical Review E*, (2009) **80**,

[115] Du, Y.; Ghodousi, M.; Lo, E.; Vidula, M. K.; Emiroglu, O.; Khademhosseini, A., *Biotechnology and bioengineering*, (2010) **105**, 655.

[116] Fernandez, J. G.; Khademhosseini, A., *Adv Mater*, (2010) **22**, 2538.

[117] Yanagawa, F.; Kaji, H.; Jang, Y. H.; Bae, H.; Yanan, D.; Fukuda, J.; Qi, H.; Khademhosseini, A., *Journal of biomedical materials research. Part A*, (2011),

[118] Harada, A.; Kobayashi, R.; Takashima, Y.; Hashidzume, A.; Yamaguchi, H., *Nat Chem*, (2011) **3**, 34.

[119] Scott, E. A.; Nichols, M. D.; Kuntz-Willits, R.; Elbert, D. L., *Acta Biomater*, (2010) **6**, 29.

[120] Azzam, R. M. A. B., N.M. , *Ellipsometry and polarized light* North-Holland: Amsterdam, (1987); p 539.

[121] Minko, S.; Patil, S.; Datsyuk, V.; Simon, F.; Eichhorn, K. J.; Motornov, M.; Usov, D.; Tokarev, I.; Stamm, M., *Langmuir : the ACS journal of surfaces and colloids*, (2002) **18**, 289.

[122] Dean, J. A., *Langes's handbook of chemistry*, McGraw-Hill Inc.: US, (1999).

[123] Kasarova, S. N.; Sultanova, N. G.; Ivanov, C. D.; Nikolov, I. D., *Optical Materials*, (2007) **29**, 1481.

[124] Chen, R. T.; Phillips, W.; Jannson, T.; Pelka, D., *Opt. Lett.*, (1989) **14**, 892.

[125] Arndt, K.-F. M., G. , *Polymercharakterisierung* Carl Hanser Verlag: München, Wien, New York, (1996).

[126] Spector, D. L.; Goldman, R. D., *Basic Methods in Microscopy: Protocols And Concepts from Cells, a Laboratory Manual*, Cold Spring Harbor Laboratory Press: (2006).

[127] Murphy, D. B., *Fundamentals of Light Microscopy and Electronic Imaging*, Wiley: (2002).

[128] Wayne, R., *Light and Video Microscopy*, Academic Press/Elsevier: United Kingdom, (2009).

[129] Sheppard, C. J. R. S., D.M. , *Confocal laser scanning microscopy (Microscopy handbook 38)*, BIOS Scientific Publishers: (1997).

[130] Optical Microscopy Primer, In http://micro.magnet.fsu.edu/primer/index.html.

[131] Price, R. L., *Basic Confocal Microscopy*, Springer New York: (2011).

[132] http://www.olympusconfocal.com/theory/confocalintro.html, In.

[133] *A Practical Guide to Scanning Probe Microscopy*, Veeco Instruments Inc.: (2005).

[134] Horcas, I.; Fernandez, R.; Gomez-Rodriguez, J. M.; Colchero, J.; Gomez-Herrero, J.; Baro, A. M., *Review of Scientific Instruments*, (2007) **78**,

[135] Bae, W. K.; Char, K.; Hur, H.; Lee, S., *Chemistry of Materials*, (2008) **20**, 531.

[136] Qu, L. H.; Peng, X. G., *J. Am. Chem. Soc.*, (2002) **124**, 2049.

[137] Maity, D.; Agrawal, D. C., *Journal of Magnetism and Magnetic Materials*, (2007) **308**, 46.

[138] Puretskiy, N.; Ionov, L., *Langmuir : the ACS journal of surfaces and colloids*, (2011) **27**, 3006.

[139] Kern, W.; Puotinen, D. A., *Rca Review*, (1970) **31**, 187.

[140] Bowden, N.; Brittain, S.; Evans, A. G.; Hutchinson, J. W.; Whitesides, G. M., *Nature*, (1998) **393**, 146.

[141] Guvendiren, M.; Yang, S.; Burdick, J. A., *Advanced Functional Materials*, (2009) **19**, 3038.

[142] Lin, P.-C.; Yang, S., *Applied Physics Letters*, (2007) **90**, 241903.

[143] Song, J., *Applied Physics Letters*, (2010) **96**, 051913.

[144] Schmidt, S.; Zeiser, M.; Hellweg, T.; Duschl, C.; Fery, A.; Möhwald, H., *Advanced Functional Materials*, (2010) **20**, 3235.

[145] Huber, D. L.; Manginell, R. P.; Samara, M. A.; Kim, B.-I.; Bunker, B. C., *Science*, (2003) **301**, 352.

[146] Ionov, L.; Stamm, M.; Diez, S., *Nano letters*, (2006) **6**, 1982.

[147] Ionov, L.; Synytska, A.; Diez, S., *Advanced Functional Materials*, (2008) **18**, 1501.

[148] Galaev, I. Y.; Mattiasson, B., *Trends in biotechnology*, (1999) **17**, 335.

[149] Ionov, L.; Diez, S., *J. Am. Chem. Soc.*, (2009) **131**, 13315.

[150] de Las Heras Alarcon, C.; Pennadam, S.; Alexander, C., *Chemical Society reviews*, (2005) **34**, 276.

[151] Sinha, V. R.; Bansal, K.; Kaushik, R.; Kumria, R.; Trehan, A., *International journal of pharmaceutics*, (2004) **278**, 1.

[152] Chiari, C.; Koller, U.; Dorotka, R.; Eder, C.; Plasenzotti, R.; Lang, S.; Ambrosio, L.; Tognana, E.; Kon, E.; Salter, D.; Nehrer, S., *Osteoarthritis and cartilage / OARS, Osteoarthritis Research Society*, (2006) **14**, 1056.

[153] Williams, J. M.; Adewunmi, A.; Schek, R. M.; Flanagan, C. L.; Krebsbach, P. H.; Feinberg, S. E.; Hollister, S. J.; Das, S., *Biomaterials*, (2005) **26**, 4817.

[154] Hollick, E. J.; Spalton, D. J.; Ursell, P. G.; Pande, M. V., *Journal of Cataract & Refractive Surgery*, (1998) **24**, 361.

[155] Lye, K. W.; Tideman, H.; Wolke, J. C.; Merkx, M. A.; Chin, F. K.; Jansen, J. A., *Clinical oral implants research*, (2013) **24 Suppl A100**, 100.

[156] Schild, H. G., *Progress in Polymer Science*, (1992) **17**, 163.
[157] Eshraghi, S.; Das, S., *Acta Biomaterialia*, (2010) **6**, 2467.
[158] 6.777J/2.751J Material Properties Database, In http://www.mit.edu/~6.777/matprops/matprops.htm.
[159] Huo, D.; Li, Y.; Qian, Q.; Kobayashi, T., *Colloids and Surfaces B: Biointerfaces*, (2006) **50**, 36.
[160] Stoychev, G.; Zakharchenko, S.; Turcaud, S.; Dunlop, J. W. C.; Ionov, L., *ACS Nano*, (2012) **6**, 3925.
[161] Zakharchenko, S.; Puretskiy, N.; Stoychev, G.; Stamm, M.; Ionov, L., *Soft Matter*, (2010) **6**, 2633.
[162] Kalinin, Y. V.; Randhawa, J. S.; Gracias, D. H., *Angewandte Chemie International Edition*, (2011) **50**, 2549.
[163] Low Kim, C.; Wheeler, A. P.; Koskan Larry, P., Commercial Poly(aspartic acid) and Its Uses, In *Hydrophilic Polymers*, American Chemical Society: (1996); Vol. 248, pp 99.
[164] Klein, T.; Moritz, R.-J.; Graupner, R., Polyaspartates and Polysuccinimide, In *Ullmann's Encyclopedia of Industrial Chemistry*, Wiley-VCH Verlag GmbH & Co. KGaA: (2000).
[165] Thombre, S. M.; Sarwade, B. D., *Journal of Macromolecular Science, Part A*, (2005) **42**, 1299.
[166] Prucker, O.; Naumann, C. A.; Rühe, J.; Knoll, W.; Frank, C. W., *J. Am. Chem. Soc.*, (1999) **121**, 8766.
[167] Frederik, C.; Erol, A. H.; Arune, G.; Demetra, S. A.; Anthi, R.; Carsten, R.; Aleksandr, O.; Xiao, S.; Costas, F.; Maria, V.; Boris, N. C.; Maria, F., *Langmuir : the ACS journal of surfaces and colloids*, (2009) **25**, 3219.
[168] Mosig, J.; Gooding, C. H.; Wheeler, A. P., *Industrial & Engineering Chemistry Research*, (1997) **36**, 2163.
[169] Karageorgiou, V.; Kaplan, D., *Biomaterials*, (2005) **26**, 5474.
[170] Zakharchenko, S.; Sperling, E.; Ionov, L., *Biomacromolecules*, (2011) **12**, 2211.
[171] Schacht, E. H., *Journal of Physics: Conference Series*, (2004) **3**, 22.
[172] Wu, X.; Liu, Y.; Li, X.; Wen, P.; Zhang, Y.; Long, Y.; Wang, X.; Guo, Y.; Xing, F.; Gao, J., *Acta Biomaterialia*, (2010) **6**, 1167.
[173] Young, S.; Wong, M.; Tabata, Y.; Mikos, A. G., *Journal of Controlled Release*, (2005) **109**, 256.
[174] Toohey, K. S.; Sottos, N. R.; Lewis, J. A.; Moore, J. S.; White, S. R., *Nat. Mater.*, (2007) **6**, 581.
[175] Esser-Kahn, A. P.; Thakre, P. R.; Dong, H. F.; Patrick, J. F.; Vlasko-Vlasov, V. K.; Sottos, N. R.; Moore, J. S.; White, S. R., *Advanced Materials*, (2011) **23**, 3654.
[176] Greil, P.; Lifka, T.; Kaindl, A., *J. European Ceram. Soc.*, (1998) **18**, 1961.
[177] Hinds, B. J.; Chopra, N.; Rantell, T.; Andrews, R.; Gavalas, V.; Bachas, L. G., *Science*, (2004) **303**, 62.
[178] Kilian, K. A.; Lai, L. M. H.; Magenau, A.; Cartland, S.; Bocking, T.; Di Girolamo, N.; Gal, M.; Gaus, K.; Gooding, J. J., *Nano letters*, (2009) **9**, 2021.
[179] King, B. H.; Gramada, A.; Link, J. R.; Sailor, M. J., *Advanced Materials*, (2007) **19**, 4044.
[180] Hermann, D.; Diem, M.; Mingaleev, S. F.; García-Martín, A.; Wölfle, P.; Busch, K., *Physical Review B*, (2008) **77**, 035112.
[181] Johnson, M. F. L.; Stewart, W. E., *J. Catal.*, (1965) **4**, 248.
[182] Nakajima, H., *Prog. Mater. Sci.*, (2007) **52**, 1091.
[183] Prasher, R., *J. Appl. Phys.*, (2006) **100**,
[184] Khaleghi, E.; Olevsky, E.; Meyers, M., *J. Am. Ceram. Soc.*, (2009) **92**, 1487.
[185] Feil, F.; Cauda, V.; Bein, T.; Brauchle, C., *Nano letters*, (2012) **12**, 1354.
[186] Yucel, D.; Kose, G. T.; Hasirci, V., *Biomacromolecules*, (2010) **11**, 3584.
[187] Li, J. M.; Rickett, T. A.; Shi, R. Y., *Langmuir : the ACS journal of surfaces and colloids*, (2009) **25**, 1813.

[188] Ma, P. X.; Zhang, R. Y., *Journal of Biomedical Materials Research*, (2001) **56**, 469.

[189] Mathieu, L. M.; Mueller, T. L.; Bourban, P. E.; Pioletti, D. P.; Muller, R.; Manson, J. A. E., *Biomaterials*, (2006) **27**, 905.

[190] Zhang, H.; Cooper, A. I., *Advanced Materials*, (2007) **19**, 1529.

[191] Zhang, H. F.; Hussain, I.; Brust, M.; Butler, M. F.; Rannard, S. P.; Cooper, A. I., *Nat. Mater.*, (2005) **4**, 787.

[192] Zhang, H. F.; Long, J.; Cooper, A. I., *J. Am. Chem. Soc.*, (2005) **127**, 13482.

[193] Stokols, S.; Tuszynski, M. H., *Biomaterials*, (2004) **25**, 5839.

[194] Nakamichi, Y.; Hirai, Y.; Yabu, H.; Shimomura, M., *Journal of Materials Chemistry*, (2011) **21**, 3884.

[195] Uetani, K.; Yano, H., *Soft Matter*, (2013) **9**, 3396.

[196] Li, Q. W.; Zhu, Y. T.; Kinloch, I. A.; Windle, A. H., *J. Phys. Chem. B*, (2006) **110**, 13926.

[197] Carbone, L.; Nobile, C.; De Giorgi, M.; Sala, F. D.; Morello, G.; Pompa, P.; Hytch, M.; Snoeck, E.; Fiore, A.; Franchini, I. R.; Nadasan, M.; Silvestre, A. F.; Chiodo, L.; Kudera, S.; Cingolani, R.; Krahne, R.; Manna, L., *Nano letters*, (2007) **7**, 2942.

[198] Gu, Z. Y.; Chen, Y. M.; Gracias, D. H., *Langmuir : the ACS journal of surfaces and colloids*, (2004) **20**, 11308.

[199] Mayer, C. R.; Neveu, S.; Cabuil, V., *Advanced Materials*, (2002) **14**, 595.

[200] Boal, A. K.; Rotello, V. M., *Langmuir : the ACS journal of surfaces and colloids*, (2000) **16**, 9527.

[201] Mattoussi, H.; Mauro, J. M.; Goldman, E. R.; Anderson, G. P.; Sundar, V. C.; Mikulec, F. V.; Bawendi, M. G., *J. Am. Chem. Soc.*, (2000) **122**, 12142.

[202] Mirkin, C. A., *Inorg. Chem.*, (2000) **39**, 2258.

[203] Shenton, W.; Davis, S. A.; Mann, S., *Advanced Materials*, (1999) **11**, 449.

[204] Kim, Y. J.; Johnson, R. C.; Hupp, J. T., *Nano letters*, (2001) **1**, 165.

[205] Doi, M.; Edwards, S. F., *The Theory of polymer dynamics*, Clarendon Press [etc.]: Oxford [etc.], (1988).

[206] Onsager, L., *Ann.NY Acad.Sci.*, (1949) **51**, 627.

Acknowledgments

This work would not be possible without support and help of a large number of people.

First of all I would like to thank **Prof. Manfred Stamm** for giving me the opportunity to carry out this work in the Leibniz Institute of Polymer Research Dresden, for his guidance and advices.

I want to express my heartfelt gratitude to my supervisor **Dr. Leonid Ionov** for inexhaustible feedback throughout course of my doctoral work, for his encouragement and enthusiasm, everyday support, and of course for the wonderful atmosphere he created in his group. It was a great pleasure for me to work with him.

I greatly appreciate **Prof. Oliver G. Schmidt** for taking the time to be a referee for my thesis.

Particular thanks to all my colleges in IPF for the friendly and scientific atmosphere and possibility to combine effective work with fun. Especially I would like to thank **Georgi Stoychev** for suggesting I come in Germany to pursue my PhD, for moral support, sharing his polymers with me and for the help with SEM imaging; **Nikolay Puretskiy** for the help with synthesis and contact angle measurements; **Ivan Raguzin** for his humor and illustrator talent; **Dr. Ekaterina Biehlig** for sharing her experience in AFM measurements, and all of them for their friendship and a lot of fun both during scientific and leisure activities.

I really appreciated the technical assistance of my IPF colleagues: **Dr. Petr Formanek** for the introduction in SEM investigations, **Andreas Janke** for his help in AFM measurements, **Petra Treppe** for GPC and **Dr. Ulrich Ortel** for measuring UV-vis spectra. My thanks to the secretary of department of Nanostructures Materials **Janett Forkel** for the excellent organizational support.

I'm grateful to **Dr. Alla Synytska** for the possibility to use her lab, devices, and solvents, as well as for her support and understanding.

Thanks to **Prof. Jens-Uwe Sommer**, **Prof. Hans-Peter Wiesmann** and **Dr. Jörg Neunzehn** for the fruitful discussions.

I wish to thank all the people I have collaborated with during these years: **Prof. Stefan Diez** (B-CUBE, Dresden and MPI-CBG) and **Jan Peychl** (Light Microscopy Facility, MPI-CBG) for assistance with confocal microscopy experiments; **Dr. Christian Waurisch**, **Dr. Stephen G. Hickey**, **Prof. Alexander Eychmüller** (TU Dresden) for providing quantum dots; **Prof. Oliver G. Schmidt**, **Dr. Samuel Sanchez Ordonez** and **Britta Koch** (IFW Dresden) for experiments with HeLa cells.

I owe a debt of gratitude to my first supervisor **Dr. Ekaterina Litmanovich** for advising me throughout my study in Moscow State University and for her never-ending believe in me as a researcher.

I’m deeply grateful to my husband **Dirk** who helped me to feel comfortable in a new country, led me through the difficulties of German language, and all these years was very supportive, patient and kind to me.

My hearty thanks to my **family** in Russia, who always believed in me. Particularly, I would like to acknowledge my **grandfather** who taught me to finish what I’ve started.

I am most grateful for my dear friend **Dr. Natalia Dadivanyan** for the help whenever needed and for critical reading of this thesis.

My thanks to all my friends in Russia and in Germany: **Jenja Demina**, **Dr. Tatiana Sitnikova**, **Ekaterina Schukina**, **Ekaterina Musaliamova**, **Claudine Dawson**, **Clara Schröder**, for their friendship over the years.

List of publication

10) V. Stroganov, **S. Zakharchenko**, E. Sperling, G. Stoychev, A. Meyer, O.G. Schmidt and L. Ionov, Biodegradable polymer films with controlled thermo-triggered folding, in preparation

9) **S. Zakharchenko**, N. Puretskiy, G. Stoychev, C. Waurisch, S.G. Hickey, J-U. Sommer, L. Ionov, Stimuli-responsive hierarchically self-assembling 3D porous hydrogel-based materials with aligned pores, *Journal of Materials Chemistry B,* 2013, **1**, 1786–1793.

8) L. Ionov, **S. Zakharchenko**, G Stoychev, Soft Microorigami: Stimuli-responsive Self-folding Polymer Films, *Advances in Science and Technology*, 2013, **77**, 348-353.

7) G. Stoychev, **S. Zakharchenko**, S. Turcaud, J. Dunlop, L. Ionov, Shape programmed folding of stimuli-responsive polymer bilayers, *ACS Nano*, 2012, **6 (5)**, 3925–3934.

6) **S. Zakharchenko**, E. Sperling, L. Ionov, Fully biodegradable self-rolled polymer tubes: a candidate for tissue engineering scaffolds, *Biomacromolecules,* 2011, **12**, 2211–2215.

5) **S. Zakharchenko**, N. Puretskiy, G. Stoychev, M. Stamm, L. Ionov, Temperature controlled encapsulation and release using partially biodegradable thermo-magneto-sensitive self-rolling tubes*, Soft Matter*, 2010, **6**, 2633-2636

4) E.A. Litmanovich, E.V. Chernikova, G.V. Stoychev, **S.O. Zakharchenko** Unusual Phase Behavior of the Mixture of Poly(acrylic acid) and Poly(diallyldimethylammonium chloride) in Acidic Media, *Macromolecules*, 2010, **43(16)**, 6871-6876

3) E.A. Litmanovich, **S.O. Zakharchenko**, G.V. Stoichev, A.B. Zezin, Phase separation in a Poly(acrylic acid)-Polycation system in acidic solutions, *Polymer Science. Series A*, 2009, **51(6)**, 616-621

2) E. Litmanovich, **S. Zakharchenko**, G. Stoichev, Influence of Chain Charge and Complexation on the Overlap and Entanglements Formation in Poly(acrylic acid) Salt-Containing Aqueous Solutions, *J.Phys.Chem. B*, 2007, **111 (29)**, 8567-8571

1) **S. Zakharchenko**, E. Litmanovich, F. Radchenko, A. Pastukhov, A. Zezin, I. Novakov, and V. Kabanov, Photon Correlation Spectroscopic Study of the Aggregative Stability of Colloidal Particles of Aluminum Pentahydroxide Chloride, *Colloid Journal*, 2006, **68 (4)**, 425–429

Journal of
Materials Chemistry B
Materials for biology and medicine
RSC Publishing

Journal cover pages

Journal of Materials Chemistry B, 2013, 1, 1786–1793

Contributions to academic conferences

Oral presentations

- S. Zakharchenko and L. Ionov, *Hierarchically self-assembled hydrogel-based materials with aligned pores for tissue engineering scaffolds*, Jülich Soft Matter Days, 13th – 16th of November 2012, Bad Honnef, Germany
- S. Zakharchenko and L. Ionov, *Biomimetic soft microorigami: Smart 3D micro-constructs from self-folding polymer films.* 9th International Nanotechnology Symposium Nanofair, 12th – 13th of June 2012, Dresden, Germany
- L. Ionov, S. Zakharchenko, G. Stoychev, E. Sperling, K. Köhler, *Soft microorigami: self-folding polymer films for cell encapsulation and release.* Nanomaterials for Biomedical Technologies. 6th – 7th of March 2012, Frankfurt am Main, Germany
- S. Zakharchenko, E. Sperling, L. Ionov, *Fully biodegradable self-rolled polymer tubes: novel candidate for tissue engineering scaffolds.* 3rd European Science Foundation Summer School “Nanomedicine”, 19th – 24th of June 2011, Lutherstadt Wittenberg, Germany
- E. Litmanovich, S. Zakharchenko, E. Lysenko, *Polyelectrolyte complexes formed in semidilute solutions*, 6-th International Symposium on Polyelectrolytes, 4th – 8th September 2006, Dresden, Germany

Poster Presentations

- S. Zakharchenko, B. Koch, S. Sanchez, O.G. Schmidt, C. Waurisch, S.G. Hickey, A. Eychmüller and L. Ionov, *Self-rolled polymer tubes for bioapplications*, Bayreuth Polymer Symposium, 15th – 17th of September 2013, Bayreuth, Germany – poster prize.
- S. Zakharchenko and L. Ionov, *Biomimetic Soft Microorigami: Smart 3D Micro-Constructs from Self-folding Polymer films*, Material Science and Engineering Congress, 25th – 27th of September 2012, Darmstadt, Germany.
- G. Stoychev, L. Ionov, S. Zakharchenko, S. Turcaud, J. W. C Dunlop, *Shape programmed folding of stimuli-responsive polymer bilayers.* Material Science and Engineering Congress, 25th – 27th of September 2012, Darmstadt, Germany.
- S. Zakharchenko, J. Neunzehn, L. Ionov, *Fully Biodegradable Self-rolled Polymer Tubes: A Candidate for Tissue Engineering Scaffold*, 13th Dresden Polymer Discussion and 8th Max Bergmann Symposium “Molecular bioengineering meets polymer science”, 1st – 4th of April 2012, Meissen, Germany.
- G. Stoychev, S. Zakharchenko, S. Turcaud, , J. W. C. Dunlop, L. Ionov, *Shape-programmed folding of stimuli-responsive polymer bilayers.* 13th Dresden Polymer

Discussion and 8th Max Bergmann Symposium “Molecular bioengineering meets polymer science”, 1st – 4th of April 2012, Meissen, Germany.

- S. Zakharchenko, E. Sperling, L. Ionov, *Fully biodegradable self-rolled polymer tubes: novel candidate for tissue engineering scaffolds.* 3rd European Science Foundation Summer School “Nanomedicine”, 19th – 24th of June 2011, Lutherstadt Wittenberg, Germany
- S. Zakharchenko, N. Puretskiy, G. Stoychev, M. Stamm, L. Ionov, *Temperature Controlled Encapsulation and Release Using Partially Biodegradable Thermo-magneto-sensitive Self-rolling Tubes*, Third International NanoBio Conference, 24th – 27th of August 2010, Zurich, Switzerland
- S. Zakharchenko, G. Stoychev, E. Litmanovich, *Structure formation in solutions of sodium polyacrylate and its complexes with tetradecyltrimethylammonium bromide,* XIII All-Russian Conference “Structure and dynamics of molecular systems”, 2006, Yalchik, Russia
- S. Zakharchenko, E. Litmanovich, *Concentration regime of PEI solution and its influence on the properties of PEI – PAA complexes,* X All-Russian Conference “Structure and dynamics of molecular systems”, 2003, Yalchik, Russia

Versicherung

Hiermit versichere ich, dass ich die vorliegende Arbeit ohne unzulässige Hilfe Dritter und ohne Benutzung anderer als der angegebenen Hilfsmittel angefertigt habe; die aus fremden Quellen direkt oder indirekt übernommenen Gedanken sind als solche kenntlich gemacht. Die Arbeit wurde bisher weder im Inland noch im Ausland in gleicher oder ähnlicher Form einer anderen Prüfungsbehörde vorgelegt.

Dresden, 13.11.2013

Svetlana Zakharchenko

Erklärung

Die vorliegende Arbeit wurde in der Zeit von September 2009 bis Oktober 2013 unter der wissenschaftlichen Betreuung von Prof. Dr. Manfred Stamm und Dr. Leonid Ionov am Leibniz-Institut für Polymerforschung Dresden e.V. in der Abteilung Nanostrukturierte Materialien angefertigt. Es haben keine früheren erfolglosen Promotionsverfahren stattgefunden. Ich erkenne die Promotionsordnung der Fakultät Mathematik und Naturwissenschaften an der Technischen Universität Dresden vom 23.02.2011 an.

Dresden, 13.11.2013

Svetlana Zakharchenko